Development and application of µXRF-CS Cl as a proxy for late Holocene drought and hurricane conditions in the Yucatan Aquifer, Mexico

Development and application of μXRF-CS Cl as a proxy for late Holocene drought and hurricane conditions in the Yucatan Aquifer, Mexico

CHELSI ANASTASIA MCNEILL-JEWER
Honours B.Sc McMaster University

A Thesis

Submitted to the School of Graduate Studies

in Partial Fulfillment of the Requirement

for the Degree

Doctor of Philosophy

McMaster University

McMaster University
Doctor of Philosophy (2020)
Hamilton, Ontario, Canada
School of Geography and Earth Sciences

TITLE:

Development and application of μXRF-CS Cl as a proxy for late Holocene drought and hurricane conditions in the Yucatan Aquifer, Mexico

AUTHOR: Chelsi A. McNeill-Jewer B.Sc (Honours)
McMaster University

SUPERVISOR: Eduard G. Reinhardt Professor
McMaster University

NUMBER OF PAGES: xx, 149

ABSTRACT

The highly porous karst limestone of the Yucatan Peninsula promotes infiltration of rainwater into the subsurface, where it becomes part of the Yucatan Aquifer. The combination of high subsurface porosity, high evapotranspiration, and seasonal droughts results in relative scarcity of lakes or drinkable water at the surface. The majority of past and present people living on the Yucatan Peninsula have depended on groundwater resources for domestic purposes. Whereas coastal karst aquifers such as the one in the Yucatan Peninsula are important water resources, they are highly vulnerable to climate-related changes such as sea level (SL) rise, increased hurricane intensity and extended droughts. With ongoing development along the eastern coast of the Yucatan Peninsula (Quintana Roo), predicted increases in storm intensity, and rising population and potential pollutant output, it has become imperative to study the seasonal and long-term effects of climate and human activity on the Yucatan Aquifer.

Like many coastal karst aquifers, the Yucatan Aquifer is stratified according to density, with the Meteoric Water Mass (MeWM) flowing towards the coast on top, and the Marine Water Mass (MaWM) flowing inland on the bottom. The current basis of our knowledge about how the two water masses interact has been from short-term instrumental monitoring and numerical modelling, which is useful for understanding straightforward relationships between salinity, precipitation and temperature across the two water masses and have paved the way for more complex analyses to be completed using the simple principles to guide

geochemical studies of sediment within the systems. Generally, sediment cores have been analysed discretely using various methods including grain size analysis, micropaleontology, WD-XRF, and others, however the recent rise of µXRF Core Scanning provides a quicker, more cost effective and higher-resolution method for studying climate-related patterns in sediment cores.

This thesis outlines and provides robust evidence for three new methods of using µXRF-CS to determine past and present climatological changes and their relationship to sediment elemental counts. We provide the first outline of the seasonal and spatial controls of geochemical changes in sedimentation in a coastal cave system (Yax Chen), using four years of *in situ* sediment collection. We then provide the first calibrated record of past salinity based on Cl counts within sediment cores taken from shallow lakes. Although instrumental monitoring has provided evidence that the aquifer is impacted by modern wet and dry periods, the effect of past climate on the aquifer has not been investigated. We provide the first record of water-column mixing at three locations within coastal Quintana Roo. This demonstrates that there has been a long-term climate impacts to coastal Yucatan Peninsula groundwater, which may be scaled to other karst islands and provides evidence that increased hurricane frequency and/or magnitude could change the baseline salinity of the fresh MeWM.

ACKNOWLEDGEMENTS

I dedicate this thesis to my mother, Norma Anne McNeill, who loved and supported me unconditionally before and throughout my PhD, up until the day she passed from an aggressive form of brain cancer on December 20, 2018. Completing a doctorate is a difficult enough task for anyone, but going through the loss of my mother and main supporter at the same time was devastating to say the least. My heart aches that she isn't here with me to celebrate this lifelong dream of mine, but I am forever grateful for the lessons she taught me and the weird personality she helped me cultivate. Thank you mama, I am going to savour this bottle of 1992 Dom Perignon in our honour. If you're actually reading this, go call/ hug your mom!

I grew up obsessed with National Geographic documentaries about anything related to the Earth and it's past. My secret dream growing up was always to be a paleontologist and I have countless rocks and fossils scattered about my house. As I grew older, I felt compelled to get a doctorate, not for the title of Dr, but for the sake of the original research and being able to delve deep into it. The 10 years I spent at McMaster have changed me into a completely different person, mostly for the better. I accomplished dreams I never thought I would get the chance to do.

To Sian, and Nick, my bbs, I feel so lucky to have met two of my best friends during my time here, and for the support we have been able to give each other before we all sashay away to our big-girl jobs. Special shoutout to all the SGES/SEES grads and all of the times we had at the Phoenix. Obviously, I also need to include the Phoenix and Jimmy for always being there for us in our times of need! Speaking of

being there in times of need, I have to thank Gaia and Romulus for the unconditional cuddles and goofiness, even though they can't read this and will never understand how grateful I am for them.

Speaking of grateful - Anya (Onie-sorry!), thank GORD you were there with me for the majority of our time as grad students. I don't think I would have been able to make it out of here without you. We have had so many times I can't even count and even though we don't spend 100% of our time together anymore I love you so much and never forget that!!!!!!!!!!!!!!!

Aarón, Mónica, y Alberto (y Kalhua!), mi nueva familia - Los amo a todos, y el amor, y el apoyo incondicionales me han ayudado mucho en el año pasado. Estoy tan emocionado de pasar el resto de mi vida con todos ustedes! Prometo que mi próximo esfuerzo será llegar a ser completamente fluido en Español y no solo en Spanglish!

My above-water family: Dad, Michelle, Missy, Aaron, Felice, Hayden and Lucas (and Bruno!), as well as all of my aunts, uncles and cousins - thank you for grounding me (pun not intended). My underwater family: Kelvin, Anabelle, Buddy, Alex, Fred, Chris, Emoke, Ivo, Peter, Manu, Ally, Cam and everyone I ever met at Zero Gravity, I need to thank for welcoming me and supporting me, and also being a constant inspiration for diving (and source of tequila shots)! I hope one day to be half as talented as you guys underwater. This is extended to everyone I ever dived with and the whole international GUE community - you guys are the coolest.

I spent the last 5 years visiting the city of Tulum, Mexico approximately every 6 months, and spent the summer of 2019 living there. We are lucky to have access to Alberto's condo there and I will always have a connection to Tulum. All of my hope and love goes out to all of the hard-working people living in Tulum and I hope that the government will be able to ensure the future protection of the incredible ecosystems found there. Lo mismo para todas las ciudades de Mexico - Las amo a todas, incluso Pac Chen, Isla Mujeres (y las hamburguesas), Bacalar, Valladolid, Sotuta de Peon, San Cristobal de las Casas, Palenque (viejo y nuevo), todo de el Jefe y sus gentes, Oaxaca, Monterrey, y mas y mas!

This thesis was powered by tacos.

DECLARATION OF ACADEMIC ACHIEVEMENT

CHAPTER 2: THE EFFECT OF SEASONAL RAINFALL ON NUTRIENT INPUT AND BIOLOGICAL PRODUCTIVITY IN THE YAX CHEN CAVE SYSTEM (OX BEL HA), MEXICO, AND IMPLICATIONS FOR XRF CORE STUDIES OF PALEOHYDROLOGY

Sediment traps were put in Yax Chen by S. Collins, EGR, and 2011-2012 Mexico Cave Exploration Project (MCEP) volunteers. Laboratory samples were processed and analysed by S. Collins, EGR and me. Water level data were collected by S. Kovacs and A. Coutino. Microfossil analysis of samples was completed by W.M Chan, G. Mushet and C. Baroulliet. µXRF-CS scanning and calibration were completed by EGR. Manuscript was prepared by me and EGR. This manuscript was published in *Palaeogeography, Palaeoclimatology, Palaeoecology* in July 2019 https://doi.org/10.1016/j.palaeo.2019.109289 .

CHAPTER 3- SALINITY CHANGES DURING THE MAYA TERMINAL CLASSIC DROUGHTS DOCUMENTED THROUGH CALIBRATED µXRF-CS CL IN SEDIMENT CORES FROM QUINTANA ROO, MEXICO

For this paper, the Chumkopo sediment core was collected in the field by me, A. Coutino, A. Krywy-Janzen, W.M Chan, S. Kovacs and EGR. The Pac Chen core was collected in the field by A. Krywy-Janzen and EGR. The calibration cores were collected by 2015 Mexico Cave Exploration Project (MCEP) volunteers. Lake water column characteristics and water depth monitoring for Pac Chen were completed by EGR, S. Kovacs and A. Coutino. Laboratory samples for Pac Chen were processed and analysed by A. Krywy-Janzen and B. Waltham. Microfossil analyses of Pac Chen were completed by A. Krywy-Janzen. Microfossil analyses of Chumkopo were completed by me. Lake column characteristics and water depth monitoring for Chumkopo were completed by EGR in 2015. µXRF-CS scanning and calibration were completed by EGR. Salinity calibration and data analysis were performed by me, with input from EGR. Salinity standard deviation drought tool was created by me, with input from A. Coutino, who also calculated all wavelet time series. Manuscript was prepared by me and EGR, with input from A. Coutino, M. Stastna and D. Rissolo. This manuscript is currently in review with the journal *Quaternary Science Reviews*.

CHAPTER 4: MIXING-INDUCED SALINITY CHANGE IN THE DEEP COASTAL YUCATAN AQUIFER CAUSED BY HURRICANES OVER THE PAST 4 KY

For this paper, cores were collected by EGR, Meacham, Gabriel, Van Hengstum, and volunteers from the 2016 Mexico Cave Exploration Project (MCEP). Lake column characteristics for Angelita were completed by EGR, Gabriel and Van Hengstum in 2007. Water column characteristics for ISOD were completed by EGR and MCEP volunteers. Water column characteristics for Zapote were completed by Stinnesbeck et al. (2017). Microfossil analysis of all cores was done by me. µXRF-CS scanning and calibration were completed by EGR. Data analysis for the gamma method was done by me and Aaron Coutino. The manuscript was prepared by me and EGR.

TABLE OF CONTENTS

LIST OF FIGURES

CHAPTER 2

Figure 6. Principal Components Analysis shows first two components (PC1 and 2) encompass ~ 54% of the data variability. Biogenic-influenced elements (Si, K, S) strongly correlate with sediment flux, which has an inverse relationship with station distance and depth. Lithogenic elements show intercorrelations (Ti, Fe, Sr), but do not correlate directly with water depth.

Figure 7. Crossplots showing relationships between lithologic (blue) and biogenically influenced elements. Error bars represent standard deviations of the analysis mean for each sample cuvette.

Figure 8. Crossplots showing relationships with station depth over the study period. All parameters are averaged over the study period. 1) Upstream distance along the cave passage from the Yax Chen Cenote; 2) Sediment Flux; 3 - 5) Biogenic-influenced elements; and 6 – 9) Lithologic elements. Error bars represent the variation in depth for each station (n= 3 sediment traps) and the variability (standard deviation) in sediment flux and elements over the analysis period.

Figure 9. Crossplots showing relationships with average precipitation (deviation from mean; mm) over the collection intervals (6 months). 1) Mean water depth (deviation from mean; m); 2) Sediment flux; 3 - 5) Biogenic-influenced elements (red); and 6 – 9) Lithologic elements (blue). Error bars represent the variation in monthly precipitation over the collection periods, and the variability (standard deviation) of sediment flux and elements for all the stations (2-17) for each collection period. Green symbols and trendline (Ti) are individual values for Station 14.

Figure 10. Map of Yax Chen cave system with locations of sediment collection sites and mangrove coverage (top). Cozumel precipitation (in mm) and water level in Yax Chen (in m) are indicated with dark grey bars representing monthly collection. Sediment flux (light grey - sediment amount in g/cm^2), Si/Ti (red - biogenic sediments), and Ti/K (blue - lithogenic sediments) are arranged by collection period and sediment collection location.

Figure 11. Plots showing relationships between precipitation and water level (deviation from mean; mm, m) with sediment flux, Si/Ti, which maybe a useful hurricane/tropical storm indicator and Ti/K as a paleorainfall proxy.

Figure 12. Conceptual diagram showing the relationship between groundwater and rainfall (low and high) along with differences between mangrove and upland forest/shrub terrains, which have also been established with monitoring of groundwater characteristics and modeling (Coutino et al., submitted).

CHAPTER 3

CHAPTER 4

LIST OF TABLES

CHAPTER 3

CHAPTER 4

CHAPTER 1- INTRODUCTION

Groundwater systems on tropical islands and peninsulas, such as the Yucatan Peninsula (Mexico) are both extremely valuable and vulnerable resources, given the increasing human development and exploitation (e.g., water extraction, pollution, alteration of catchments), as well as climate controls such as sea level rise and hurricanes. This makes it imperative to understand the past and present evaporation and mixing dynamics within coastal groundwater systems to ensure proper planning and protection of important resources. The heavily karstified limestone geology of the coastal Yucatan Peninsula in Quintana Roo (the most eastern state) exhibits high permeability and porosity as a consequence of dissolution processes and sea level change (Smart et al., 2006; Bauer-Gottwein et al., 2011). Dissolution processes throughout the Holocene have also given rise to extensive coastal cave systems and sinkholes that provide points of access to the groundwater mass (Smart et al., 2006). Because of the high porosity, the majority of rainwater quickly percolates through the substrate and into the unconfined aquifer where it forms a distinct fresh water mass (the meteoric water mass, or MeWM), which sits atop the underlying marine water mass (MaWM) that intrudes from the coast (Kambesis and Coke, 2013). The two water masses are separated by a zone of intermediate salinity, termed the halocline, or mixed water mass (MxWM), which changes vertical position based on sea level rise, seasonal dry periods, and periods of intense rainfall (Coutino et al, 2017; Ritter et al., 2018). The high porosity that influences rapid subsurface drainage also contributes to a lack

of surface water bodies in the region, making lakes and rivers extremely rare (rivers are completely absent in Quintana Roo). The lack of surface water and abundance of groundwater has made the MeWM of the Yucatan Aquifer the primary source of potable water for domestic and agricultural use (Escolero et al., 2002).

Current knowledge about the Yucatan Peninsula aquifer comes from instrumental monitoring and preliminary studies of sedimentation within the cave systems. It is known that the groundwater mass responds to modern controls such as tidal fluctuations, hurricanes, seasonal drought and sea level rise (Coutino et al., 2017; Kovacs et al., 2017a; Coutino et al., submitted). There is, however, a recognized gap in knowledge about how the groundwater responded to these controls in the past, especially to changes in the frequency and intensity of precipitation events, which are predicted to be the biggest impacts on the aquifer in coming decades (van Hengstum et al., 2016, Kovacs et al., 2017a). The study of sedimentation within the aquifer and development of paleoclimate records from caves and cenotes will provide tangible evidence of groundwater movement and interaction with climate in the late Holocene. The development and application of paleoclimate proxies using µXRF elemental counts will provide a basis for understanding long term groundwater behaviour and will aid in increasing the spatial network of groundwater based paleoclimate records across the eastern Yucatan Peninsula.

Conventional XRF analysis is completed on discreetly sampled powdered sediment using either a fusion or pelletization of the sample for further determination of major and trace elements (Croudace, Rindby & Rothwell, 2015).

Nondestructive X-Ray Fluorescence core scanners have become a major innovation in the analysis of sediment cores within the past decade and have radically improved the capacity to record and understand environmental processes and change from annual to even subannual levels (Croudace & Rothwell, 2015). Benefits of this method include non-destruction of samples, rapid analysis, and high resolution. A number of elemental proxies have been recognized as indicators of climate, weathering, erosion, productivity, redox conditions, pollution, and water chemistry changes that can be easily and rapidly detected in sediment cores using XRF-Core Scanning. The depositional setting of the sediment is an important control on the selection of proxy elements and the development of calibration strategies (Croudace, Rindby & Rothwell, 2015). While XRF-CS has not been extensively applied to cave and cenote sediments in the Yucatan Peninsula, it stands to be a promising tool for developing understanding of sedimentation in these new depositional settings.

This dissertation is divided into three manuscripts, one that was published (Chapter 1; July 2019), one that has been submitted (Chapter 2; August 2020), and one that has been prepared for publication (Chapter 3). All three papers investigate the relationships between μXRF elemental counts and environmental variables. The introduction of μXRF core scanning as an analytical method enables high-resolution analyses of relative elemental changes, which can be employed as paleoclimate proxies. The three chapters in this thesis demonstrate that the water table of the eastern Yucatan Peninsula responds to dry and wet periods, expressed

through changes in salinity that are controlled by evaporative processes, or addition of rainfall to the system, respectively. Evaporation and mixing-driven salinity changes have occurred in the eastern Yucatan Peninsula for thousands of years and are tied to changes in Caribbean Sea characteristics such sea surface salinity (SSS) and sea surface temperature (SST), but are also linked to broader climate patterns such as movement of the Inter-Tropical Convergence Zone (ITCZ) and its modulations from the El Niño Southern Oscillation (ENSO) and North Atlantic Oscillation (NAO), as well as to Northern Hemisphere (NH) temperature change. Hurricanes, or lack of them, has a profound impact on surface water and groundwater in the Yucatan Peninsula.

The first manuscript examines four years of rainfall, water level and *in situ* sediment flux data collected from Yax Chen, a coastal cave system 300 m from the coast, to determine the seasonal and spatial relationship between elemental inputs into the cave system. Relationship among cave depth, adjacent sinkhole size, distance from the coast, and vegetation cover were investigated. Prior to this study, it was known that increased rainfall causes greater sediment flux, but the mechanisms surrounding this phenomenon were not fully understood. Collins et al. (2015a) showed that low-porosity mangrove peat deposits adjacent to certain cenotes promote flooding of the peat surface, which prevents water from immediately percolating downward. Knowledge of mangrove and forest cover along cave system-cenote complexes is important to properly protect the cave systems and ecosystems downstream from them. Furthermore, future development along the

coastal Playa Del Carmen-Tulum coast will result in destruction of mangroves, which we have shown are important environmental controls on sediment inputs into the cenotes. Reduction of mangrove peat, in combination with additions of pollutants (e.g. from sunscreen, insect repellent, car oil, cleaning products, etc.) could have deleterious effects downstream, as water in the cave systems flows toward the vulnerable coast (McNeill-Jewer et al., 2019)

The second manuscript investigates the utility of a calibrated paleosalinity proxy based on micro-XRF Chlorine counts. Sixteen cores were taken in locations that exhibited a wide range of sediment types and salinities. Cl concentrations in uppermost deposits were related to salinity in the overlying waters and this calibration was then applied to sediment cores from two shallow lakes in Quintana Roo (Chumkopo and Pac Chen) to infer past salinity. Prior to this study, there was no method to estimate paleo-salinity using sediment cores, however in Chapter 3 we show that high-resolution μXRF core scanner records can provide reliable inferences regarding past salinity changes. This provides critical information regarding the magnitude of droughts that occurred in the Terminal Classic Maya Period, and also provides a robust way to estimate salinity based on elemental Cl counts that will be useful for developing management plans for the future.

The last manuscript provides evidence of long-term interactions between the MeWM, MxWM and MaWM from two deep sinkholes (Angelita, Zapote), and one cave location (ISOD2; Yax Chen) that span the MeWM to MaWM water masses. Instrumental monitoring has shown that hurricanes and associated high rainfall

induces mixing of the MeWM and MaWM of the aquifer, however until this study it was unknown whether or not this occurred in the past, or if this phenomenon could even be detected in the paleorecord. Chapter 4 addresses this by investigating the geochemical differences in 'mixing' between the MeWM and MaWM of the Yucatan sub-surface water column. We provide evidence that successive hurricanes or intense storms can result in salinization of the MeWM, which is important given ongoing climate change and predictions about how this will influence future hurricane magnitude and intensity.

CHAPTER 2: THE EFFECT OF SEASONAL RAINFALL ON NUTRIENT INPUT AND BIOLOGICAL PRODUCTIVITY IN THE YAX CHEN CAVE SYSTEM (OX BEL HA), MEXICO, AND IMPLICATIONS FOR XRF CORE STUDIES OF PALEOHYDROLOGY

Manuscript published in *Palaeogeography, Palaeoclimatology, Palaeoecology 534* July 2019 https://doi.org/10.1016/j.palaeo.2019.109289

Chelsi A. McNeill-Jewer [a*], Eduard G. Reinhardt [a], Shawn Collins [a, b], Shawn Kovacs [a, c], Winnie May Chan [a, d], Fred Devos [e], Chris LeMaillot [e]

[a] McMaster University, School of Geography and Earth Sciences, Hamilton, ON, L8S 4K1, Canada
[b] Wireline Services Group, Unit 28 – 80 Barbados Blvd., Toronto, ON, Canada, M1J 1K9, shawncollins@wirelineservices.com.au
[c] GEM Systems Inc., 135 Spy Court, Markham, ON, Canada, L3R 5H6, shawn.kovacs@gemsystems.ca
[d] CNRS - Université de Lyon 2, UMR 5133, Archéorient de Maison de l'Orient et de la Méditerranée
7 Rue Raulin 69007, Lyon, France, winniemay.chan@gmail.com
[e] Mexico Cave Exploration Project (MCEP), Centro Investigador del Sistema Acuifero de Quintana Roo A.C. (CINDAQ), Global Underwater Explorers (GUE), Mexico, fred@zerogravity.com.mx, chris@zerogravity.com.mx

*Corresponding author. Email mcneic3@mcmaster.ca

HIGHLIGHTS

- 4 years of µXRF data offers interpretation of paleo-rainfall from sediment cores
- Lithogenic elements (Fe, Ti, Sr) correlate to seasonal rainfall
- Biogenic elements (K, S, Si) have a seasonally lagged response to hurricanes
- Ti/K and Si/Ti are suitable proxies for paleo-rainfall in karst basins
- Intense rainfall can increase metal release from mangrove to the aquifer and coast

Key words: sediment traps, weathering proxies, Yucatan Peninsula, anchialine caves, µXRF core scanning, hurricanes, mangrove

ABSTRACT

Though the paleoclimate history of Mexico's Yucatan Peninsula has gained much attention as a topic of study over the past decades, hydrologically sealed lake basin records are not abundant as most basins are partially or fully connected to the regional aquifer. Sediments of cenotes (sinkholes) and coastal caves in the region present a new and unique archive to be investigated, though little is known about sedimentation in these systems. Whereas μXRF analyses of cores can achieve sub-annual resolution because of small analysis increments, short-period studies examining weathering inputs and rainfall have not yet been undertaken, hindering paleoenvironmental interpretations of lake and aquifer sediment records. This study examines the spatial and temporal relationship of cave sediment geochemistry in the anchialine cave system Yax Chen (Quintana Roo, Mexico). Sediment traps (n = 51) were placed at seventeen stations along the 2.7-km flooded cave system, which transitions from a mangrove-dominated to upland-forest terrain, with cenotes of variable size and frequency. Sediment traps were collected every 6 months from May 2013 - May 2017 along with rainfall and groundwater level data. There are distinct responses of lithogenic (Fe, Ti, Sr - limestone weathering) and biogenic-influenced (Si, K, S - phytoplankton and mangrove sediment) elemental proxies in the sediment traps associated with seasonal rainfall and hurricanes. Whereas lithogenic elements (TI/K) show a direct relationship to seasonal rainfall, sedimentation of biologically influenced (Si/Ti) elements exhibit a 6-12-month lagged response and showed correlation with large

rainfalls such as Hurricane Ingrid in 2013 and other tropical storms throughout the study period.

1. INTRODUCTION

Weathering proxies are commonly used for paleoenvironmental analysis of lake and ocean sediments, and often include measurements of potassium (K), iron (Fe) and titanium (Ti) (Haug et al., 2001; Kylander et al., 2011). Recent instrumental advances have now enabled measurement of these elements at high resolution, with more efficiency, using automated µXRF core scanners. Earlier studies used bulk sediment analyses (e.g. ICP-MS, XRF, etc.) of these elements and others (e.g. Ca and Sr) to understand changing weathering inputs and relationships with climate change (i.e. wet/dry), but these studies were of relatively low-resolution and thus only document large trends (Zhao and Zheng, 2015). A significant amount of research has been devoted to understanding rock weathering rates over geological timescales because of their importance in carbon cycling. Climate change and core studies often rely on this body of research to make inferences about changing environmental conditions (Gaillardet et al., 2018; Lo et al., 2017). The recent advent of µXRF core scanners has enabled development of an increased number of high-resolution weathering records that reveal smaller, annual to sub-annual trends in periodicity (e.g. Orme et al., 2016), however there is a lack of data to assess the sensitivity of these proxies to seasonal or spatial trends on a basin level.

In order to estimate the sensitivity of weathering proxies to seasonal changes, one can use previous studies such as those examining dissolved and suspended sediment loads of rivers and streams, and spatial patterning of surface sediments from lake or ocean basins (Dauvalter and Rognerud, 2001; Froger et al., 2018). Such studies, however, may not be applicable to certain regions, as they may not include elements of interest or record the necessary weather patterns (e.g. rainfall). Catchment geology may also be quite different from the location of interest. Further complications arise when comparing data generated by different analytical instrumentation (XRF, ICPMS, etc.) and sampling strategies (e.g. dissolved and suspended load, surface sediment samples). µXRF core scanning measures bulk sediment including porewater and sediment, which limits comparisons with data acquired earlier (e.g. Gregory et al., in press). Surface samples collected within the basin, along environmental gradients of interest (e.g. proximity to fluvial input) can be used, but surface samples are subject to variable time averaging and thus have limitations when examining short-term seasonal or weather-related trends (Gregory et al., 2017; Roy et al. 2018). Sediment-trap studies are more useful in this regard, but as sediment traps are more logistically intensive in terms of deployment and recovery, there are only a few studies to draw upon (Urban et al., 2004; Bischoff, Cummins and Shamp, 2005; Collins et al., 2015a).

Here we present four years of µXRF elemental data from sediment traps, analyzed using the Sequential Sample Reservoir (SSR), which can be directly compared with µXRF core records (Gregory et al., 2017). Sediment trap samples

were collected every ~ 6 months from Yax Chen, which is part of the Ox Bel Ha cave system in the Yucatan Peninsula, Mexico. Yax Chen is the location of an ongoing environmental monitoring project that began in 2011 to document aquifer hydrology and sedimentation (Collins et al., 2015a, 2015b; Coutino et al., 2017; Kovacs et al., 2017a). These data are important as they provide baseline information on the sensitivity and response of weathering and productivity proxies (Fe, Ti, K, Si) for paleohydrological assessment of cave sediment records (µXRF) on which there is little prior research, and also provide insights for other paleolimnological studies in karst terrains (Roy et al., 2018).

2. SITE BACKGROUND

2.1. YUCATAN KARST

The Yucatan Peninsula (Fig. 1) is a Cretaceous-Cenozoic karstified limestone platform over 350,000 km^2 in area, located in southeast Mexico and bordered by the Gulf of Mexico and the Caribbean Sea (Smart et al., 2006). The coastal Quaternary deposits are relatively flat, resulting in a low hydraulic gradient (10-15 cm/km) and flow towards the coast (Beddows, 2004). The limestone has a high net porosity, ranging from 14-23% that is both vertically and horizontally anisotropic (Smart et al., 2006; Beddows et al., 2007). The coastal systems have multiple-scale porosity that consist of matrix, fracture, and cave conduit flow, with the majority of flow (~99%) within the conduits (Beddows et al., 2004; Smart et al., 2006). The high porosity focuses percolation of rainwater to the subsurface, preventing its ponding on the surface and resulting in a relative scarcity of surficial

lakes and rivers in the coastal region. Multiple phases of dissolution associated with sea-level change have created extensive wet and dry cave conduits, sinkholes/karst windows (locally known as cenotes), and submarine vents that discharge meteoric water at various points along the coast (Back and Hanshaw, 1970, Beddows, 2004; Paytan et al., 2005; Smart et al., 2006). The conduits are generally aligned perpendicular to the coast and cause increased turbulent flow and transmissivity within the groundwater mass (Beddows, 2004; Bauer-Gottwein et al., 2011). The morphologies of the conduits are important controls on the distribution of groundwater characteristics throughout the region (Beddows, 2004; Smart et al., 2006). Though the majority of caves do not have substantial sediment accumulation, depending on vegetation cover and sinkhole size, some passages downstream of cenotes contain organic material from the open water where aquatic primary productivity occurs (Pohlman et al., 1997; Sànchez et al., 2002; Smith et al., 2002; Collins et al., 2015a). Compared to other regions of Mexico, the chemical composition of sediment archives from the Yucatan Peninsula has received comparatively little attention (Curtis et al., 1996; Hodell et al., 2005; Carillo-Bastos et al., 2010), though there are many studies that focus on other methods of paleoecological reconstruction.

2.2. YUCATAN AQUIFER AND YAX CHEN HYDROLOGY

Within the Yucatan subsurface, the Meteoric or fresh water mass (MeWM) (<1 ppt) lies atop a denser Marine water mass (MaWM) (>30 ppt). The two water masses are separated by a boundary of intermediate salinity (halocline/pycnocline)

that responds to wet/dry cycles, sea-level rise, tidal mixing and storms. Response to storms has recently been documented by salinity sensors within the Ox Bel Ha cave system and elsewhere (Coutino et al., 2017; Kovacs et al., 2017a; Brankovits et al., 2018). Because the Yucatan Peninsula lacks major surficial fresh water sources, the MeWM is the main source of water for the local population as well as millions of vacationers who visit the region each year. The Yucatan aquifer system is one of the most extensive transboundary anchialine aquifers in the world, with 165,000 km^2 covering the Yucatan Peninsula regions of Mexico, Guatemala and Belize (Bauer-Gottwein et al., 2011). Decades of widespread tourism focused on the coasts have created long-term logistical concerns for wastewater and groundwater management, which will be a future issue because of the high sensitivity of the karst subsurface and unconfined aquifer, combined with increasing development (Molina et al., 2001; Escolero, 2002; Beddows 2004; Bauer-Gottwein et al., 2011).

Because the MeWM is rain-derived, it has low salinity, dissolved solids, and ions (Beddows et al., 2004; Stoessell and Coke, 2006). Specific Electrical Conductivity (SEC) of the MeWM is low (<2.5 mS/cm) and decreases moving inland as the influence of coastal mixing declines (Beddows, 2004). Total Dissolved Solids (TDS) and ion concentrations are generally low as well, other than in areas where there is carbonate dissolution, marine water intrusion, or concentration from evaporation (Smith et al., 2002; Beddows et al., 2004; Stoessell and Coke, 2006). Significant departures from the low SEC are generally a consequence of

environmental factors such as concentration by evaporation, saline intrusion, dissolution, and changes in productivity) (Perry et al., 2002; Beddows et al., 2004; Stoessell and Coke, 2006).

Groundwater flow in the Yucatan aquifer is decoupled, with the cooler MeWM (~25°C) and warmer MaWM (~27°C) moving in opposite directions (Beddows, 2004; Stoessell and Coke, 2006). The MeWM typically flows towards the coast at a velocity of approximately ~ 2.32 ± 5.21 cm/s and has been measured specifically in Ox Bel Ha at ~ 8-10 cm/s and increasing to 25-30 cm/s during large rainfall events (Beddows, 2004; Brankovits et al., 2018). The MaWM flows inland at a much slower rate of approximately 0.86 ± 0.52 cm/s (Beddows, 2004). There are also observations of saline intrusion inland during drought, when the regional hydraulic head is not forceful enough to create outflow from the submarine groundwater vents (Parra et al., 2016). Water table heights in the Yucatan Peninsula can also be controlled by seasonal trends in rainfall (Marin et al., 1989; Collins et al., 2015a; Kovacs et al., 2017a). Water table data recorded in the region of Tulum show broad variations in height from tidal movement, dryness, and storm-induced rainfall (Collins et al., 2015a; Coutino et al., 2017; Kovacs et al 2017a; Kovacs et al., 2018). Some recharge masses, such as that seen during the 2013 hurricane season, are so large that they periodically raise the water table on the order of meters for a number of days (Marin et al., 1989; Collins et al., 2015a; Kovacs et al., 2017a). For example, the passing of Hurricane Ingrid in 2013 and Tropical Storm Hanna in 2014 resulted in increases in water table height (~1m),

which lasted days to weeks after the event, as excess rainwater slowly discharged at the coast (Collins et al., 2015a; Coutino et al., 2017; Kovacs et al., 2017a). During rainfalls, increased flow in the fresh water mass (FWM) causes marine water entrainment at the halocline and increases FWM salinity as it moves towards the coast (1-2 ppt) (Escolero et al., 2002; Coutino et al., 2017; Kovacs et al., 2017; Brankovits et al., 2018).

2.3. YUCATAN CLIMATE

The Yucatan Peninsula has a warm, dry, evaporation-dominated climate (Metcalfe et al., 2000). Seasonal variation in rainfall is prominent and is primarily controlled by the north or southward position of the Inter Tropical Convergence Zone (ITCZ) (Magaña et al., 1999). Average annual rainfall across the Yucatan Peninsula ranges from 550-1500 mm/y, though values from single events have totaled from 700 mm (Wilma, 2005) to over 1000 mm (Ingrid, 2013) associated with the passing of large storms and hurricanes (Bauer-Gottwein, 2011; Farfan et al., 2014; Collins et al., 2015a; Coutino et al., 2017; Kovacs et al., 2017a). There is a notable east-west rainfall gradient driven by higher rainfall along the Caribbean coast of the peninsula (>1500 mm/y) (Neuman and Rahbek, 2007). Localized storms can cause variability in the spatial patterning of rainfall, and can deliver up to 80% of annual rainfall during the summer season (González-Herrera et al., 2002). Though the Yucatan Peninsula is generally warm and dry from November to May, occasional winter storms and strong seasonal winds may occur from November to February. A “double-peak” rainy season begins in June and

continues until the hurricane season occurs in September-November (Magaña et al., 1999; Boose et al., 2003; Brown et al., 2013; Farfan et al., 2014).

2.4. YAX CHEN CAVE SYSTEM

Yax Chen is a 2.7-km-long coastal subsection of the longer Ox Bel Ha cave system (270 km; Quintana Roo Speleological Survey, 2019), which is ~ 9 km south of Tulum. Research on this cave system was conducted by Collins et al (2015a, b), who investigated the onset of sedimentation, as well as external controls on sediment flux and composition within the cave passages (Fig. 2). The cave network trends northwest-southeast and there are 7 large cenotes (1600-9000 m^2) along the Yax Chen portion of the cave system, which are surrounded by fringing and dwarf mangrove (*Rhizophora mangle, Avicennia germinans, Laguncularia racemosa*) in the downstream section, and forest in the upstream reaches (Meacham, 2012; Collins et al., 2015a). The downstream vs upstream classification used for this system is based on a transition from large, mangrove-dominated cenotes in the coastal reaches, to the relatively smaller, forest-dominated inland zone, which occurs ~ 100 m upstream of cenote ISOD 2 (Fig 2). The main passage of Yax Chen is generally shallow, with a depth of 10 -11 m upstream of L-Shaped cenote and ~ 8 m in the downstream section. The water column within Yax Chen is stepped, with haloclines defining each water mass. Here, we define the MeWM as the upper portion (0-11 m depth) which has a salinity of ~ 6 ppt, and the MaWM includes an intermediate portion at ~ 17 ppt (11-15 m depth) and the basal marine

water that intrudes from the coast (>15 m depth ~ 35 ppt; Kovacs et al., 2017a). Water level in the system responds to tidal fluctuations, drought periods and seasonal rainfall, including extreme events such as Hurricane Ingrid (2013), which caused the water table to rise by ~ 0.75 m in Yax Chen. (Coutino et al., 2017; Kovacs et al., 2017a).

The Yax Chen cave system has a substantial accumulation of organic sediment, and sedimentation within the cave is primarily controlled by productivity within adjacent cenotes and the presence/absence of mangrove (Collins et al., 2015a). The presence of large cenotes surrounded by mangrove contributes to higher bi-annual sedimentation rates in the downstream section of the cave following the rainy season (Collins et al., 2015a). Sediment flux in the upstream section of the cave (station 1 to 8) is significantly lower (0.014 mg/cm^2/day) than the downstream section (0.22 mg/cm^2/day) (Fig 2.). Large rainfalls can induce instantaneous physico-chemical changes and increase flow within the conduits, but significant impact on sedimentation is lagged by ~ 6-12 months (Collins et al., 2015a). As noted in Collins et al. (2015a), however, increased flow during high rainfalls does not appear to cause significant resuspension of sediment, as no obvious scour marks were observed in the sediment after the large influx of water during Hurricane Ingrid.

3. METHODS

3.1. SEDIMENT TRAP PLACEMENT AND COLLECTION

Sediment traps have been used in lakes, estuaries and oceans to determine biological and chemical fluxes in aqueous environments for over 100 years (Gardner, 1980a). The goal of most sediment trap studies is to use the bulk organic and elemental data to understand nutrient cycling and sediment composition within the water column (Gardner, 1980; Urban et al., 2004). There are, however, only a few studies for which sediment traps were used for paleolimnological applications (Teranes & Bernasconi, 2000; Rioual et al., 2009; Collins et al., 2015a, b). In 2011, 51 traps were placed at 17 stations along the Yax Chen cave system to identify downstream effects of cenote size and vegetation cover (see Collins 2015a for original study). Placement was intended to document the controls of cenote size and vegetation on downstream sedimentation. The collection periods were set up to capture the majority of the seasonal rainfall and drought periods, and the sediment traps were switched *in situ* every time they were collected, to ensure continuous data recovery. Traps were constructed from PVC tubing following the design and dimensions of Gardner (1980 a,b). At each station, traps were placed in groups of three, spanning the width of the cave, and were located just above (~30 cm) the sediment-water interface (Fig. 3). See Collins et al. (2015a) for further details on the construction, placement and collection of the sediment traps. The traps were collected bi-annually by cave-trained SCUBA divers every May and

December since May 2012. Data spanning the 2013-2017 collection period are included in this analysis.

3.2 RAINFALL AND WATER LEVEL DATA

Daily weather data (2013-2017) were collected from the Cozumel weather station as in Kovacs et al. (2017a). Water level data (± 1.3 cm) were collected at 30-minute intervals with a ReefNet Sensus Ultra dive logger fixed in the MeWM near station 7, and were corrected for atmospheric barometric change using a surface-deployed sensor (Kovacs et al., 2017) (Fig. 2). Depths (m) and rainfall (mm) are shown as departures from mean water level over the analysis period.

3.3 SEDIMENT FLUX DATA

Bi-annual sediment flux (mg/cm^2/day) for each station was measured to document the influence of seasonal rainfall on sedimentation within Yax Chen, using the methods described in Collins et al. (2015a). Sediment flux data from May 2011 to May 2014 are shown in Collins et al. (2015a), and here we include new data from June 2014 to May 2016.

4. µXRF CORE SCANNING

Sediment traps were recovered every six months (June - November, December – May) for 4 years (2013-2017) and the water was filtered with a 20-µm paper filter to concentrate the sediment. The sediment traps contained mostly organic matter. Sediment from the three traps at each station was homogenized and packed into a ~ 1-cm^3 cuvette. Samples were loaded in a Sequential Sediment Reservoir (SSR) using a spatula, while evenly compacting the sediment to minimize potential matrix

effects (Gregory et al, 2018). Each sequential cuvette was analyzed using the Cr heavy element (Cr-HE) X-ray source (30 Kv, 28 mA, exp. time = 15 s, step-size 1 mm) on a Cox ITRAX µXRF-CS at the McMaster University Core Scanning Facility (MUCS). Ten measurements from the central portion of each sample reservoir were averaged and the standard deviation was calculated to document variability. Data are shown as total counts over the 15 sec integration time.

A subset of elements that are commonly used as weathering/lithological or biological productivity proxies were used in the PCA analysis using R's default function prcomp(). Each entry was normalised using the default scaling function and the dataset was reduced to elements of interest (Mg, Al, Si, K, Ca, S, Ti, V, Fe, Ni, Cu, Zn, Sr) highlighted in Rothwell and Croudace (2014). Consideration of elemental abundance (i.e. high counts) relative to the variability of the measurements (standard deviation) was used to further narrow the elements of interest to Si, K, Ca, S, Fe, and Sr.

4. RESULTS

4.1 RAINFALL AND GROUNDWATER LEVEL

Over the four years of the study period (June 2013 to May 2017) there were different amounts of rainfall (Fig. 4). As described in Kovacs et al. (2017a), there is a strong positive relationship between Cozumel rainfall and groundwater level in Yax Chen ($r = 0.79$, $p(a) < 0.01$, Fig. 9). In terms of seasonal patterning, the 2013 wet season had high rainfall, though it occurred late in the season (Fig. 5), and included several large events such as Hurricane Ingrid (Beven, 2004). Since the

accumulation of sediment is more related to seasonal (monthly) ecosystem dynamics, it is expected that small rainfalls and dryness immediately preceding data collection have little to no impact on the results. Relatively dry conditions followed in 2014 and 2015, with a limited wet season characterized by several large events (Tropical Storms Dolly and Hannah). The 2015 wet season had frequent smaller rainfalls, but also several large events that peaked in October-November, and extended into 2016 (March), which was unusual compared to the other years. The 2016 wet season, like that of 2014, was short and did not have any large rainfalls (Fig. 5). As will be discussed, there is generally good correspondence between the sediment trap collection periods and the wet/dry seasons, though there are some deviations from that likely have to do with individual characteristics of each cenote (i.e. size, vegetation cover).

4.2 SEDIMENT LITHOLOGY

Trap samples consisted of organic matter (OM)-rich sediment (gyttja) and were sieved at 45 and 63 µm before being examined using an Olympus binocular microscope at 80x magnification. Components included abundant diatoms, opaline spicules (sponges) and OM flocs, and to a lesser degree, carbonate particles of calcite and tan-coloured particles of limestone. Abundant diatoms are thought to be the main contributor to the Si observed within the sediments, and classification of diatom species within the cave system will be addressed with further study. Calcareous foraminifera (*Ammonia* spp., *Elphidium* spp.) and agglutinated taxa

(testate amoebae - *Centropyxis* spp.; foraminifera - *Trochammina* spp.) were also present. Though this study did not estimate OM content (LOI), Collins et al. (2015a) found that sediment upstream from the L-Shaped Cenote had much lower OM (18-20%) than downstream sediment (40-42%), a consequence of the smaller sizes of upstream cenote openings, coupled with reduced mangrove cover.

4.3 ELEMENT DISTRIBUTIONS

Overall, there were both temporal and spatial variations in the elemental distributions throughout the study period (Fig. 5). Elements of interest were further grouped into lithologically derived (Ti, Fe, Sr) and biologically influenced elements (K, S, Si). Although these have some overlap in terms of their origins and inputs, based on the PCA analysis and other aspects that will be discussed, these groupings of elements do seem to be largely sourced from either limestone/soil and OM or biological productivity (Fig. 6). Provenance and controls of elements will be discussed further in section 5.1. Over the four-year study period, the biologically influenced elements tended to be highly variable and almost binary in response, with a large increase from June 2014 to May 2015, specifically in Si and S (Fig. 5). There was less variability observed in lithogenic elements, though there was a distinctive decline in the June 2016 to May 2017 collection periods (n = 2), following the pattern of reduced rainfall (Fig. 5). The crossplots in Fig. 7 indicate that biogenic (K, S, Si) and lithogenic (Ti, Fe, Sr) elements all have strong positive relationships, with K and S exhibiting bimodal relationships that may have to do with influences

on sediment caused by organic matter accumulation upstream vs downstream. Upstream cenotes without much mangrove cover have less potential for nutrients to enter the water source and therefore have less diatom growth in them, resulting in less Si accumulation.

In Figure 7, K correlates strongly with S ($r = 0.81$. $p(a) < 0.01$), which is a known indicator of organic matter and organic matter decay. Ca generally has poor correlations (except with Sr, $r = 0.61$, $p(a) < 0.01$, Fig. 7), and likely comes from both lithological and biological sources (e.g. limestone pieces, shells) in the sediment. The PCA plot (Fig. 6) shows distinct groupings in the elements of interest (Mg, Al, Si, K, Ca, S, Ti, V, Fe, Ni, Cu, Zn, Sr), with smaller groupings of lithogenic (Ti, Fe, Sr), and biogenically influenced clusters (K, S, Si, sediment flux). Distance upstream and depth of station are both orthogonal to sediment flux (Fig. 6).

Rainfall and water level in Yax Chen correspond very well to sediment flux (Kovacs et al., 2017a, Collins et al., 2015), though comparison of elements with rainfall show different relationships (Fig. 9). Generally, the biogenic elements are poorly correlated to rainfall, however this is likely a consequence of time lags associated with biological growth that complicate the temporal relationship (discussed further in section 5.3). This inverse relationship between rainfall and sediment flux was shown in Collins et al. (2015a), and was attributed to the lagged response of sedimentation to extreme rainfalls as a result of delayed drainage and high water tables. Individual elements show little relationship to rainfall, except for Ti ($r = 0.52$, $p(a) < 0.05$ overall, $r = 0.60$, $p(a) < 0.05$ for station 14) and S ($r = -0.62$,

$p(a) < 0.05$). A similar trend was found in a range of Yucatan sediments by Roy et al. (2018), who suggested that elemental proxies for rainfall in the region should be ratioed with Ca rather than used individually. Upstream or downstream location and timing of rainfall seem to have an impact on the overall correlation between rainfall and element counts. Small variations in parent lithology may also slightly influence element values in the trap sediment, though this is likely negligible as the study area covers a short distance (2.7 km). These factors probably account for some poor correlations, as overall trends with rainfall seem predictable and individual locations seem to have slightly better relationships (e.g. Ti for station 14; Fig. 5, 9).

5. DISCUSSION

5.1. SOURCE AND CONTROLS OF WEATHERING PRODUCT AND NUTRIENTS

As mentioned in section 2.1, the Yucatan Peninsula is comprised primarily of karstified calcium carbonate ($CaCO_3$), i.e. limestone. Dissolution of the limestone rock results in the accumulation of thin and patchy fine-grained soils (Leptosols, Regosols, Vertisols) (Bautista et al., 2011) that commonly contain elements such as Ca, Fe, Sr, K and Ti (Calvert and Pederson, 2007; Gaillardet et al., 2018; Roy et al., 2018) and little siliciclastic material (e.g. Si, Ti, Fe, K, and others). Based on surface samples from lakes, the calcium carbonate rock has a diluting effect that results in sediments that contain less K, Ti, and Fe than typical clastic terrains, and thus has been found to show a weak relationship with broad patterns of rainfall

(Roy et al., 2018). Soils of the Yucatan Peninsula also often include localized deposits of fine-grained *terra rossa* with abundant Al, Si and Fe oxides (Cabadas et al., 2010; Bautista et al., 2011). In the limestone, Sr concentration is closely related to Ca, as Sr is included in aragonite, which is the mineral form of much of the biogenic carbonate in Tertiary limestones (Banner, 1995). Ti and Fe are commonly used individually and as ratios as lithological weathering proxies, though Ti is often preferred because it is not sensitive to changes in redox conditions, which is an important consideration for sources of Fe from the mangrove sediment (Haug et al., 2001; Davies et al., 2004; Machlachlan et al., 2015). Fe and Ti, however, are highly correlated in our sediment trap results, suggesting that there are only minor redox effects within the cave sediment itself.

K/Ti is commonly used as a proxy for weathering rates, with K as a proxy for soil weathering (clays) and Ti as a clastic sediment indicator. In this study, however, we found the inverse relationship to be stronger, where Ti/K is strongly correlated with rainfall because there is little clay observed in the sediment and source soils are clay-poor (Revel et al., 2017; Roy et al., 2018). Ti is likely derived from a limestone weathering and present as oxyhydroxides like Fe, which are then flushed into the cenotes from flooded land areas and the mangrove with rainfall. K, which has a limestone source, but is also a biologically influenced contribution from the mangrove and primary productivity in the cenotes, has a slightly time-lagged response and increases during dry periods when Ti is lower, thus emphasizing the response to rainfall and making the ratio more sensitive (Ti/K $r = 0.759$, $p(a) < 0.05$

Fig. 11). Other studies in the region have indicated that individual elements tend to be variable within sites, which can complicate the relationship with rainfall (Roy et al., 2018). For example, Roy et al. (2018) identified K/Ca as a more reliable recorder of rainfall because of the regional carbonate geology. However, because of the abundance of calcium carbonate shell material in the cenotes and poor correspondence of Ca with other elements, this ratio was not useful in identifying trends in Yax Chen, as Ca seems to be also affected by variable benthic productivity (i.e. foraminifera, gastropod shell). Relating the geochemistry of surface samples with long-term spatial averages of rainfall can be useful, but does not allow for examination of the relationship between geochemistry and the intra-annual pattern of rainfall (seasonal quantity and rates), which seems to be important, as we show here (Roy et al., 2018).

Biogenic silica (SiO_2) is an indicator of diatom abundance in lacustrine sediment, and the contribution from siliciclastic sediment can often be identified effectively with Si/Ti or Si/Al (Johnson et al., 2011; Liu et al., 2013; Barron et al., 2015). In our data, K, S and sediment flux show similar responses to Si, indicating a shared biological influence, since the PCA and cross plots show S and Si are well correlated to K ($r = 0.81$, $p(a) = < 0.01$, and $r = 0.63$, $p(a) = < 0.01$ Fig. 6, 7). During decomposition of mangrove leaf litter, the greatest total loss is for K, with up to 95% lost within two weeks of inundation (Steinke, Holland and Singh, 1993; Kathiresan, and Bingham, 2001). K and S are associated with nutrient-rich particulate organic matter (POM) derived from mangrove peat (Clark et al., 1998;

Kathiresan, and Bingham, 2001; Thompson et al., 2006). S is closely linked to OM and organic-rich muds, and is a product of reducing and oxidizing conditions that occur when mangrove is waterlogged and then subsequently dried (Clark et al., 1998; Croudace, Rindby and Rothwell, 2006; Bayen, 2012). It is associated with the biomass of marine plants and bacterial reduction, and can be bound within organic-rich muds (Ivanov, 1981; Croudace and Rothwell, 2015). Most mangrove sediment contains high amounts of reduced inorganic S in the form of pyrite (FeS_2) and elemental S (Kristensen et al., 2008).

In the case of coastal Yucatan Peninsula, Si/Ti is an excellent candidate for estimating biogenic silica, with higher ratios indicating increased amounts of biogenic silica vs clastic or oxyhydroxide inputs (Brown, 2015). This ratio works well as a productivity proxy because siliciclastics and clays within the regional sediment are scarce, and the majority of Si is attributable to diatom and other phytoplankton productivity (Sánchez et al., 2002). The sediments (composed of biogenic-influenced and lithological elements) are released after the high water level floods the soils and dry areas surrounding the mangrove, which are then flushed through adjacent cenotes, cracks and fissures as water level drops after substantial rainfalls. This sediment introduces a load of nutrients from mangrove areas, possibly through a change in redox conditions with the flushing into the sunlit cenotes, where primary productivity occurs and is then swept into the cave. This is discussed further in section 5.3.

5.2. SPATIAL AND TEMPORAL VARIATION IN ELEMENT TRENDS

There are site-specific differences in element concentrations related to cenote characteristics such as vegetation cover (mangrove vs. forest), position upstream or downstream of L-Shaped Cenote, and area of open water. As described in Collins et al. (2015a), there is a strong relationship between site location and sediment flux, with higher values in downstream locations (station 5 to 17) vs upstream, which is likely attributable to the presence of mangrove and larger cenotes at downstream sites. This also corresponds with a change in depth and water density (MeWM vs MaWM), which could play a role in concentrating phytoplankton and heavier elements within the less dense fresh water in the shallower downstream sections. In some instances, element distributions (K, S, Si) display relationships with distance upstream, though none are particularly strong, and there is statistical overlap in their mean values, suggesting that distance and depth both influence distribution of elements (Fig. 8). This sounds contradictory

Increases in the lithogenic proxy Ti/K are observed in all sediment traps from the 2013 and 2015 wet season collection period associated with the passing of Hurricane Ingrid in September 2013, and a prolonged summer 2015 wet season (Fig. 10). Though there was no instantaneous reaction of biogenic proxy Si/Ti to the 2013 hurricane, there was a distinct lag in response within the next collection periods (June-November 2014), which complicates the correlation between Si/Ti and water level (Fig. 11). The Si, K and S proxies all show a lagged response to

both low and high rainfall rates (Fig. 5), so it is likely that a combination of high rainfall followed by dry conditions is required to elicit a detectable response. During high rainfalls, MeWM flow is higher and there is limited residence time for the nutrients to be used by phytoplankton in the sunlit cenotes, whereas during low rainfalls flow is correspondingly lower, thus allowing phytoplankton blooms (Brankovits, 2018). This is in line with results from multiple studies of the biogeochemistry and biology of cenotes in the Yucatan Peninsula, which indicate that the highest number of phytoplankton and chlorophycean species are found in cenotes in the winter season (Schmitter-Soto et al., 2002). The seasonal delay likely represents the time it takes for the water table to transfer nutrients into the open water, and for primary productivity to increase to a detectable amount in the summer season following Hurricane Ingrid (further discussed in section 5.3). These findings also reflect those of Collins et al. (2015a), who noted higher sedimentation rates in the 6 months following the 2013 rainy season (0.2 vs. 0.5 $mg/cm^2/day$), and higher organic matter in downstream traps. Seasonality in sedimentation was also observed in a hyper-eutrophic lake in Florida after the occurrence of hurricanes (James et al., 2008; Beaver et al., 2013). In the months after Hurricanes Frances and Jean (September 2004), percent biovolume of diatoms in Lake Okeechobee, Florida increased to over 60% in the nearshore region and over 80% in the offshore region (James et al., 2008; Beaver et al., 2013).

The large peak in rainfall that occurred during the 2015 summer wet season was not associated with a known hurricane or tropical storm, but a series of smaller rainfalls over a longer period, however it further demonstrates the immediate response of lithogenic proxy Ti/K and the prominent lag in sediment flux and biogenic proxy Si/Ti (Fig. 10). The lowest element counts overall coincided with the prolonged dry period from December 2015-May 2017 (Fig. 5), associated with reduced weathering and runoff. This is observed more dramatically in Ti/K and the upstream stations (Fig. 10), indicating mangrove peat may have more of an influence on sedimentation in the downstream sections during drier periods. Although Ti/K shows a coincident response to large rainfall events such as the passing of Hurricane Ingrid (2013) and the summer 2015 wet season, the biological proxy Si/Ti shows a significantly higher and seasonally lagged response to these events (Fig. 10). With this in mind, Si/Ti seems to be a better recorder of extreme events such as hurricanes, whereas Ti/K is more sensitive to gradual changes in rainfall. As discussed, deployment of sediment traps is very time consuming and our study offered a unique opportunity to examine weather-related effects in greater detail.

5.3 CONCEPTUAL MODEL OF SEDIMENTATION

We hypothesize that changes in Si abundance between stations and over time was a product of biological growth within cenote water. Because the caves themselves are light-limited, the only way for biogenic Si and particulate organic

matter (POM) to enter the sediment traps is through connection with sunlit cenotes (Pohlman, 1997; Smith et al., 2002; Schmitter-Soto et al., 2002). Furthermore, it is the mangrove peat cover adjacent to certain cenotes that causes higher sediment flux rates in the downstream reaches of the system (Collins et al., 2015a) (Fig. 12b). This is because peat acts as an aquitard that reduces permeability to the subsurface, which would otherwise be rapid, as is the case in forest terrain, which has thin soil cover and exposed karst (Fig. 12d). When a large amount of rainwater enters the system (Fig 12a, c), the high-flow MeWM has little to no residence time in the sunlit cenotes, so that nutrients cannot be immediately used by diatoms and other phytoplankton to produce large blooms. The reduction in permeability caused by peat occlusion of the karst causes ponding of water in the mangrove area, which allows the water to warm and leach nutrients (such as K, N, P) from the surrounding leaf litter (Steinke, Holland and Singh, 1993; Li & Ye, 2014), which then flush into the cenotes when water level drops after the rainy season and into the dry season.

When drainage begins and the water table height is returned to baseline (or below), the warm ponded water is released into the sunlit cenotes, cracks and fissures in the karst (Fig. 12c; Coutino et al., submitted). Primary productivity, which yields biogenic silica (diatom SiO_2), is then enhanced in the open waters, which influences sedimentation in downstream areas months after the original rainfall event.

5.4 CONSIDERATIONS FOR CORE LOCATIONS

This study demonstrates that cave sediment geochemistry from Yax Chen reflects seasonal hydrological conditions associated with intense rainfall events and prolonged dry periods. More importantly, it highlights the spatial variability of the cave system as a sensitive recorder of paleoclimate, and provides guiding information for future coring locations for reconstructing paleohydrology. Future considerations for choosing coring locations for the best time resolution include: locations with a high sedimentation rate; areas of the sediment surface above the halocline, as lighter material may be preferentially concentrated in this range (e.g. Schmitter-Soto et al., 2002); and it is suggested that cores taken downstream of L-Shaped Cenote, or generally downstream of a large cenote, will have the best temporal records, and will also capture the greatest range of variability in the elemental proxies with shifts in rainfall. The time lag of 6 to 12 months in some of the proxies (Si, K, S) is negligible for long-term core studies, but is useful for understanding and comparing long-term change from location to location.

Good potential rainfall proxies include Ti/K, which is sensitive throughout the cave system to total precipitation, and Si/Ti which is indicative of extreme rainfalls. Site-specific variations may play a role in elemental response, but the pattern of change should be reproducible. Though the correlation between Si/Ti and rainfall is not as robust as Ti/K, this is likely influenced by a variable lag in response that has to do with other controls of primary productivity (such as rainfall/drought timing,

solar heating, cenote size, etc.; Fig. 10, 11). Nonetheless, the data shows clear impacts of large rainfall events (e.g., Hurricane Ingrid, 2015 wet season; Fig 10).

5.5 IMPLICATIONS FOR FUTURE MANGROVE-CENOTE INTERACTIONS

This study provided information on how the geochemistry of the cenote-cave environments in the Yax Chen system respond to intense wet and dry events, and how this can be identified in the paleo-record. Changing climate and warming ocean temperatures are expected to exacerbate hurricane intensity and frequency, leading to more climate uncertainty, including more frequent and powerful storms and droughts that will increase the vulnerability of the aquifer to both natural and anthropogenic perturbations (Boose et al., 2003; Bauer-Gottwein et al., 2011; Farfan et al., 2014). This is becoming a more pressing issue as mangrove forests become one of the most threatened tropical ecosystems (Bayen, 2012; Torrescano-Valle & Islebe, 2012). Redox potential of the mangrove sediment is controlled by seasonal waterlogging (Marchand, Allanbach and Lallier-Verges, 2011; Bayen, 2012), and provides an important control on the accumulation of many trace metals (Clark et al., 1998). Mangrove peat is naturally a heavy metal sink because mangrove roots baffle sediment and accumulate fine-grained sulphidic organic matter and heavy metals under anoxic conditions, however they become more oxic during flushing events, and as we showed here, the peat could become a source of metals released to the aquifer and shallow coastal ocean and reef systems (Clark et al., 1998; Defew et al., 2005; Marchand, Allanbach and Lallier-Verges, 2011). There are also substantial amounts of P in mangrove

environments, which have the potential to be mobilized into oligotrophic environments during large storms and cause harmful algal blooms at the coast (Hernández-Terrones et al., 2011). It is likely that when large storms flood and waterlog the mangrove, leaching from decomposition is enhanced, which introduces more nutrients and heavy metals into the water, which is then drained into the open water during the dry season. Human activity is quickly increasing in areas adjacent to mangrove-covered cenotes, which may increase the concentration of nitrates, sulphates, sulphide-bound metals and hydrocarbons in mangrove peat (Harbison, 1989; Ellison & Farnsworth, 1996; Defew et al., 2005; Kalnejais et al., 2011; Bayen, 2012). This is important to consider going forward because groundwater management problems in many of these regions are related to insuring long-term water quality in the face of impacts from development (Molina et al., 2001; Escolero et al., 2002; Hausman, 2009). Increases in coastal development, coupled with the potential for higher magnitude and frequency of hurricanes may result in a detrimental impact to the local coastal ecosystems in the future (Torrescano-Valle & Islebe, 2012). This has already been observed in the coastal region of the northern Yucatan Peninsula (Escolero et al., 2002; Hernandez-Terrones et al., 2011), and in some pockets of the Maya Riviera (Baker et al., 2012).

6. CONCLUSIONS

Broad seasonal trends (wet/dry) and large-magnitude events can be identified in the sediment geochemistry of Yax Chen. Though individual elements averaged

throughout the cave system did not show strong correlations with hydroclimate (except for Ti, which showed moderate relationships), in general, lithologically derived elements (Ti, Fe, Sr) fit the broad patterning of rainfall. Biologically influenced elements (K, S, Si) also showed a rainfall response, reflecting primary productivity and mangrove-derived sediment, but exhibited a lagged response to hurricanes and tropical storms. The ratio Ti/K is the most robust proxy for rainfall and shows a strong relation, whereas Si/Ti has a lagged response, but is a good indicator of large rainfall events, i.e. hurricanes and tropical storms.

This study shows how sediment geochemistry and μXRF core scanning of cave sediments can provide paleoclimate records of rainfall, and also has potential applications for lake sediments, as it shows overall elemental responses to rainfall. Our high-temporal-resolution study shows that the rate and duration of rainfall plays a role in sedimentation, and that elements display variable responses, with lags in their response timing.

ACKNOWLEDGEMENTS

The authors gratefully acknowledge the support of The Mexican Cave Exploration Project (MCEP), CINDAQ, and the staff at Zero Gravity for dive support and logistics. This research was possible through the MCEP Science Week volunteers from around the world. Special thanks go to Jan Duikt, Peter Gaertner and Manuela Schoch for repeated support each year and photography. Natural Sciences and Engineering Research Council (NSERC) Discovery Grants (EGR - 2015-057250) and the Canada Foundation for Innovation John R. Evans Leaders Fund (CFI-JELF grant 105-04523).

REFERENCES

1. Back, W., & Hanshaw, B. B. (1970). Comparison of chemical hydrogeology of the carbonate peninsulas of Florida and Yucatan. Journal of Hydrology, 10(4), 330-368.
2. Bauer-Gottwein, P., Gondwe, B. R., Charvet, G., Marín, L. E., Rebolledo-Vieyra, M., & Merediz-Alonso, G. (2011). Review: The Yucatán Peninsula karst aquifer, Mexico. Hydrogeology Journal, 19(3), 507-524.
3. Bautista, F., Palacio-Aponte, G., Quintana, P., & Zinck, J. A. (2011). Spatial distribution and development of soils in tropical karst areas from the Peninsula of Yucatan, Mexico. Geomorphology, 135(3-4), 308-321.
4. Bayen, S. (2012). Occurrence, bioavailability and toxic effects of trace metals and organic contaminants in mangrove ecosystems: a review. Environment international, 48, 84-101
5. Banner, J. L. (1995). Application of the trace element and isotope geochemistry of strontium to studies of carbonate diagenesis. Sedimentology, 42(5), 805-824.
6. Beaver, J. R., Casamatta, D. A., East, T. L., Havens, K. E., Rodusky, A. J., James, R. T., ... & Buccier, K. M. (2013). Extreme weather events influence the phytoplankton community structure in a large lowland subtropical lake (Lake Okeechobee, Florida, USA). Hydrobiologia, 709(1), 213-226.

7. Beddows P. A (2004) Groundwater hydrology of a coastal Conduit carbonate aquifer: Caribbean Coast of the Yucatán Peninsula, México, PhD Thesis, University of Bristol, UK
8. Beddows, P. A., Smart, P. L., Whitaker, F. F., and Smith, S. L., 2007, Decoupled fresh saline groundwater circulation of a coastal carbonate aquifer: Spatial patterns of temperature and specific electrical conductivity: Journal of Hydrology, v. 346, p.18-32.
9. Beven, J. L. I., 2014, Hurricane Ingrid, National Hurricane Centre Tropical Cyclone Report, Volume 2014, National Weather Service.
10. Bischoff, J. L., Cummins, K., & Shamp, D. D. (2005). Geochemistry of sediments in cores and sediment traps from Bear Lake, Utah and Idaho (No. 2005-1215).
11. Boose, E. R., D.R. Foster, A. Barker Plotkin, and B. Hall, 2003, Geographical and historical variation in hurricanes across the Yucatan Peninsula, in Gomez-Pompa, A., M.F. Allen, S. F., and Jimenez-Osornio, J. J., eds., Lowland Maya Area:Three Millennia at the Human-Wildland Interface: New York, Haworth Press, p.495-516.
12. Brankovits, D., Pohlman., J.W., Ganju, N.K., Iliffe., T.M., Lowell, N., Roth, E., Sylva, Emmert, Lapham (2018). Hydrologic controls of methane dynamics in karst subterranean estuaries
13. Brown, Erik. (2015). Estimation of Biogenic Silica Concentrations Using Scanning XRF: Insights from Studies of Lake Malawi Sediments. 10.1007/978-94-017-9849-5_9.
14. Brown, A. L., Reinhardt, E. G., van Hengstum, P. J., & Pilarczyk, J. E. (2013). A coastal Yucatan sinkhole records intense hurricane events. Journal of Coastal Research, 30(2), 418-428
15. Cabadas, H. V., Solleiro, E., Sedov, S., Pi, T., & Alcalá, J. R. (2010). The complex genesis of red soils in Peninsula de Yucatan, Mexico: mineralogical, micromorphological and geochemical proxies. Eurasian soil science, 43(13), 1439-1457.
16. Calvert SE, Pedersen TF (2007) Elemental proxies for palaeoclimatic and palaeoceanographic variability in marine sediments: interpretation and application. In: Hillaire-Marcel C, De Vernal A (eds) Proxies in Late Cenozoic Paleoceanography, Dev Mar Geol, Elsevier, pp 567–644
17. Clark, M. W., McConchie, D., Lewis, D. W., & Saenger, P. (1998). Redox stratification and heavy metal partitioning in Avicennia-dominated mangrove sediments: a geochemical model. Chemical Geology, 149(3-4), 147-171.
18. Collins, S.V., Reinhardt, E.G., Werner, C.L., Le Maillot, C., Devos, F., Meacham, S.S., (2015a). Regional response of the coastal aquifer to Hurricane Ingrid and sedimentation flux in the Yax Chen cave system (Ox

Bel Ha) Yucatan, Mexico. Palaeogeograp. Palaeoclimatol. Palaeoecol. 438, 226–238.
19. Collins, S. V., Reinhardt, E. G., Werner, C. L., Le Maillot, C., Devos, F., & Rissolo, D. (2015b). Late Holocene mangrove development and onset of sedimentation in the Yax Chen cave system (Ox Bel Ha) Yucatan, Mexico: Implications for using cave sediments as a sea-level indicator. Palaeogeography, Palaeoclimatology, Palaeoecology, 438, 124-134.
20. Coutino, A., Stastna, M., Kovacs, S., & Reinhardt, E. (2017). Hurricanes Ingrid and Manuel (2013) and their impact on the salinity of the Meteoric Water Mass, Quintana Roo, Mexico. Journal of Hydrology.
21. Coutino, A., Stastna, M., Reinhardt, E (submitted). Mangroves modulate the mixing response of the Yucatan Aquifer: observations and modelling. Journal of Hydrology.
22. Croudace, I. W., Rindby, A., & Rothwell, R. G. (2006). ITRAX: description and evaluation of a new multi-function X-ray core scanner. Geological Society, London, Special Publications, 267(1), 51-63.
23. Dauvalter, V., & Rognerud, S. (2001). Heavy metal pollution in sediments of the Pasvik River drainage. Chemosphere, 42(1), 9-18.
24. Davies SJ, Metcalfe SE, MacKenzie AB, Newton AJ, Endfield GH, Farmer JG (2004) Environmental changes in the Zirahuén basin, Michoacán, Mexico, during the last 1000 years. J Paleolimnol 31:77–98.doi:10.1023/B:JOPL.0000013284.21726.3d
25. Defew, L. H., Mair, J. M., & Guzman, H. M. (2005). An assessment of metal contamination in mangrove sediments and leaves from Punta Mala Bay, Pacific Panama. Marine Pollution Bulletin, 50(5), 547-552.
26. Ellison, A. M., & Farnsworth, E. J. (1996). Anthropogenic disturbance of Caribbean mangrove ecosystems: past impacts, present trends, and future predictions. Biotropica, 549-565.
27. Escolero, O. A., Marin, L. E., Steinich, B., Pacheco, A. J., Cabrera, S. A., & Alcocer, J. (2002). Development of a protection strategy of karst limestone aquifers: the Merida Yucatan, Mexico case study. Water Resources Management, 16(5), 351-367.
28. Farfán, L. M., D'Sa, E. J., Liu, K. B., & Rivera-Monroy, V. H. (2014). Tropical cyclone impacts on coastal regions: the case of the Yucatán and the Baja California Peninsulas, Mexico. Estuaries and coasts, 37(6), 1388-1402.
29. Froger, C., Ayrault, S., Evrard, O., Monvoisin, G., Bordier, L., Lefèvre, I., & Quantin, C. (2018). Tracing the sources of suspended sediment and particle-bound trace metal elements in an urban catchment coupling elemental and isotopic geochemistry, and fallout

radionuclides. Environmental Science and Pollution Research, 25(28), 28667-28681.
30. Gaillardet, J., Calmels, D., Romero-Mujalli, G., Zakharova, E., & Hartmann, J. (2018). Global climate control on carbonate weathering intensity. Chemical Geology.
31. Gardner, W. D., 1980a, Field Assessment of Sediment Traps: Journal of Marine Research, v. 38, no. 1, p. 41-52.-, 1980b, Sediment trap dynamics and calibration: A laboratory evaluation: Journal of Marine Research, v. 38, no. 1, p. 17-39.
32. Gregory, B. R., Reinhardt, E. G., Macumber, A. L., Nasser, N. A., Patterson, R. T., Kovacs, S. E., & Galloway, J. M. (2017). Sequential sample reservoirs for Itrax-XRF analysis of discrete samples. Journal of Paleolimnology, 57(3), 287-293.
33. Gregory, B.R., Patterson, R.T., Reinhardt, E.G., Galloway, J.M. and Roe, H.M. (2019). An evaluation of methodologies for calibrating Itrax X-ray fluorescence counts with ICP-MS concentration data for discrete sediment samples. Chemical Geology, In Press.
34. González-Herrera, R., Sánchez-y-Pinto, I., & Gamboa-Vargas, J. (2002). Groundwater-flow modeling in the Yucatan karstic aquifer, Mexico. Hydrogeology Journal, 10(5), 539-552.
35. Harbison, P. A. T. (1986). Mangrove muds—a sink and a source for trace metals. Marine Pollution Bulletin, 17(6), 246-250.
36. Haug, G. H., Hughen, K. A., Sigman, D. M., Peterson, L. C., & Röhl, U. (2001). Southward migration of the intertropical convergence zone through the Holocene. Science, 293(5533), 1304-1308.
37. Hausman, H. (2009). Responsible Development in Tulum, Mexico: Considering Water Quality and Subaqueous Cave Locations. Master of Environmental Management Thesis, Duke University.
38. Ivanov MV (1981). The global biogeochemical sulphur Cycle. In: Likens GE (ed) Some perspectives
39. of the major biogeochemical cycles SCOPE, pp 61–78
40. James, T. R., Chimney, M. J., Sharfstein, B., Engstrom, D. R., Schottler, S. P., East, T., & Jin, K. R. (2008). Hurricane effects on a shallow lake ecosystem, Lake Okeechobee, Florida (USA). Fundamental and Applied Limnology/Archiv für Hydrobiologie, 172(4), 273-287.
41. Johnson, T. C., Brown, E. T., & Shi, J. (2011). Biogenic silica deposition in Lake Malawi, East Africa over the past 150,000 years. Palaeogeography, Palaeoclimatology, Palaeoecology, 303(1), 103-109.
42. Kathiresan, K., & Bingham, B. L. (2001). Biology of mangroves and mangrove ecosystems.

43. Kalnejais, L. H., Martin, W. R., & Bothner, M. H. (2010). The release of dissolved nutrients and metals from coastal sediments due to resuspension. Marine Chemistry, 121(1-4), 224-235.
44. Kovacs, S. E., Reinhardt, E. G., Stastna, M., Coutino, A., Werner, C., Collins, S. V., & Le Maillot, C. (2017a). Hurricane Ingrid and Tropical Storm Hanna's effects on the salinity of the coastal aquifer, Quintana Roo, Mexico. Journal of Hydrology.
45. Kovacs, S. E., Reinhardt, E. G., Chatters, J. C., Rissolo, D., Schwarcz, H. P., Collins, S. V., & Erreguerena, P. L. (2018). Calcite raft geochemistry as a hydrological proxy for Holocene aquifer conditions in Hoyo Negro and Ich Balam (Sac Actun Cave System), Quintana Roo, Mexico. Quaternary Science Reviews, 175, 97-111.
46. Kylander, M. E., Ampel, L., Wohlfarth, B., & Veres, D. (2011). High-resolution X-ray fluorescence core scanning analysis of Les Echets (France) sedimentary sequence: new insights from chemical proxies. Journal of Quaternary Science, 26(1), 109-117.
47. Liu, X., Colman, S. M., Brown, E. T., Minor, E. C., & Li, H. (2013). Estimation of carbonate, total organic carbon, and biogenic silica content by FTIR and XRF techniques in lacustrine sediments. Journal of Paleolimnology, 50(3), 387-398.
48. Lo, F. L., Chen, H. F., & Fang, J. N. (2017). Discussion of suitable chemical weathering proxies in sediments by comparing the dissolution rates of minerals in different rocks. The Journal of Geology, 125(1), 83-99.
49. Magaña, V., Amador, J. A., & Medina, S. (1999). The midsummer drought over Mexico and Central America. Journal of Climate, 12(6), 1577-1588.
50. Marchand, C., Allenbach, M., & Lallier-Vergès, E. (2011). Relationships between heavy metals distribution and organic matter cycling in mangrove sediments (Conception Bay, New Caledonia). Geoderma, 160(3-4), 444-456.
51. Meacham, S. S., 2012, Using Landsat 5 TM Data to Identify and Map Areas of Mangrove in Tulum, Quintana Roo, Mexico [Masters of Science: University of New Hampshire, 105 p.
52. Metcalfe, S. E., O'Hara, S. L., Caballero, M., & Davies, S. J. (2000). Records of Late Pleistocene–Holocene climatic change in Mexico—a review. Quaternary Science Reviews, 19(7), 699-721.
53. Neuman, B. R., & Rahbek, M. L. (2007). Modeling the Groundwater Catchment of the Sian Ka'an Reserve, Quintana Roo. Association for Mexican Cave Studies.
54. Orme, L. C., Reinhardt, L., Jones, R. T., Charman, D. J., Croudace, I., Dawson, A., & Barkwith, A. (2016). Investigating the maximum resolution

of µXRF core scanners: A 1800 year storminess reconstruction from the Outer Hebrides, Scotland, UK. The Holocene, 26(2), 235-247.
55. Parra, S. M., Valle-Levinson, A., Mariño-Tapia, I., Enriquez, C., Candela, J., & Sheinbaum, J. (2016). Seasonal variability of saltwater intrusion at a point-source submarine groundwater discharge. Limnology and Oceanography, 61(4), 1245-1258.
56. Paytan, A., Shellenbarger, G. G., Street, J. H., Gonneea, M. E., Davis, K., Young, M. B., & Moore, W. S. (2006). Submarine groundwater discharge: an important source of new inorganic nitrogen to coral reef ecosystems. Limnology and Oceanography, 51(1), 343-348.
57. Perry, E., Paytan, A., Pedersen, B., & Velazquez-Oliman, G. (2009). Groundwater geochemistry of the Yucatan Peninsula, Mexico: constraints on stratigraphy and hydrogeology. Journal of Hydrology, 367(1), 27-40.
58. Pohlman, J. W., Iliffe, T. M., & Cifuentes, L. A. (1997). A stable isotope study of organic cycling and the ecology of an anchialine cave ecosystem. Marine Ecology Progress Series, 17-27.
59. Quintana Roo Speleological Survey, 2019, List of Long Underwater Caves in Quintana Roo, Mexico: Tulum, Quintana Roo Speleological Survey.
60. Revel, M., Bayon, G., Vigier, N., Bastian, L., & Dufour, A. (2017). Abrupt response of chemical weathering to Late Quaternary hydroclimate changes in northeast Africa. Scientific Reports, 7(1). https://doi.org/10.1038/srep442
61. Rioual, P., Chu, G. Q., Li, D., Mingram, J., Han, J., & Liu, J. (2009). Climate-induced shifts in planktonic diatoms in lake Sihailongwan (North-East China): a study of the sediment trap and palaeolimnological records. In 11th International Paleolimnology Symposium (p. 120).
62. Roy, P. D., Torrescano-Valle, N., del Socorro Escarraga-Paredes, D., Vela-Pelaez, A. A., & Lozano-Santacruz, R. (2018). Comparison of elemental concentration in near-surface late Holocene sediments and rainfall regimes of the Yucatán Peninsula (Mexico): a preliminary study. BOLETIN GEOLOGICO Y MINERO, 129(4), 693-706.
63. Sánchez, M., Alcocer, J., Escobar, E., & Lugo, A. (2002). Phytoplankton of cenotes and anchialine caves along a distance gradient from the northeastern coast of Quintana Roo, Yucatan Peninsula. Hydrobiologia, 467(1), 79-89.
64. Schmitter-Soto, J. J., Comín, F. A., Escobar-Briones, E., Herrera-Silveira, J., Alcocer, J., Suárez-Morales, E., & Steinich, B. (2002). Hydrogeochemical and biological characteristics of cenotes in the Yucatan Peninsula (SE Mexico). Hydrobiologia, 467(1-3), 215-228.
65. Servicio Meteorológico Nacional, 2014, Daily Weather Data: Tulum Mexico, Servicio Meteorológico Nacional

66. Smart, P. L., Beddows, P. A., Coke, J., Doerr, S., Smith, S., & Whitaker, F. F. (2006). Cave development on the Caribbean coast of the Yucatan Peninsula, Quintana Roo, Mexico. Geological Society of America Special Papers, 404, 105-128.
67. Smith, S. L., Whitaker, F. F., Parkes, R. J., Smart, P. L., Beddows, P. A., & Bottrell, S. H. (2002). The geochemistry and geomicrobiology of saline groundwaters: Yucatan Peninsula, Mexico. Hydrogeology and Biology of Post-Paleozoic Carbonate Aquifers, Karst Waters Institute Special Publication, 7, 135-137.
68. Sobel, A. H., Camargo, S. J., Hall, T. M., Lee, C. Y., Tippett, M. K., & Wing, A. A. (2016). Human influence on tropical cyclone intensity. Science, 353(6296), 242-246.
69. Steinke, T. D., Holland, A. J., & Singh, Y. (1993). Leaching losses during decomposition of mangrove leaf litter. South African Journal of Botany, 59(1), 21-25.
70. Stoessell, R. K., and Coke, J. G., 2006, An Explanation for the lack of a Dilute Freshwater Lens in Unconfined Tropical Coastal Aquifer: Yucatan Example: Gulf Coast Association of Geological Societies Transactions, v. 56, p. 785-792.
71. Teranes, J. L., & Bernasconi, S. M. (2000). The record of nitrate utilization and productivity limitation provided by δ15N values in lake organic matter—a study of sediment trap and core sediments from Baldeggersee, Switzerland. Limnology and Oceanography, 45(4), 801-813.
72. Thomson J, Croudace IW, Rothwell RG (2006) A geochemical application of the ITRAX scanner to a sediment core containing eastern Mediterranean sapropel units. In: Rothwell RG (ed) New Techniques in Sediment Core Analysis. Geol Soc Spec Publ 267:65–77. doi:10.1144/ GSL. SP.2006.267.01.05
73. Torrescano-Valle & Islebe, 2012. Mangroves of Southeastern Mexico: Palaeoecology and Conservation
74. Urban, N. R., Lu, X., Chai, Y., & Apul, D. S. (2004). Sediment trap studies in Lake Superior: Insights into resuspension, cross-margin transport, and carbon cycling. Journal of Great Lakes Research, 30, 147-161.
75. Vera, I., Mariño-Tapia, I., & Enriquez, C. (2012). Effects of drought and subtidal sea-level variability on salt intrusion in a coastal karst aquifer. Marine and Freshwater Research, 63(6), 485-493.
76. Zhao, M. Y., & Zheng, Y. F. (2015). The intensity of chemical weathering: Geochemical constraints from marine detrital sediments of Triassic age in South China. Chemical Geology, 391, 111-122.

CHAPTER 2 FIGURES

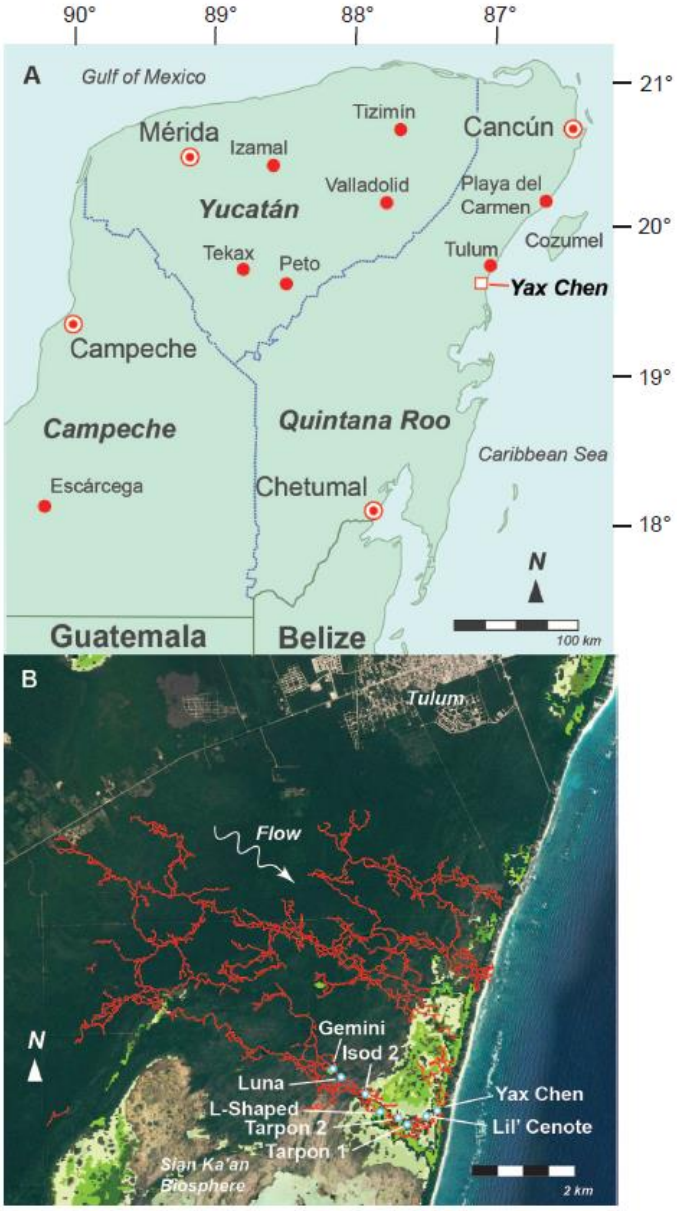

Figure 1. A) Map of the Yucatan Peninsula showing location of Yax Chen Cave System. B) Map of the Ox Bel Ha Cave System (red lines) which at present has ~ 270 km of mapped passage (QRSS, 2019). Yax Chen is a 2.7 km NW-SE trending section of Ox Bel Ha to the north of the Sian Ka'an Biosphere preserve. Shown are the cenotes as in Figure 2, with the classified mangrove type of fringe and dwarf mangrove (dark and light green; see Collins et al., 2015a for full description).

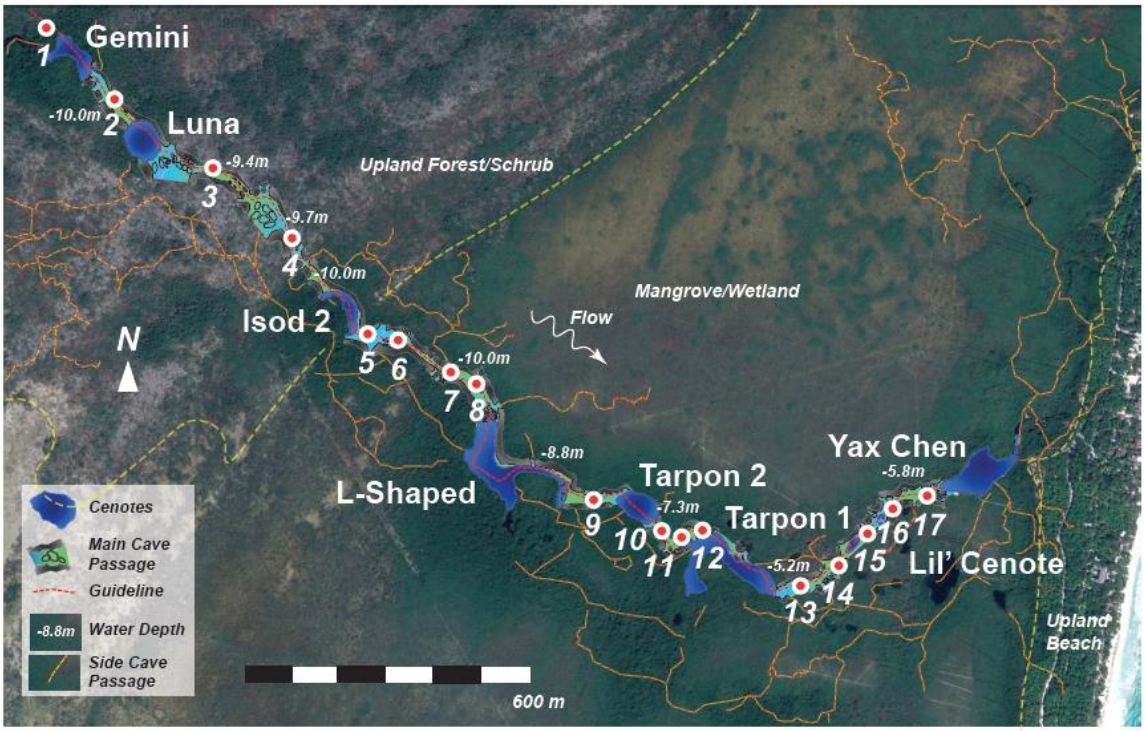

Figure 2. Sidewall map of Yax Chen Cave System showing the cenotes and connecting cave passage with the sediment trap stations. Smaller red and yellow dashed lines represent sidewall passages which have not been mapped in detail. The mangrove/wetland transition to the upland forested/shrub terrain is also demarcated as in Figure 1B.

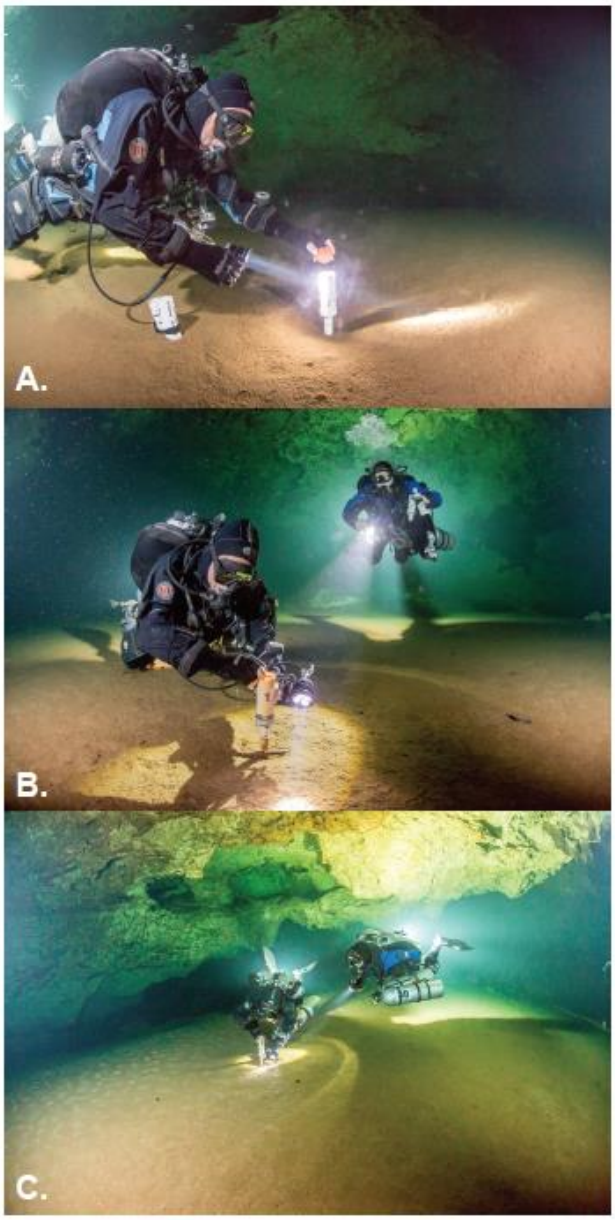

Figure 3. Sediment trap recovery includes placing a cap on the trap prior to removal, followed by replacement of the new trap. Good buoyancy control on the part of the diver is necessary to prevent resuspension of the loose OM flocs of sediment and placement of the cap immediately upon approach prevents any percolation from entering the trap. Percolation is caused by the diver's exhalent bubbles dislodging limestone particles from the cave ceiling which fall to the cave bottom. (Photo: Peter Gaertner)

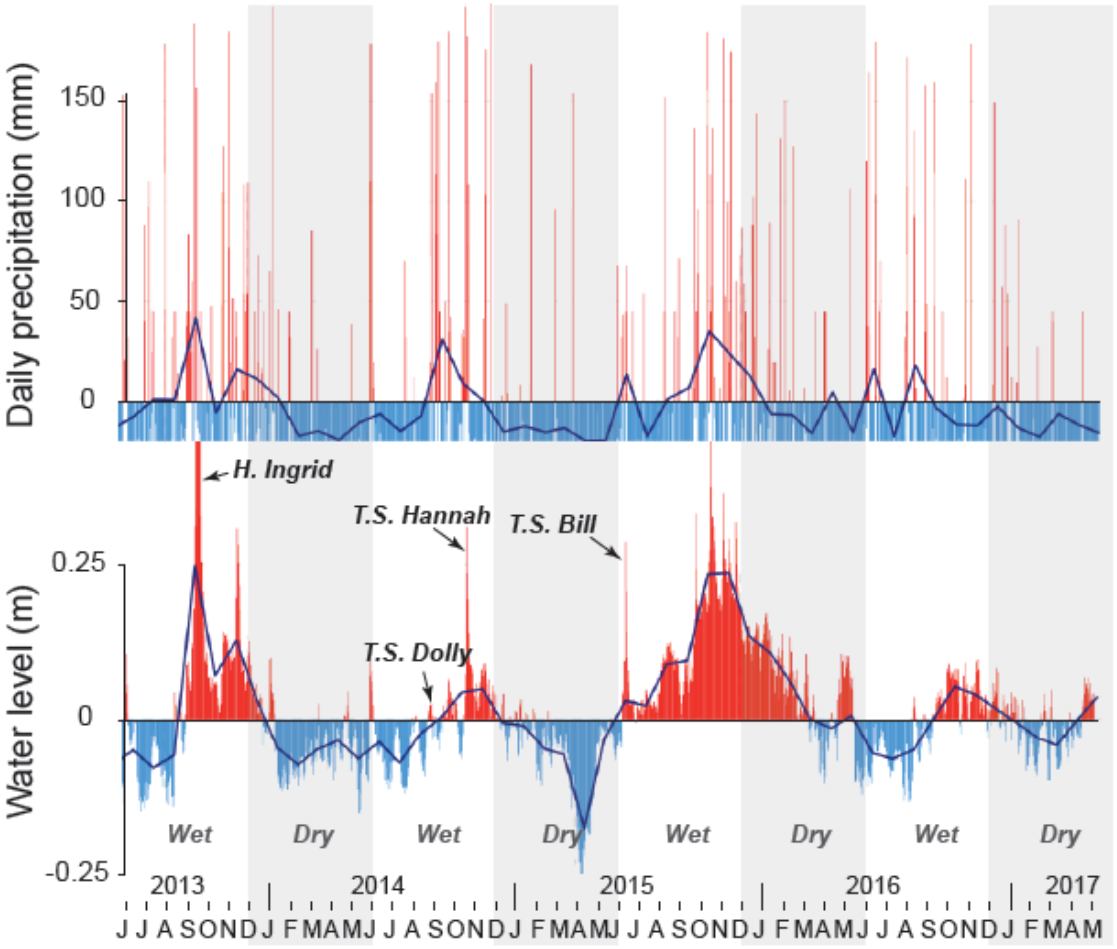

Figure 4. Daily rainfall from the Cozumel Weather Station shown as departure from the mean over the analysis period (mm) with monthly mean (dark blue line). Below is daily water level in Yax Chen also shown as departure from mean over the analysis period (m) with the monthly mean (dark blue line). Positive and negative departure from mean water level are shown in red (positive) and blue (negative). Sediment trap collection periods and the wet/dry season are in grey shading along with notable large rainfall events (hurricanes and tropical storms).

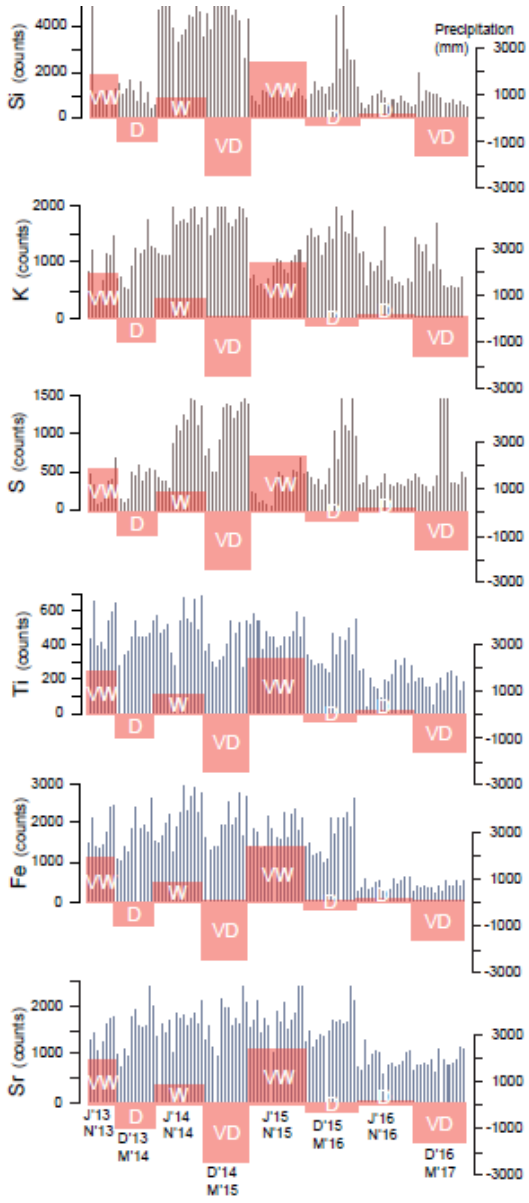

Figure 5. Sediment trap XRF results from the eight collection periods spanning 6 months each, with notations of seasonal collection and year (i.e. January 2013 corresponds to J'13, November 2013 corresponds to N'13). Rainfall over the collection periods is reported in deviation from mean in mm as in Figure 4 and notations indicate very wet (VW), wet (W), dry (D) and very dry (VD) seasonal periods. Biogenic-influenced elements (Si, K, S; see text for discussion) as well as lithogenic elements (Ti, Fe, Sr) are shown. Individual lines plotted are ordered by relative position in the cave. Of note is the distinct increase in biogenic elements from the Jun 2014 – May 2015 collection periods, and the decrease in lithogenic elements with reduced rainfall from December 2015 to May 2017.

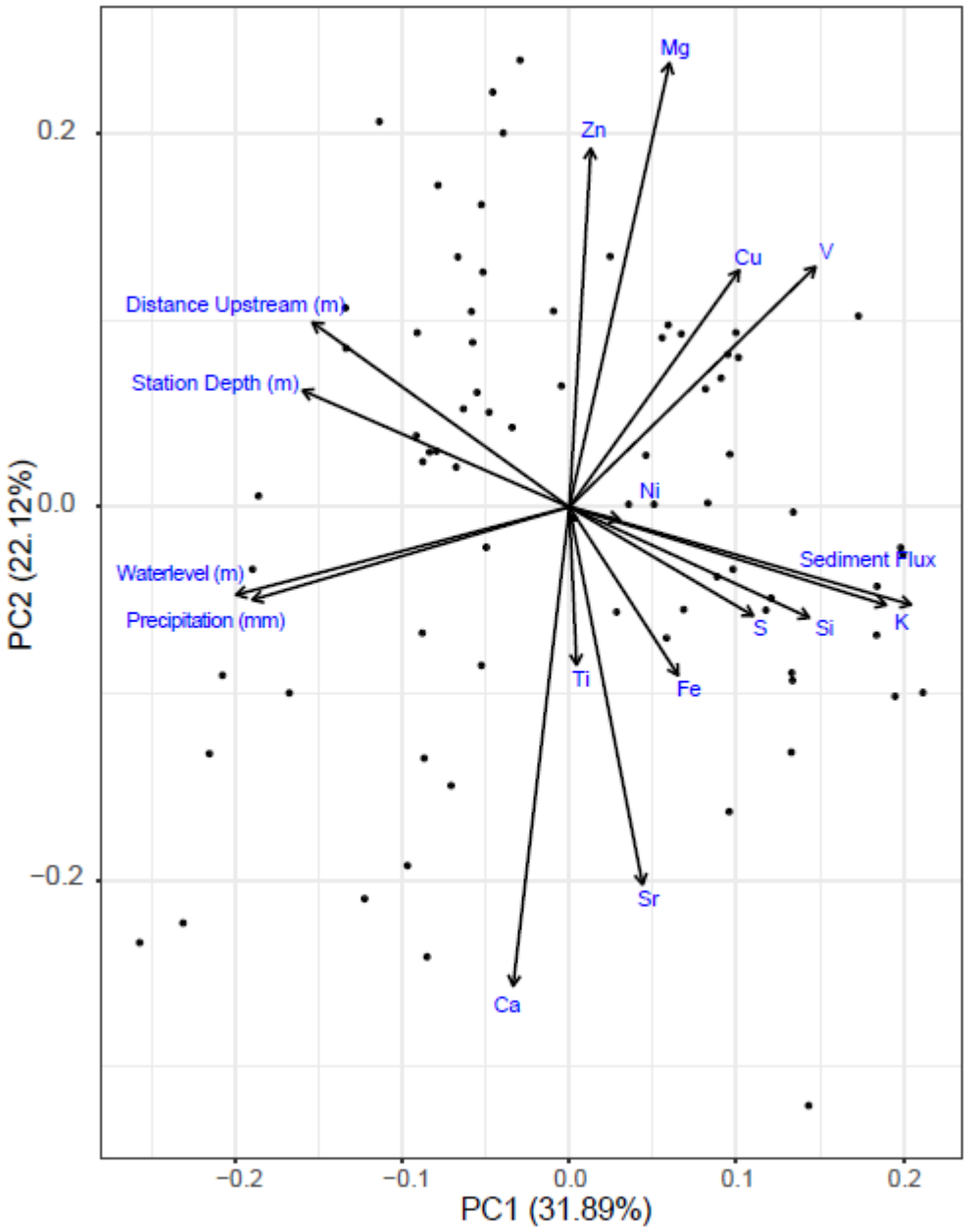

Figure 6. Principal Components Analysis shows first two components (PC1 and 2) encompass ~ 54% of the data variability. Biogenic-influenced elements (Si, K, S) strongly correlate with sediment flux, which has an inverse relationship with station distance and depth. Lithogenic elements show intercorrelations (Ti, Fe, Sr), but do not correlate directly with water depth.

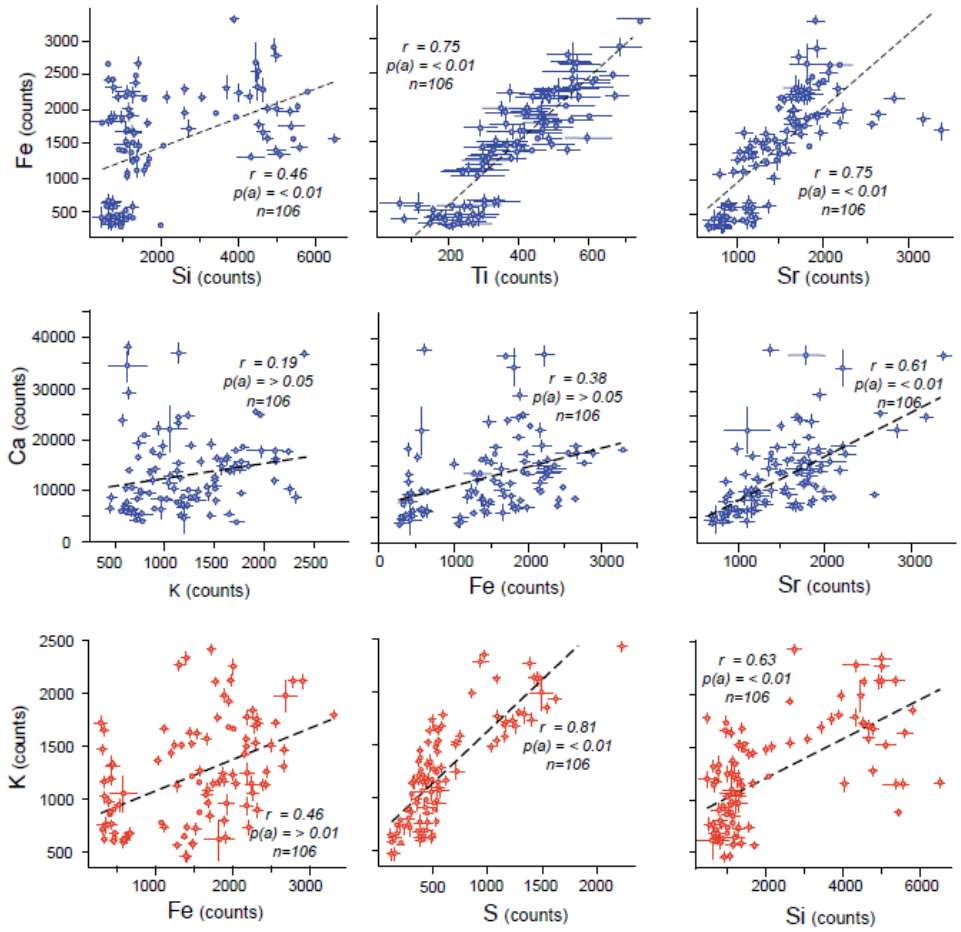

Figure 7. Crossplots showing relationships between lithologic (blue) and biogenically influenced elements. Error bars represent standard deviations of the analysis mean for each sample cuvette.

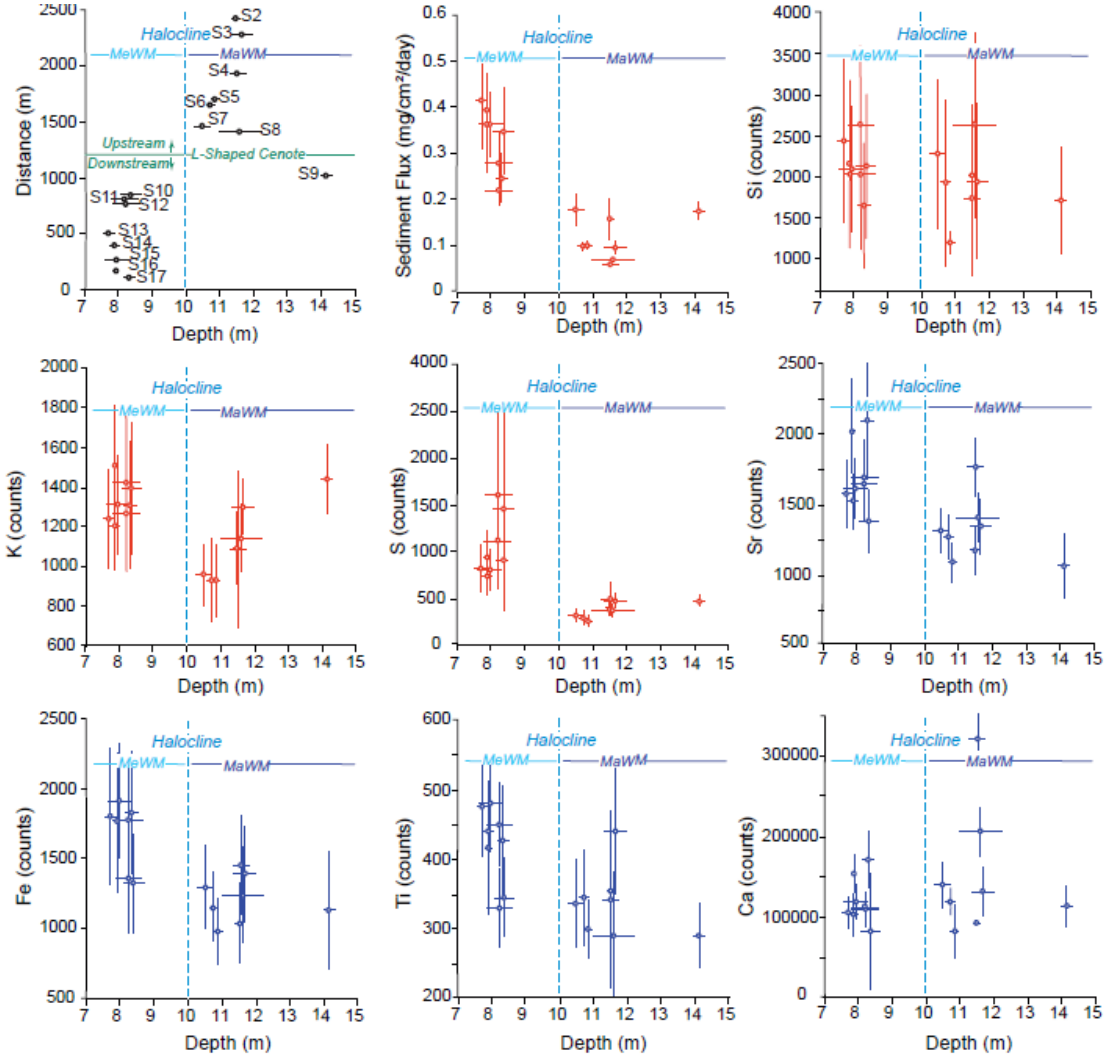

Figure 8. Crossplots showing relationships with station depth over the study period. All parameters are averaged over the study period. 1) Upstream distance along the cave passage from the Yax Chen Cenote; 2) Sediment Flux; 3 - 5) Biogenic influenced elements; and 6 – 9) Lithologic elements. Error bars represent the variation in depth for each station (n= 3 sediment traps) and the variability (standard deviation) in sediment flux and elements over the analysis period.

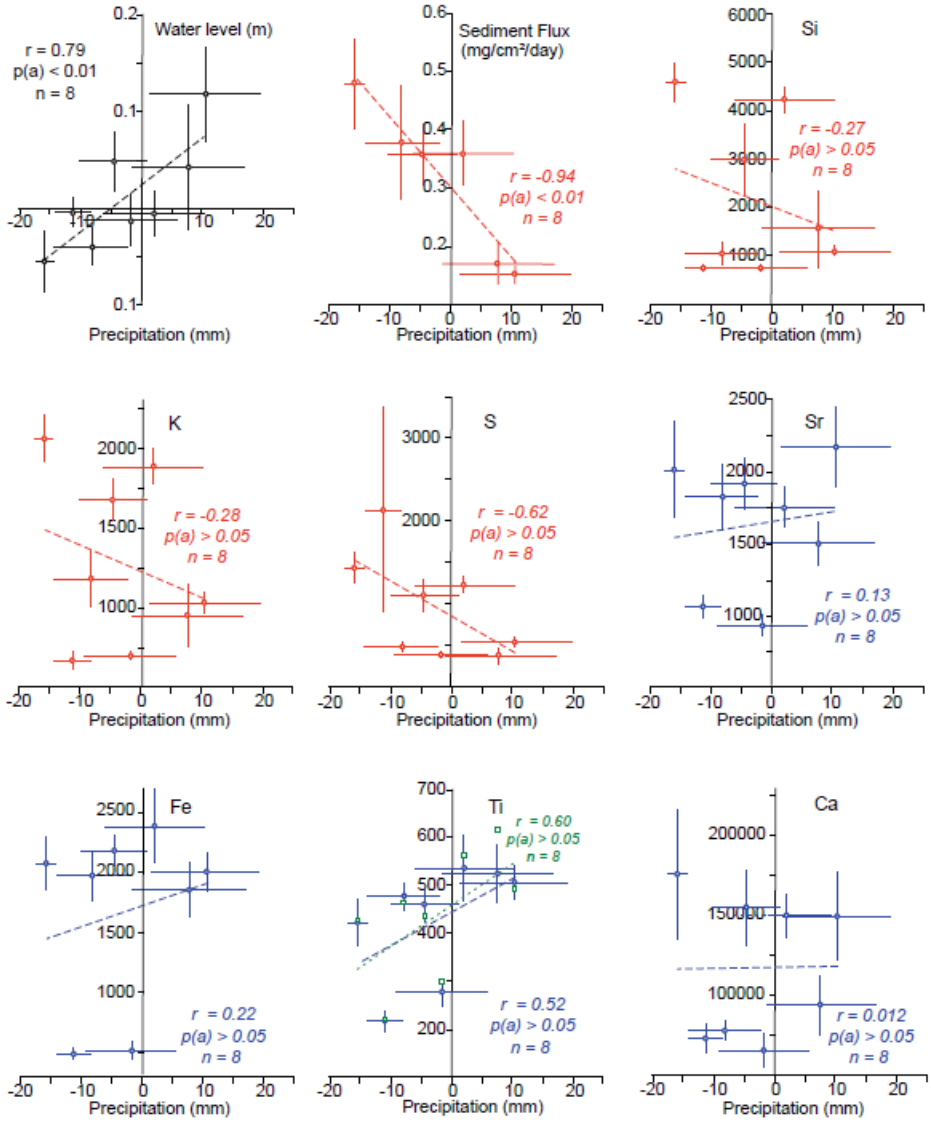

Figure 9. Crossplots showing relationships with average precipitation (deviation from mean; mm) over the collection intervals (6 months). 1) Mean water depth (deviation from mean; m); 2) Sediment flux; 3 - 5) Biogenic influenced elements (red); and 6 – 9) Lithologic elements (blue). Error bars represent the variation in monthly precipitation over the collection periods, and the variability (standard deviation) of sediment flux and elements for all the stations (2-17) for each collection period. Green symbols and trendline (Ti) are individual values for Station 14.

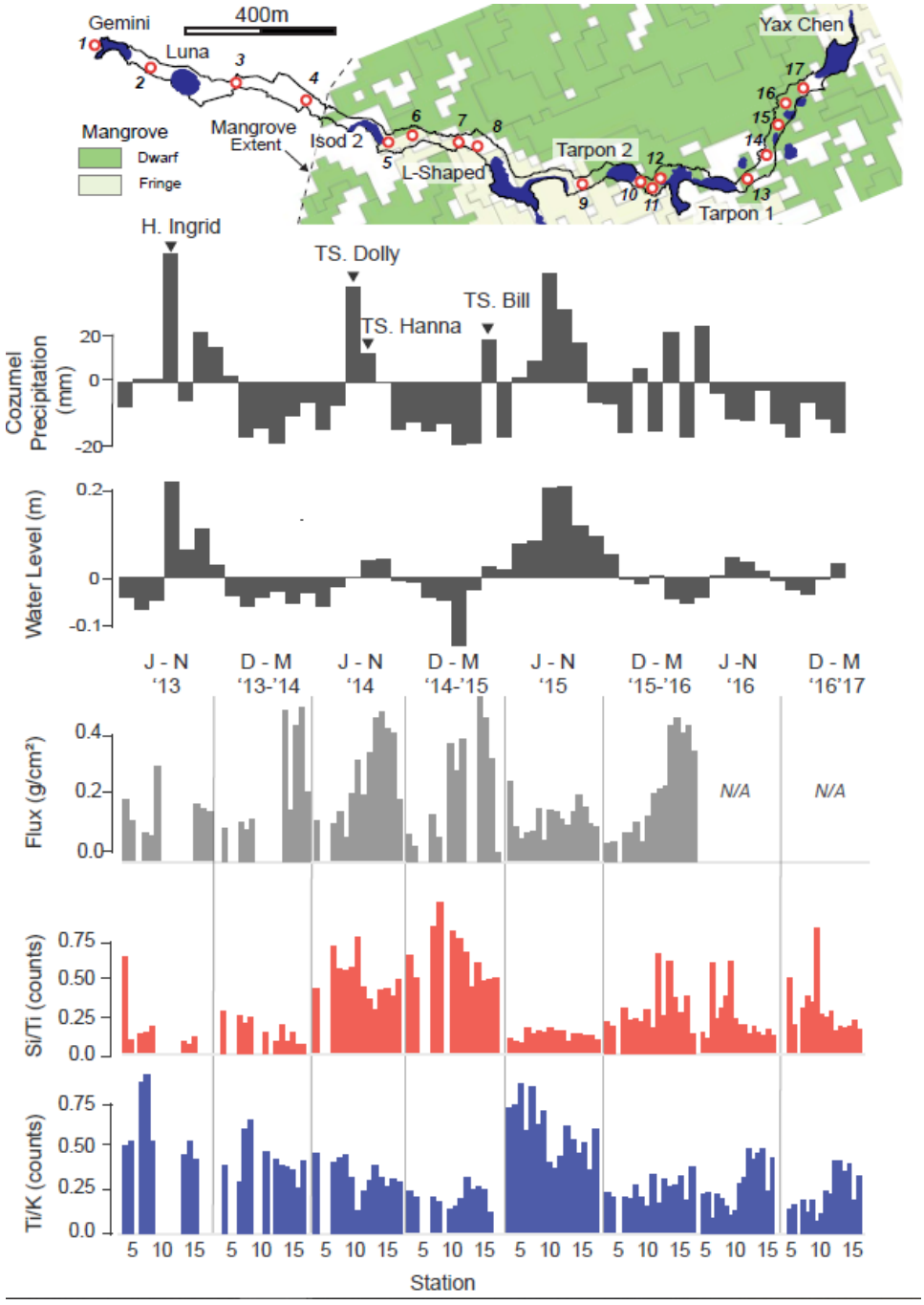

Figure 10. Map of Yax Chen cave system with locations of sediment collection sites and mangrove coverage (top). Cozumel precipitation (in mm) and water level in Yax Chen (in m) are indicated with dark grey bars representing monthly collection. Sediment flux (light grey - sediment amount in g/cm^2), Si/Ti (red - biogenic sediments), and Ti/K (blue - lithogenic sediments) are arranged by collection period and sediment collection location.

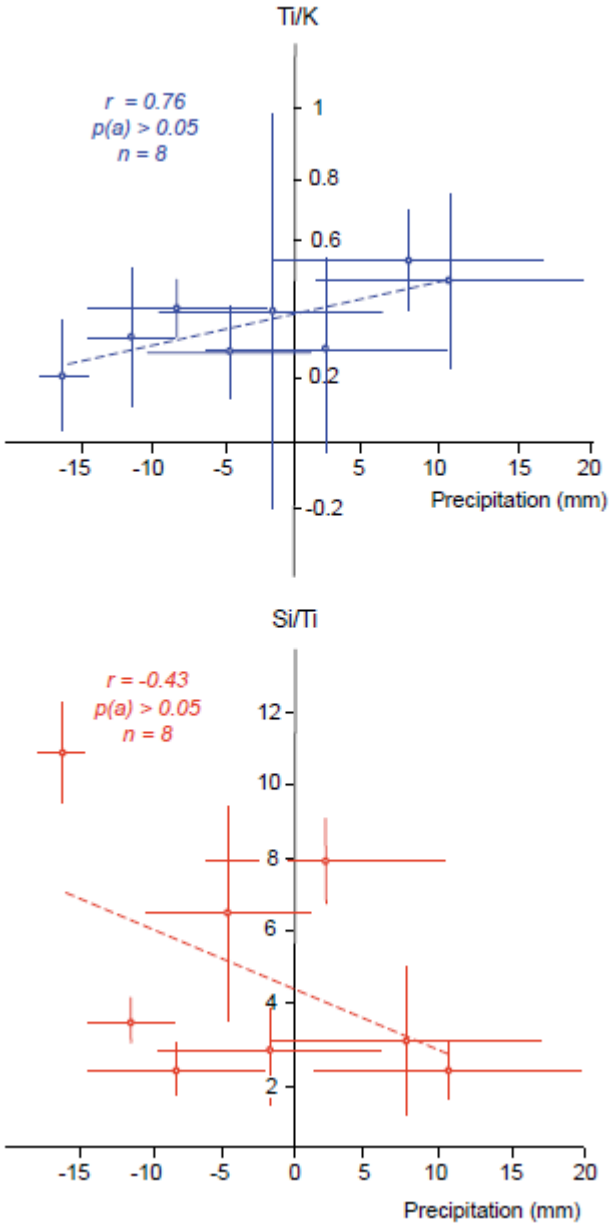

Figure 11. Plots showing relationships between precipitation and water level (deviation from mean; mm, m) with sediment flux, Si/Ti which maybe a useful hurricane/tropical storm indicator and Ti/K as a paleorainfall proxy.

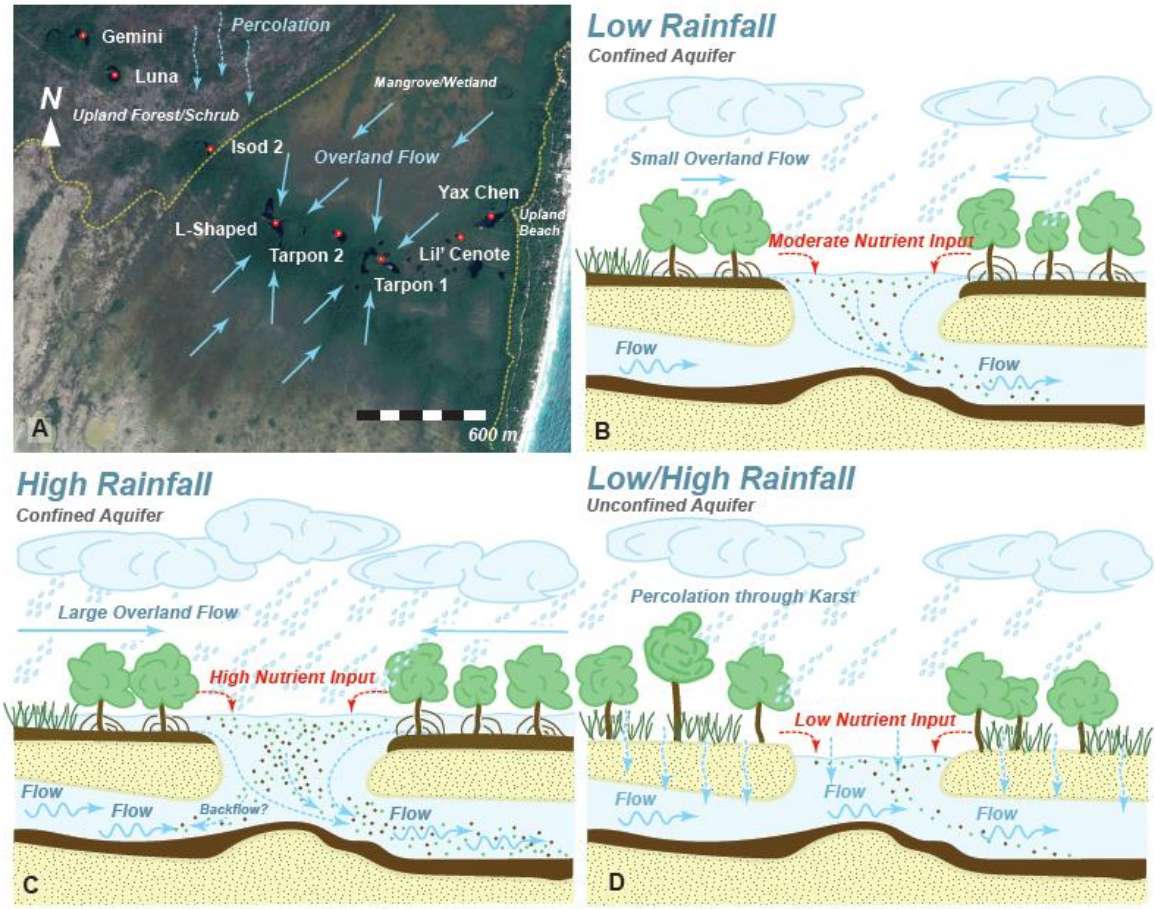

Figure 12. Conceptual diagram showing the relationship between groundwater and rainfalls (low and high) along with differences between mangrove and upland forest/shrub terrains which have also been established with monitoring of groundwater characteristics and modeling (Coutino et al., submitted).

CHAPTER 3- SALINITY CHANGES DURING THE MAYA TERMINAL CLASSIC DROUGHTS DOCUMENTED THROUGH CALIBRATED µXRF-CS CL IN SEDIMENT CORES FROM QUINTANA ROO, MEXICO

Chelsi A. McNeill-Jewer*[a], Eduard Reinhardt[a], Anya Krywy-Janzen[a], Aaron Coutino[b], Marek Stastna[b], Dominique Rissolo[c], Sam Meacham[d,e]

[a] School of Earth, Environment and Society, McMaster University, 1280 Main st W, Hamilton Ontario
[b] Department of Applied Mathematics, University of Waterloo, 200 University ave, Waterloo Ontario
[c] Qualcomm Institute, University of California, San Diego, La Jolla, CA 92093-0436
[d] CINDAQ, Puerto Aventuras, Quintana Roo, Mexico
*corresponding author: mcneic3@mcmaster.ca

KEYWORDS: *Caribbean climate, uXRF-CS, paleosalinity, drought, Maya Civilization, paleoclimate proxies, Chlorine, Yucatan Peninsula, paleo-drought records, evaporative lakes*

HIGHLIGHTS

- Calibrated µXRF-CS Cl counts have a direct relationship to salinity in ppt
- Cl records from evaporative lakes provide high-resolution paleoclimate data
- Classic Maya droughts were sub-decadal in duration
- Paleo-salinity records in agreement with recent Caribbean SSS and SST change
- High-resolution Cl core records provide estimates of water potability

ABSTRACT

Linking regional- and global-scale climate change to events in human history is often difficult because of the lack of high-resolution records regarding the availability of potable water resources, especially in arid tropical regions such as the Yucatan Peninsula. Though there is general consensus regarding the role of prolonged droughts as a catalyst of the collapse of southern lowland Classic Period

Maya civilization, there are challenges regarding temporal resolution when comparing climate proxies to archaeological data, as the broad timespans and differing sensitivities of most records complicate associations between drought and the principal drivers or spatial distribution of droughts during the Maya Terminal Classic. I developed a high-resolution paleosalinity proxy using Cl from µXRF-scanned sediment cores, which successfully identified drought periods on the eastern Yucatan Peninsula during the Classic Maya disintegration. A salinity calibration curve was created from 16 sediment cores and applied to two inland lake cores from Quintana Roo, Mexico to document sub-decadal to sub-annual dry periods over the past 4000 years. Most severe dry periods occurred around 2.8 ky ago, during the Maya Preclassic Hiatus (200-250 CE) and during the Classic Maya collapse (800-1000 CE). The records are in agreement with instrumental and reconstructed indicators of SST and SSS change across the tropical Atlantic and Caribbean, indicating there is a common control driving evaporation and salinity change in the Yucatan Peninsula and beyond. This method provides a paleo-salinity proxy that can be used to infer the potability of past water, and shows that orbital-scale climate change impacted water resources in the past.

1.0 INTRODUCTION

Many studies have focused on reconstructing the late Holocene climate history of the Yucatan Peninsula and the wider Caribbean region to determine the timing of arid periods and their links to larger ocean-atmosphere phenomena. Paleoclimate research has used geochemical and sedimentological methods to look at

precipitation changes across the Yucatan Peninsula, and include studies of carbon and oxygen isotopes in microfossils from lake sediment cores (Curtis et al., 1996) and speleothems (Kennett et al., 2012; Medina-Elizalde et al., 2010; Medina-Elizalde and Rohling, 2012; Akers et al., 2016), pollen (Carillo-Bastos et al., 2012; Cook et al., 2012), elemental analysis of marine and freshwater sediment (Haug et al., 2001; Hodell et al., 2001), and sedimentology (Hodell et al., 2005). Though wet and dry trends over the past millennia have been defined across the Yucatan Peninsula, the sensitivity, dating and sampling resolution for each proxy and study site is unique, making cross-comparison difficult. There may also be issues of temporal resolution, as many paleoclimate analyses sacrifice temporal resolution for time and cost. Though some studies have generated quantifiable measures of past precipitation reduction using $\delta^{18}O$ (Medina-Elizalde et al., 2016; Evans et al. 2018), or pollen (Carillo-Bastos et al., 2012), this does not translate directly to the water balance of the local water table or potability of water resources, which are important factors to consider because water for domestic and agricultural consumption is a major control on societal wellbeing. Determining the direct impacts of drought on freshwater resources remains difficult as there is no clear relationship between paleoclimate proxies and the potability of past water. The regional setting of climate changes within the Caribbean is also important to investigate to better understand how drought across the Yucatan Peninsula is linked to local and regional climate connections.

We developed and applied a sedimentary Cl paleo-salinity proxy, which may

eventually guide understanding of regional evaporation patterns and their connection to global climate phenomena. Sediment cores (n=16) from eastern Quintana Roo, Mexico were used to calibrate µXRF Core Scanner (µXRF-CS) Cl counts with measured environmental salinity (ppt), to create a paleo-salinity proxy that was applied to infer salinity changes from sediment cores collected in two shallow lakes, one close to the coast (Chumkopo) and one further inland (Pac Chen). Cl responds conservatively to mixing of fresh and marine waters, or though concentration by evaporation, and responds without a temporal lag. It is a salinity proxy that can be broadly applied, providing spatial and temporal data that have thus far been unavailable in paleoclimatology studies.

1.2 CHLORINE AS A PROXY FOR SALINITY

Chlorine (Cl) is a conservative element with an aqueous concentration that reflects the mixing between fresh (<1 ppt) and marine water (~35 ppt), but also concentrates in restricted or closed water bodies with evaporation during months that are warmer and/or drier (Perry et al., 2009). Porewater Cl measured from sediment cores can record water condition at the time of deposition, and has been used to document changes in aridity and evaporation in the Dead Sea (Lazar et al., 2014; Kiro et al., 2017) and in a Cuban sinkhole (Peros et al., 2017). Traditionally, Cl has been measured at coarse resolution through extraction of pore fluids at intervals in sediment cores, but the approach is time-consuming and relatively low-resolution. µXRF core scanning, however, enables measurement of Cl within pore spaces in sediment cores at high resolution (200 µm), potentially

recording at sub-annual scales, even in sediments that are not laminated (Orme et al., 2015). Chlorine µXRF records were used to document seawater intrusion from storms and tsunamis in a coastal lake from the Cook Islands (Chague-Goff et al., 2016). µXRF-CS Cl data have also been applied in cave and cenote sediments from Quintana Roo, Mexico to document changes in aquifer dynamics with respect to the mixing of meteoric and marine water, and proved to be a useful tool for paleoenvironmental studies when endmember salinity is not known (Kovacs et al., 2017a). Furthermore, µXRF analysis simultaneously provides other elemental data, including proxies of terrigenous weathering (e.g., Fe, Ti, K), which can be compared with Cl data (Krywy-Janzen et al., 2019; McNeill-Jewer et al., 2019).

2.0 REGIONAL SETTING

2.1 YUCATAN PENINSULA HYDROGEOLOGY

The Yucatan Peninsula (Figure 1), is a flat, karstified limestone platform with extensive cave systems and sinkholes proximal to the coast. The coastal karst system has multiple-scale porosity consisting of matrix, fracture, and cave conduit flow with a meteoric water mass (MeWM) on top of a marine water mass (MaWM). The MeWM flows towards the coast, whereas the MaWM flows inland (Beddows, 2004; Smart et al., 2006; Beddows et al., 2007; Perry et al., 2009; Bauer-Gottwein et al., 2011). Surface waters of the Yucatan Peninsula generally have low Total Dissolved Solids (TDS) and Specific Electrical Conductivity (SEC). Most ions in the rainfall-derived MeWM originate from carbonate dissolution rather than from seawater intrusion (Beddows, 2004; Stoessel and Coke, 2006). Generally, any

increase in the SEC above 2.5 mS/cm is attributed to concentration of Cl in the upper layer, via evaporation or mixing with underlying saline water (Smith et al., 2003; Beddows et al., 2004). The MeWM lies within porous limestone and is only exposed at karst windows (cenotes), freshwater wetlands (sabanas), low-lying swamps (aguadas) and coastal lagoons, resulting in a relative scarcity of freshwater across the landscape in the east. The study by Krywy-Janzen et al. (2019) reconstructed the flooding history of Lake Pac Chen and found that it was tied to Holocene sea-level rise. This implies that the lakes are directly connected to the MeWM, and thus cannot be considered hydrologically closed systems. Furthermore, Krywy-Janzen et al. (2019) and Coutino et al. (submitted) showed that the inland water bodies display semi-diurnal tidal oscillations, indicating they are connected to the ocean through the aquifer.

2.2. YUCATAN PENINSULA CLIMATE

The annual precipitation cycle over south Mexico and Central America has a bimodal distribution, with maxima in June and September-October, and a midsummer drought in July and August, known as ‘canicula,’ which is related to Sea Surface Temperature (SST) fluxes over the tropical Pacific (Magaña et al., 1999; Mendez and Magaña, 2010). Climate across the eastern Yucatan Peninsula is evaporation-dominated with regional local rainfall annual maxima of about 1500 mm/y, and minima reaching 500 mm/y, and evaporation potentials of 350-2500 mm/y (300-400 mm/y at Lake Chichancanab;Is this important here? Hodell et al., 2005; Brenner et al., 2001; Gianinni et al., 2001; Bauer-Gottwein et al., 2011). The

region is dependent on tropical depressions, storms and hurricanes to maintain a positive net water balance, in light of the high rates of evapotranspiration (Bauer-Gottwein et al., 2011; Medina-Elizalde and Rohling, 2012; Nooren et al., 2018). Interannual variability in Mesoamerican rainfall is linked with climate patterns and features such as the Intertropical Convergence Zone (ITCZ), El Niño Southern Oscillation (ENSO), North Atlantic Oscillation (NAO), and Atlantic Multidecadal Oscillation (AMO), as well as changes in tropical North Atlantic SST and Sea Surface Salinity (SSS) (Gianinni et al., 2000; Magaña et al., 2003; Wang et al., 2009; Stephenson et al., 2014; Bhattacharya et al., 2017; Wu et al., 2017).

The Caribbean Basin experiences wet and dry extremes associated with ENSO cycles and local changes in SST. ENSO is a positive feedback between the ocean and atmosphere and has highest power at 2-7-year periods (Clement et al., 1999). El Niño can result in drier-than-average conditions in summer, and wetter-than-average conditions in spring throughout southern Mexico (Gianinni et al., 2001). Warm El Niño conditions are a direct response to warmer SST in the northern equatorial Pacific, whereas cooler spring/summer ocean temperatures result in less summer rainfall for the Caribbean region (Giannini et al., 2001). There is a southward migration of the ITCZ during El Niño years that causes enhanced dryness over Mexico and Central America (Walisser and Gautier, 1993; Magaña et al., 1999). The ITCZ is a persistent feature of deep convective clouds and plays a crucial role in global energy redistribution (Lechleitner et al., 2017). The mean

position of the ITCZ in the Northern Hemisphere (NH) is linked to atmospheric energy transport, cloud feedback, distribution of water vapor and ocean energy uptake (Schneider et al., 2014). Observational data suggest that tropical Atlantic SSTs and the mean position of the ITCZ are strongly coupled, with anomalous cooling of one hemisphere resulting in an ITCZ migration towards the warmer hemisphere because of energy differentials (Schneider et al., 2014; Chiang and Friedman, 2012). The behaviors and interactions of these climate phenomena influence seasonal rainfall across the Caribbean and the Yucatan Peninsula.

2.3 SITE BACKGROUND

Laguna Pac Chen and Laguna Chumkopo (Laguna Ka'an Luum) are two fresh-water lakes located on the east coast of Quintana Roo, Mexico. The lakes differ significantly in their physical and chemical characteristics, including area, location, bathymetry, depth profiles, and sediment type. Pac Chen and Chumkopo were included in previous studies of flooding (Pac Chen; Krywy-Janzen et al., 2019) and hurricane history (Chumkopo; Brown et al., 2014).

Pac Chen (20°38.07' N, 87°35.12'W) is a ~16-m-deep lake with an area of 0.04 km^2 across three basins. It is located approximately 40 km west of the Caribbean coast and 20 km northeast of the Maya city of Coba. Surface salinity in Pac Chen is 0.5 ppt, and there is a minor salinity change associated with greater depth (Figure 2). The base of the lake contains a thick drape of organic sediment with occasional beds of gastropods. Krywy-Janzen et al. (2019) reconstructed the flooding history

of Pac Chen using multiple sediment cores to show that it flooded and developed in accordance with rising sea level during the late Holocene. Water depth measured over 6 months shows semi-diurnal tidal variations, indicating a connection to the aquifer (and sea), but the level of interchange between lake water and the aquifer is not known (Krywy-Janzen et al., 2019).

Laguna Chumkopo (20°9.75' N, 87°33.23'W) is substantially larger (0.41 km^2) than Pac Chen and has two deep sinkholes (>80 m deep) adjacent to a shallow platform (Brown et al., 2014). It is located 10 km west of the coast and 15 km south of the Postclassic Maya port Tulum. The main basin is covered with a thick unit of lime mud, but there is a connection with groundwater through the deep sinkhole. Brown et al. (2014) investigated the hurricane record of Chumkopo using sediment cores from the deep sinkhole. Chumkopo has a surface salinity of 1.1 ppt and a sharp halocline at ~22 m (Figure 2), where the transition between the MeWM and MaWM occurs. The thermal profile reflects a combination of seasonal and annual groundwater processes, and temperature in the MeWM is higher within the upper 6.9 m (32.7°C vs 30.4 °C below 6.9 m; Brown et al., 2014).

3.0 MATERIALS AND METHODS

3.1 SEDIMENT CORE RETRIEVAL AND ANALYSIS

Two sediment cores were collected from Lake Pac Chen (PC4; Krywy-Janzen et al., 2019) and Laguna Chumkopo (CKC3). The cores were analyzed at the McMaster University Core Scanning Laboratory (MUCS Lab) using a Cox

Analytical iTRAX X-Ray Fluorescence Core Scanner (µXRF-CS) with a Cr X-Ray source. PC4 was scanned at a resolution of 500 µm with a 15-second exposure time, whereas CKC3 was scanned at 200-µm resolution with a 15-second exposure time. Radiocarbon samples were of bulk fine particulate organic material, small twigs and charcoal for Pac Chen while all radiocarbon samples for CKC3 were bulk organic material from carbonate rich marl (Table A.1). A reservoir correction of 1244 years, which was developed in Kovavs et al (2015b) was applied to Chumkopo to counteract any Hard Water Effect (HWE) as the water body of Chumkopo is significantly connected to the MaWM and the sediment is primarily carbonate mud. Calibrated radiocarbon age-depth models were calculated using the Bayseian linear modelling package BACON in statistical software R (Figure A.1; Table A.1; Blaauw and Christen, 2011). Wavelet spectral analyses of both core records were completed using the Wavelet Toolbox from MATLAB ® (MATLAB, 2020; see supplemental material).

3.2 SALINITY CALIBRATION AND EXPERIMENT

Sixteen short (<0.5 m) push cores and *in situ* water samples that span a range of salinities (0.4 to 30 ppt) were collected by SCUBA divers throughout the Ox Bel Ha and Sac Actun cave systems (Tulum, Quintana Roo) (Table A.2). Water samples were measured using a handheld YSI 30 salinity, conductivity and temperature meter. The cores were split and analysed at the MUCS Lab using a Cox Analytical ITRAX core scanner at a resolution of 1000 µm, with a Cr tube and 15-second

exposure time. There was a linear relationship between ppt values in water samples and the averaged Cl^- counts from the corresponding top 5 cm of sediment in cores (Figure 3). After scanning, sediment from the upper 5 cm was sampled and rinsed with deionized water and re-scanned using a sequential sediment sample reservoir (SSR) (Gregory et al., 2017).

Cl values for PC4 and CKC3 were converted to ppt using the equation in Figure 3. Annual dry periods were defined using statistical software R, by calculating the overall average and standard deviation of salinity for each core to produce a threshold. The data were then filtered to display only points above this value. Definitions of 'common,' 'severe,' and 'extreme' drought markers correspond to times when salinity increased by 1, 2 or >2 σ above the baseline salinity for at least 2 data points, representing sub-annual to multi-year droughts. Drought records are shown in Figures 7c and 8a.

Chlorine data from cores CKC3 (Chumkopo) and PC4 (Pac Chen) were normalized and combined to create a single Cl record (salinity) using MATLAB. The normalized records were interpolated to match their ages by year before combining them to create the composite record named "Chumpac."

4.0 RESULTS

4.1 CORE LITHOLOGY AND μXRF

CKC3 contains laminated marl mud, organic matter (OM) and gastropods (Figure 4A). PC4 is composed of fine-grain OM with increasing carbonate content towards the surface and deposits of darker OM around 95-91, 22-16, and 12-9 cm (Figure 4B; Krywy-Janzen et al., 2019). There is no facies change associated with the Cl in CKC3, which has consistent laminations throughout the core (Figure 4A). Increases of Cl in PC4 between 55 and 45 cm correspond to a layer of gastropods at 55-40 cm, which may represent a matrix effect, however continued K fluctuation below the gastropod layer indicates that the values represent a primary signal (Krywy-Janzen et al., 2019).

The Cl counts for CKC3 (500 to 3000, average ~1000) are approximately double those in PC4 (250 to 1000, ~ average 300), which was expected, given the measured salinities in the two lakes. The K counts for CKC3 (0-250) were approximately half those in PC4 (0-500), which was also expected, given the abundance of OM in PC4 compared to CKC3. Cross-plots of the Cl and K values, and incoherent/coherent backscatter (incoh/coh), indicate no direct relationship among Cl, K and porosity (Figure 4C). There is a weak relationship between depth and incoh/coh in PC4 caused by changes in porosity near the top of the core (60-0 cm; Figure 4B), which was discussed in Krywy-Janzen et al. (2019), along with the slight matrix effect of K in PC4 and its dependence on OM.

4.2 AGE MODELS

The age-depth models show linear sediment accumulation rates in CKC3 and PC4, though there is a small change between 50 and 0 cm in CKC3 **(**Figure A.1**)**. There are no age reversals or outliers associated with the age models and all points were interpolated linearly. The maximum age of CKC3 is ~4000 years, whereas the PC4 maximum age is ~2000 years (Figure A.1). See supplemental material for details (Table A.1).

4.3 SALINITY CL CALIBRATION

The salinity calibration yielded a strong correlation between sediment Cl and water-column ppt (r = 0.94, n=16). Outliers may have been a consequence of low sedimentation rates, such that time-integrated Cl values in the upper deposits do not reflect accurately the “snapshot” salinity of the overlying water. The majority of the water samples used for the calibration had rather low salinity, which may account for why higher values do not fit the trend as well (Figure 3A). After rinsing with deionized water, the Cl counts for all samples consistently dropped to near zero (Figure 3B), regardless of lithology, indicating the Cl was effectively trapped in pore space within the sediment. Mean inferred salinity over the spans of the two records were 1.48 +/- 0.43 and 1.07 +/- 0.56 ppt, for Chumkopo and Pac Chen, respectively. There were, however, intervals in which the Cl was as high as 14 ppt in Chumkopo and 12 ppt in Pac Chen.

4.4 CKC3 AND PC4 CL TRENDS

The paleo-salinity records from both Chumkopo and Pac Chen show gradual changes and rapid events, and display trends similar to other indicators of past dryness and environmental change. The Cl records from CKC3 and PC4 reflect records of Caribbean SST, rainfall, and NH temperature, suggesting a link between global temperature, insolation and rainfall across the coastal Yucatan Peninsula (Figures 5, 6, and A.2). The longer Cl record from Chumkopo also reflects paleotemperature changes across the broader NH over the past 4000 years (Figure 6; Bond et al., 2001; Kiboshi et al., 2013). The CKC3 record shows relatively high variability from 4 to approximately 3.4 ky BP. This was followed by a period when salinity was low and stable from 3.4 to 2.8 ky BP, which was succeeded by two periods of increased aridity centered around 2.8 and 2.6 ky ago, which lasted ~100 years each and had a ~100-year hiatus in between (Figure 6c). Highlights also include higher Cl values around Bond events, namely ca. 2.8, 1.5, and 550 years ago (Figure 6a, b).

5.0 DISCUSSION

5.1 CONNECTIONS TO NORTHERN HEMISPHERE AND ITCZ

Associations between the CKC3 and PC4 Cl records and instrumental temperature and precipitation data from the Caribbean, SST data from Yucatan corals, and foraminifera from Cariaco Basin, indicate a link between climate on the Yucatan Peninsula and SST across the wider Caribbean region (Figure 5 - Black et al.,

2007; Vásquez-Bedoya, 2012; Stephenson et al., 2015). Notable dry periods in the CKC3 and PC4 records include the “Pan Caribbean Drought” (3500-2300 BCE), the Maya Preclassic Hiatus (~200-250 CE), and the Maya Terminal Classic Period (~800-1100 CE). There is also a particularly strong event around 2.8 y BP that may be associated with a documented widespread dry event across the Caribbean (Wanner et al., 2011; Kiboshi et al., 2011, 2013; van Hengstum et al., 2018). Links and similarities with Pan-Caribbean records of dryness show a period from approximately 3.3 to 2.5 ky that was particularly dry and falls within the so-called “Pan Caribbean Drought” (Berman and Pearsall, 2000; Van Hengstum et al., 2018). The northern Bahamas also experienced drought conditions around that time, and the dry spell coincides with evidence from other hydroclimate and oceanographic records that show a synchronous southward migration of the ITCZ and North Atlantic Hadley Cell (van Hengstum et al., 2018). The general drying trend observed in the CKC3 record over the last few thousand years could be related to the southward migration of the ITCZ during the late Holocene in response to orbitally forced insolation, which caused a gradual cooling in the NH (Schneider et al., 2014; Nooren et al., 2018). Ultimately, this is evidence of a larger-scale relationship between wet/cold periods in the NH and rainfall over coastal Quintana Roo, manifest through changes in the position of the ITCZ and modulations by ENSO and the NAO. The constructive behaviour of ENSO and NAO often influence dryness or wetness across the Caribbean (Gianinni et al., 2001). There is strong covariation between ITCZ and NAO records over centennial to decadal timescales

(Lechleitner et al., 2017). Paleorainfall records from caves in Belize (Yok-1) and Scotland (Uamh-an-Tartair) indicate that this is also active over annual to decadal timescales and is likely influenced by a combination of energy flux perturbations (Lechleitner et al., 2019).

5.2 CL RECORD AS A SENSITIVE PALEODROUGHT PROXY FOR THE TERMINAL CLASSIC DROUGHT

There is abundant evidence that the time period surrounding the Maya Terminal Classic (MTC) was associated with dryness. There is, however, a lack of consensus regarding the length and severity of the dry periods, as studies have yielded slightly different results regarding the timing and length of droughts. It is generally accepted that the MTC was not characterized by a single centuries-long drought, but rather a series of multi-decadal dry events separated by periods of relative moisture (Hodell et al., 2005; Frappier et al., 2014).

Both the CKC3 and PC4 records support this, showing multiple periods of enhanced salinity that are sub-decadal to annual in length, however the most profound period of aridity common to both records coincides with the MTC, from 750-1100 CE (Figures 7, 8). This represents one of the driest intervals in the late Holocene history of the region, documented by a host of climate proxy records including pollen, speleothems, microfossils and tree ring data (Brenner et al., 2001; Haug et al., 2001; Haug et al., 2003; Hodell et al., 2005; Mendoza et al., 2007; Carillo-Bastos et al., 2010; Cook et al., 2012; Kennett et al., 2012; Lachniet et al.,

2012; Medina-Elizalde and Rohling, 2012; Stahle et al., 2016). Increases in calibrated salinity of >5 ppt in Pac Chen and 3 ppt in Chumkopo, indicate that surface water salinity in each waterbody increased rapidly during the MTC.

The carrying capacity of ancient civilizations across the Yucatan Peninsula was highly sensitive to reductions in precipitation (Gill, 2000; Medina-Elizalde and Rohling, 2012). Although there is no evidence that Pac Chen and/or Chumkopo were used as drinking water sources, their locations near large settlements (e.g. Coba, Tulum), suggest that increased aridity during the MTC probably would have impacted surface water bodies utilized by populations at those sites. Daily consumption of salts in excess of 120 to 500 mg (for children and adults, respectively) can result in various health issues, though the prevalence of sodium salts in drinking water is yet to be studied in detail due to global variation in diet based salt intake (WHO, 2003). Though of relatively short duration, the past episodes of high evaporation/precipitation were unpredictable, leading to uncertainty throughout the region regarding water availability for domestic or agricultural use, and may have even induced droughts that impacted regional agriculture. Each missed seasonal rain cycle would have further reduced the ability of the ancient Maya to produce sufficient food. Even if Maya society were able to adapt to low precipitation by modifying landscapes and adopting novel agricultural practices, increased climate variability may have proved to be a serious challenge.

5.3 SENSITIVITY OF AND CONTROLS ON THE CL PROXY RECORD

We demonstrated that Cl counts in surface sediments are strongly correlated with salinity above the sediment-water interface at the time of deposition, and thus have the potential to provide information about the paleosalinity/potability of shallow surface water in Chumkopo and Pac Chen. Chloride is likely trapped within the interstices of the sediment and OM, as the Cl was easily rinsed away by one round of washing (Figure 3B). Since Pac Chen and Chumkopo are connected to the regional aquifer, they presumably experience minimal water table drawdown during droughts because they are buffered by the MeWM beneath them, though there can still be considerable concentration of Cl in the shallow areas because of marginal restriction (Figure 9a). The Cl salinity proxy is best tuned to record concentration changes driven by evaporation, rather than dilution by rainfall, making it useful for investigating cloud-free warm days, which are tied to local and regional air and SST (Clement et al., 1999; Mo and Lettenmaier, 2016). The method cannot, however, distinguish between the controls responsible for Cl dilution in sediments. For instance, it cannot discern between the impact of a succession of rainfalls from a hurricane, and a return to baseline salinity associated with water-column instability and seasonal overturn. Investigations into lake dynamics will reveal information regarding instability and overturn within the lakes themselves to better understand this aspect.

Despite these potential limitations, interpretation of the CKC3 and PC4 records is relatively straightforward, and perhaps simpler than other methods for

reconstructing dryness, such as speleothem and microfossil $\delta^{18}O$ and $\delta^{13}C$. For instance, interpretations of stable isotope measures in speleothems and lacustrine microfossils rely on multiple assumptions about factors that affect the fractionation of isotopes, such as the source and isotope value of rainfall, closed-basin hydrology of lakes, water-column mixing in lakes, and temperature of carbonate precipitation. Furthermore, hiatuses in speleothem growth or lake sedimentation can produce gaps in the paleoclimate record (Brenner et al. 2003; Lachniet et al., 2012; Medina-Elizalde et al., 2016; Lechleitner et al., 2017). These geochemical analyses are often performed discretely in the interest of time and cost, which may result in a discontinuous record that could miss or gloss over specific events, especially if a growth hiatus or change in lake hydrology occurs. Many of these issues do not apply to sediment cores scanned with µXRF-CS, as the high-resolution scanning method and direct calibration with salinity in ppt makes for a reliable continuous proxy of evaporation as we demonstrate here.

5.4 LAKE EVAPORATION AND DYNAMICS

Whereas drought indices often focus on precipitation deficits and increase in temperature, it is also important to investigate the evaporative dynamics of drought (Hobbins et al., 2016). In its simplest form, drought is an extended imbalance between moisture supply and demand. Evaporation-dominated lakes with negative water balance, such as Chumkopo and Pac Chen, reflect climate signals through increased salinity in the epilimnion, as salinity in the upper waters of lakes

increases in between spring and summer when E>P, temperatures are increased and relative humidity is low (Boehrer and Schultze, 2008; Arnon et al., 2016). Surface evaporation from the ocean is a function of SST and atmospheric variables such as wind speed, temperature, latent heat flux, and cloud-free days (Katsaros, 2011; Xie, 2009). During summer when lake evaporation exceeds precipitation, surface fluxes of energy transport are mostly controlled by insolation, which results in a net input of heat into the lake and evaporation then concentrates salinity in the upper epilimnion (Katsaros, 2001; Kettle et al, 2012; Arnon et al., 2016). As the water heats up, its saturation potential also increases, allowing it to hold a higher concentration of salinity without inducing overturn, until insolation decreases and the saline layer is able to mix and diffuse into lower layers (Boehrer and Schultze, 2008; Sirota et al., 2016).

It is not unreasonable to associate increasing salinity with reductions in precipitation, as this relation has been observed in other large water bodies. From 1880 to 2002, salinity in central Florida Bay ranged from as low as 18 ppt to as high as 57 ppt, driven by regional rainfall variability and ocean-atmosphere interactions on inter-annual to decadal timescales (Cronin et al, 2002), likely similar to the phenomena observed at Pac Chen and Chumkopo. The recurrence of “flash droughts” may also be a reasonable explanation for the quick and dramatic onset of dry periods detected in Chumkopo and Pac Chen. Flash drought refers to a confluence of heat waves and dryness, relatively short periods of warm surface

temperature, and anomalously low and rapidly decreasing soil moisture (Mo and Lettenmaier, 2016). Precipitation-deficit flash droughts are driven by positive air temperature anomalies and a reduction of precipitation that drives down soil moisture, which further raises air temperature (Mo and Lettenmaier, 2016). The lack of precipitation is likely associated with clear skies and an increase in net radiation to the surface, which increase air temperature (Mo and Lettenmaier, 2016). Flash droughts may be driven by SST anomalies, though more research is required to elucidate this relationship (Mo and Lettenmaier, 2016).

Overturning induced by instability or rainfall periods may impact the sensitivity of the sediment Cl record to changes in overlying water-column salinity, as these episodes would dampen the impact of salinity concentration from evaporation by mixing the concentrated upper surface with more dilute water (Von Rohden et al., 2010). Frequent small rainfalls or less frequent larger events (i.e. hurricanes) could also be responsible for rapid decreases in salinity observed throughout both records. One hundred and seven hurricanes have struck the Yucatan Peninsula since 1851, though only 12 events hit within 75 km of Chumkopo (Brown et al, 2014). A hurricane would not need to pass directly over the lake for there to be enough rainfall to mix the water, so it is reasonable to assume that this could be a factor that has impacted long-term water-column salinity. Frappier et al. (2014) recorded 13 cave flooding events between ~700 and 1000 CE, from mud layers in a stalagmite from the Yucatan Peninsula, which confirms that hurricanes occurred

throughout the Terminal Classic Period.

6. CONCLUSIONS

Our data support a connection between Mesoamerican drought and climate variability in the north and tropical Atlantic. This study also presents a new method of recording and interpreting high-resolution drought-induced salinity changes in lake sediment records. The use of high-resolution µXRF-CS revealed sub-annual indicators of evaporation-induced salinization of two water bodies in the eastern Yucatan Peninsula that correspond to multiple documented dry periods, including the the 2.8 y BP dry event and Maya Terminal Classic Period, ca. 800-1000 CE. The method is capable of detecting and quantifying evaporative salinity changes in low-conductivity lacustrine systems. Calibration of µXRF-CS Cl counts to detect drought-induced salinity changes is straightforward, and the assumptions associated with it (i.e., mixing parameters, climate behaviour) are quantifiable. Future modeling studies will provide a more coherent understanding of evaporation and mixing dynamics in lakes. Calibration of Cl counts with *in situ* salinity values led to better estimations of salinity in the paleo record, which may provide better spatial and temporal estimates of the availability of fresh water resources during the Classic Maya disintegration. Lake dynamics have important implications for the availability and potability of fresh water during drought intervals. Further research is required to understand this process, but it does have important implications for the availability of fresh water resources during the Classic Maya droughts. The Cl sediment records can capture more sensitive events than other sediment and

speleothem-based paleo-proxies, owing to the small step size of the iTRAX µXRF core scanner. We also determined that the Cl records of salinity match other Holocene climate records from the Caribbean, including longer regional SST records and Bond events. Dry conditions identified by the Cl record accord with previously generated climate proxy records across the Yucatan Peninsula, and also correspond well with proxy records that reflect ocean-atmosphere dynamics in the Caribbean, such as changes in SST and SSS that point to larger teleconnections with AMO, and NH temperature change, suggesting that lake evaporation at Chumkopo and Pac Chen is consistent with larger teleconnective changes.

ACKNOWLEDGEMENTS Special thanks to Chris LeMalliot, Fred Devos, the staff at Zero Gravity Dive Center, and the Mexico Cave Exploration Project dive team for collecting the sediment cores and water samples for the salinity calibration throughout the Ox Bel Ha and Sac Actun cave systems. Special thanks to the owner Carlos Marin and Fabian Arriaga of Alltournative SA de CV for allowing access to the Pac Chen facility.

DECLARATION OF FUNDING Natural Sciences and Engineering Research Council (NSERC) Discovery Grants (EGR - 2015-057250) and the Canada Foundation for Innovation John R. Evans Leaders Fund (CFI-JELF grant 105-04523).

REFERENCES

1. Bauer-Gottwein, P., Gondwe, B. R., Charvet, G., Marín, L. E., Rebolledo-Vieyra, M., and Merediz-Alonso, G. (2011). Review: The Yucatán Peninsula karst aquifer, Mexico. Hydrogeology Journal, 19(3), 507-524.
2. Beddows, P. A. (2004). Groundwater hydrology of a coastal conduit carbonate aquifer: Caribbean coast of the Yucatán Peninsula, México (Doctoral dissertation, University of Bristol).
3. Beddows, P. A., Smart, P. L., Whitaker, F. F., and Smith, S. L., 2007, Decoupled fresh saline groundwater circulation of a coastal carbonate

aquifer: Spatial patterns of temperature and specific electrical conductivity: Journal of Hydrology, v. 346, p.18-32.

4. Bhattacharya, T., Chiang, J. C., and Cheng, W. (2017). Ocean-atmosphere dynamics linked to 800–1050 CE drying in Mesoamerica. Quaternary Science Reviews, 169, 263-277.
5. Blaauw, M., and Christen, J. A. (2011). Flexible paleoclimate age-depth models using an autoregressive gamma process. *Bayesian analysis*, *6*(3), 457-474.
6. Black, D. E., Abahazi, M. A., Thunell, R. C., Kaplan, A., Tappa, E. J., and Peterson, L. C. (2007). An 8-century tropical Atlantic SST record from the Cariaco Basin: Baseline variability, twentieth-century warming, and Atlantic hurricane frequency. Paleoceanography, 22(4).
7. Bond, G., Kromer, B., Beer, J., Muscheler, R., Evans, M. N., Showers, W., ... and Bonani, G. (2001). Persistent solar influence on North Atlantic climate during the Holocene. Science, 294(5549), 2130-2136.
8. Brenner, M., Hodell, D. A., Curtis, J. H., Rosenmeier, M. F., Binford, M. W., and Abbott, M. B. (2001). Abrupt climate change and pre-Columbian cultural collapse. Interhemispheric climate linkages, 87-104.
9. Brown, A. L., Reinhardt, E. G., van Hengstum, P. J., and Pilarczyk, J. E. (2013). A coastal Yucatan sinkhole records intense hurricane events. Journal of Coastal Research, 30(2), 418-428.
10. Carrillo-Bastos, A., G.A. Islebe, N. Torrescano-Valle, and N.E. González, 2010, Holocene vegetation and climate history of central Quintana Roo, Yucatan Peninsula, Mexico: Review of Palaeobotany and Palynology, v. 160, p. 189-196.
11. Carrillo-Bastos, A., Islebe, G. A., and Torrescano-Valle, N. (2013). 3800 years of quantitative precipitation reconstruction from the northwest Yucatan Peninsula. PloS one, 8(12), e84333.
12. Chagué-Goff, C., Chan, J. C. H., Goff, J., and Gadd, P. (2016). Late Holocene record of environmental changes, cyclones and tsunamis in a coastal lake, Mangaia, Cook Islands. Island Arc, 25(5), 333-349.
13. Cook, B. I., Anchukaitis, K. J., Kaplan, J. O., Puma, M. J., Kelley, M., and Gueyffier, D. (2012). Pre-Columbian deforestation as an amplifier of drought in Mesoamerica. Geophysical Research Letters, 39(16).
14. Clement, A. C., Seager, R., and Cane, M. A. (1999). Orbital controls on the El Niño/Southern Oscillation and the tropical climate. Paleoceanography, 14(4), 441-456.
15. Cronin, T. M., Dwyer, G. S., Schwede, S. B., Vann, C. D., and Dowsett, H. (2002). Climate variability from the Florida Bay sedimentary record: possible teleconnections to ENSO, PNA and CNP. *Climate Research*, *19*(3), 233-245.

16. Croudace, I. W., Rindby, A., and Rothwell, R. G. (2006). ITRAX: description and evaluation of a new multi-function X-ray core scanner. Geological Society, London, Special Publications, 267(1), 51-63.
17. Croudace, I.W., Rothwell, R.G., (2015). Micro-XRF studies of sediment cores in Developments in Paleoenvironmental Research. Springer
18. Curtis J., Hodell D. and Brenner M. (1996) Climate variability on the Yucatan Peninsula (Mexico) during the past 3500 years, and implications for Maya cultural evolution. Journal of Quaternary Research 46, 37-47.
19. Giannini, A., Cane, M. A., and Kushnir, Y. (2001). Interdecadal changes in the ENSO teleconnection to the Caribbean region and the North Atlantic Oscillation. Journal of Climate, 14(13), 2867-2879.
20. Giannini, A., Kushnir, Y., and Cane, M. A. (2001). Seasonality in the impact of ENSO and the North Atlantic high on Caribbean rainfall. Physics and Chemistry of the Earth, Part B: Hydrology, Oceans and Atmosphere, 26(2), 143-147.
21. Gill, R. B (2000). The great maya droughts: water life and death. University of New Mexico Press.
22. Haug, G. H., Hughen, K. A., Sigman, D. M., Peterson, L. C., and Röhl, U. (2001). Southward migration of the intertropical convergence zone through the Holocene. Science, 293(5533), 1304-1308.
23. Haug G., Gunther D., Peterson L., Sigman D., Hughen K. and Aeschlimann B. (2003) Climate and the collapse of Maya civilization. Science 299, 1731-1735.
24. Hennekam, R., and de Lange, G. (2012). X-ray fluorescence core scanning of wet marine sediments: methods to improve quality and reproducibility of high-resolution paleoenvironmental records. Limnol. Oceanogr. Methods, 10(12), 991-1003.
25. Hobbins, M. T., Wood, A., McEvoy, D. J., Huntington, J. L., Morton, C., Anderson, M., and Hain, C. (2016). The evaporative demand drought index. Part I: Linking drought evolution to variations in evaporative demand. *Journal of Hydrometeorology*, *17*(6), 1745-1761.
26. Hodell D., Curtis J. and Brenner M. (1995) Possible role of climate in the collapse of Classic Maya civilization. Nature 375, 391-394.
27. Hodell, D. A., Brenner, M., Curtis, J. H., and Guilderson, T. (2001). Solar forcing of drought frequency in the Maya lowlands. Science, 292(5520), 1367-1370.
28. Hodell, D. A., Brenner, M., and Curtis, J. H. (2005). Terminal Classic drought in the northern Maya lowlands inferred from multiple sediment cores in Lake Chichancanab (Mexico). Quaternary Science Reviews, 24(12), 1413-1427.
29. Kennett D., Brietenbach S., Aquino V., Asmerom Y., Awe J., Baldini J., Bartlein P., Culleton B., Ebert C., Jazwa C., Macri M., Marwan N., Polyak

V., Prufer K., Ridley H., Sodemann H., Winterhalder B. and Haug G. (2012) Development and disintegration of Maya political systems in response to climate change. Science 338, 788-791.

30. Kobashi, T., Goto-Azuma, K., Box, J. E., Gao, C. C., and Nakaegawa, T. (2013). Causes of Greenland temperature variability over the past 4000 yr: implications for northern hemispheric temperature changes. Climate of the Past, 9(5), 2299-2317.
31. Kovacs, S. E., Reinhardt, E. G., Chatters, J. C., Rissolo, D., Schwarcz, H. P., Collins, S. V., ... and Erreguerena, P. L. (2017). Calcite raft geochemistry as a hydrological proxy for Holocene aquifer conditions in Hoyo Negro and Ich Balam (Sac Actun Cave System), Quintana Roo, Mexico. *Quaternary Science Reviews*, *175*, 97-111.
32. Krywy-Janzen, A., Reinhardt, E., McNeill-Jewer, C., Coutino, A., Waltham, B., Stastna, M., ... & van Hengstum, P. (2019). Water-level change recorded in Lake Pac Chen Quintana Roo, Mexico infers connection with the aquifer and response to Holocene sea-level rise and Classic Maya droughts. Journal of Paleolimnology, 62(4), 373-388
33. Lachniet, M. S., Bernal, J. P., Asmerom, Y., Polyak, V., and Piperno, D. (2012). A 2400 yr Mesoamerican rainfall reconstruction links climate and cultural change. Geology, 40(3), 259-262.
34. Lazar, B., Sivan, O., Yechieli, Y., Levy, E.J., Antler, G., Gavrieli, I., and Stein, M.,2014, Long-term freshening of the Dead Sea brine revealed by porewater Cl and d18O in ICDP Dead Sea deep-drill: Earth and Planetary Science Letters, v. 400, p. 94–101, doi: 10 .1016 /j .epsl .2014 .03 .019.
35. Lechleitner, F. A., Breitenbach, S. F., Rehfeld, K., Ridley, H. E., Asmerom, Y., Prufer, K. M., ... and Polyak, V. (2017). Tropical rainfall over the last two millennia: evidence for a low-latitude hydrologic seesaw. *Scientific reports*, *7*(1), 1-9.
36. Magaña, V., Amador, J. A., and Medina, S. (1999). The midsummer drought over Mexico and Central America. Journal of Climate, 12(6), 1577-1588.
37. Magaña, V. O., Vázquez, J. L., Pérez, J. L., and Pérez, J. B. (2003). Impact of El Niño on precipitation in Mexico. Geofísica internacional, 42(3), 313-330.
38. Medina-Elizalde, M., and Rohling, E. J. (2012). Collapse of Classic Maya civilization related to modest reduction in precipitation. Science, 335(6071), 956-959.
39. Medina-Elizalde, M., Burns, S. J., Polanco-Martínez, J. M., Beach, T., Lases-Hernández, F., Shen, C. C., and Wang, H. C. (2016). High-resolution speleothem record of precipitation from the Yucatan Peninsula spanning the Maya Preclassic Period. Global and Planetary Change, 138, 93-102.

40. Méndez, M., and Magaña, V. (2010). Regional aspects of prolonged meteorological droughts over Mexico and Central America. Journal of Climate, 23(5), 1175-1188.
41. Mendoza, B., García-Acosta, V., Velasco, V., Jáuregui, E., and Díaz-Sandoval, R. (2007). Frequency and duration of historical droughts from the 16th to the 19th centuries in the Mexican Maya lands, Yucatan Peninsula. Climatic Change, 83(1-2), 151-168.
42. Mo, K. C., and Lettenmaier, D. P. (2016). Precipitation deficit flash droughts over the United States. *Journal of Hydrometeorology*, *17*(4), 1169-1184.
43. Peros, M., S. Collins, A. A. G'Meiner, E. Reinhardt, and F. M. Pupo (2017), Multistage 8.2 kyr event revealed through high-resolution XRF core scanning of Cuban sinkhole sediments, Geophys. Res. Lett., 44, doi:10.1002/ 2017GL074369.
44. Perry, E., Paytan, A., Pedersen, B., and Velazquez-Oliman, G. (2009). Groundwater geochemistry of the Yucatan Peninsula, Mexico: constraints on stratigraphy and hydrogeology. Journal of Hydrology, 367(1), 27-40.
45. Schneider, T., Bischoff, T., and Haug, G. H. (2014). Migrations and dynamics of the intertropical convergence zone. Nature, 513(7516), 45-53.
46. Smart, P. L., Beddows, P. A., Coke, J., Doerr, S., Smith, S., and Whitaker, F. F. (2006). Cave development on the Caribbean coast of the Yucatan Peninsula, Quintana Roo, Mexico. Geological Society of America Special Papers, 404, 105-128.
47. Stahle, D. W., Cook, E. R., Burnette, D. J., Villanueva, J., Cerano, J., Burns, J. N., ... and Szejner, P. (2016). The Mexican Drought Atlas: Tree-ring reconstructions of the soil moisture balance during the late pre-Hispanic, colonial, and modern eras. Quaternary Science Reviews, 149, 34-60.
48. Stoessell, R. K., and Coke, J. G. (2006). An explanation for the lack of a dilute freshwater lens in unconfined tropical coastal aquifers: Yucatan example.
49. Torrence, C., and Compo, G. P. (1998). A practical guide to wavelet analysis. Bulletin of the American Meteorological society, 79(1), 61-78.
50. van Hengstum, P. J., E.G. Reinhardt, P.A. Beddows, and J.J. Gabriel, 2010. Linkages between Holocene paleoclimate and paleohydrogeology preserved in a Yucatan underwater cave: Quaternary Science Reviews, v. 29, no. 19-20, p. 2788-2798.
51. Vásquez-Bedoya, L. F., Cohen, A. L., Oppo, D. W., and Blanchon, P. (2012). Corals record persistent multidecadal SST variability in the Atlantic Warm Pool since 1775 AD. Paleoceanography, 27(3).

52. Von Rohden, C., Boehrer, B., and Ilmberger, J. (2010). Evidence for double diffusion in temperate meromictic lakes. Hydrology and Earth System Sciences, 14(4), 667.
53. Wanner, H., Solomina, O., Grosjean, M., Ritz, S. P., and Jetel, M. (2011). Structure and origin of Holocene cold events. Quaternary Science Reviews, 30(21-22), 3109-3123.
54. Wu, H. C., Felis, T., Scholz, D., Giry, C., Kölling, M., Jochum, K. P., and Scheffers, S. R. (2017). Changes to Yucatán Peninsula precipitation associated with salinity and temperature extremes of the Caribbean Sea during the Maya civilization collapse. Scientific reports, 7(1), 15825.
55. Xie, S.-P., 2009: Ocean–atmosphere interaction and tropical climate. Tropical Meteorology, Y. Wang, Ed., The Encyclopedia of Life Support Systems (EOLSS), UNESCO/EOLSS, 189–201

CHAPTER 3 APPENDIX

A.1 AGE MODELS

All ^{14}C dates were obtained from DirectAMS, Bothell, WA.

A.2 WAVELET ANALYSIS

Wavelet coherence is defined as the absolute value squared of the smoothed cross wavelet spectra, normalized by the smoothed wavelet power spectra. The wavelet coherence is closely related to the traditional statistical correlation, however it correlates the spectra rather than the raw data. This type of analysis is commonly used in geophysics (Grinsted et al., 2004; Ng et al., 2012; Torrence and Compo, 1998) and has been used to look at the periodicity of historical droughts within Mexico (Mendoza et al., 2006, 2007). By using the complex Morlet wavelet, the cross-wavelet spectrum contains phase information in addition to amplitude, and this allows for phase changes to be represented as an arrow, with a right-point arrow indicating in phase, whereas a left-point arrow indicates 180º out of phase.

A.3 COMPARISON TO LOCAL RECORDS

The Chumpac record reflects climate anomalies highlighted in other records from multiple sites in the Yucatan Peninsula, including the Punta Laguna ostracod $\delta^{18}O$ record (Figure A.2B), the Chichancanab sediment density record (Figure A.2C), and Tecoh speleothem $\delta^{18}O$ record (Figure A.2C). Punta Laguna is within 15 km of Pac Chen (84 km from Chumkopo), Chichancanab is in the middle of the Yucatan Peninsula, and the Tecoh speleothem is from the state of Yucatan. These

records were previously used to identify dry periods in the Yucatan Peninsula associated with the MTC, but have lower resolutions and sensitivities than the Chumpac record. There is good correspondence between the Chumpac Cl record and Chichancanab density because they both record evaporative trends in surface water, whereas the Punta Laguna ostracod $\delta^{18}O$ record probably reflects bottom-water isotope values and is less sensitive to short-term evaporative trends.

APPENDIX REFERENCES

1. Croudace, I. W., Rindby, A., and Rothwell, R. G. (2006). ITRAX: description and evaluation of a new multi-function X-ray core scanner. Geological Society, London, Special Publications, 267(1), 51-63.
2. Croudace, I.W., Rothwell, R.G., (2015). Micro-XRF studies of sediment cores in Developments in Paleoenvironmental Research. Springer
3. Gregory, B. R., Reinhardt, E. G., Macumber, A. L., Nasser, N. A., Patterson, R. T., Kovacs, S. E., and Galloway, J. M. (2017). Sequential sample reservoirs for Itrax-XRF analysis of discrete samples. Journal of Paleolimnology, 57(3), 287-293.
4. Grinsted, A., Moore, J. C., and Jevrejeva, S. (2004). Application of the cross wavelet transform and wavelet coherence to geophysical time series. Nonlinear processes in geophysics, 11(5/6), 561-566
5. Hennekam, R., and de Lange, G. (2012). X-ray fluorescence core scanning of wet marine sediments: methods to improve quality and reproducibility of high-resolution paleoenvironmental records. Limnol. Oceanogr. Methods, 10(12), 991-1003.
6. Kovacs S., Reinhardt G., Statsna M., Coutino A., Werner C., Collins S., Devos F., Le Maillot C. (2017) Hurricane Ingrid and Tropical Storm Hanna's effects on the salinity of the coastal aquifer, Quintana Roo, Mexico. Journal of Hydrology
7. Krywy-Janzen et al, 2017
8. Löwemark, L., Chen, H. F., Yang, T. N., Kylander, M., Yu, E. F., Hsu, Y. W., ... and Jarvis, S. (2011). Normalizing XRF-scanner data: a cautionary note on the interpretation of high-resolution records from organic-rich lakes. Journal of Asian Earth Sciences, 40(6), 1250-1256.

9. Meacham, S. S. (2012). Using Landsat 5 TM Data to Identify and Map Areas of Mangrove in Tulum, Quintana Roo, Mexico.
10. Mendoza, B., García-Acosta, V., Velasco, V., Jáuregui, E., and Díaz-Sandoval, R. (2007). Frequency and duration of historical droughts from the 16th to the 19th centuries in the Mexican Maya lands, Yucatan Peninsula. Climatic Change, 83(1-2), 151-168.
11. Ng, E. K., and Chan, J. C. (2012). Geophysical applications of partial wavelet coherence and multiple wavelet coherence. Journal of Atmospheric and Oceanic Technology, 29(12), 1845-1853.
12. Tjallingii, R., Röhl, U., Kölling, M., and Bickert, T. (2007). Influence of the water content on X-ray fluorescence core-scanning measurements in soft marine sediments. Geochemistry, Geophysics, Geosystems, 8(2).

CHAPTER 3 TABLES

Table A.1: Radiocarbon information for PC4 and CKC3. BO= Bulk Organic, T= Twig, C= Charcoal. Note: A HWE of 1266 years was added to the CKC3 bulk dates in BACON.

Core	Core Depth **(cm)**	**Conventional ^{14}C age**	**Material**	**Lab Code**	**Calibrated yrs BP (2 σ confidence interval)**
CKC3	18.5 - 19.5	1929 ± 28	BO	D-AMS 019675	565-603
CKC3	34.5- 35.5	2137 ± 38	BO	D-AMS 019674	703-786
CKC3	71 - 72	3437 ± 54	BO	D-AMS 019673	1935-2199
CKC3	99 - 100	3925 ±38	BO	D-AMS 019677	2743-2844
CKC3	152.5 - 153.5	4539 ±33	BO	D-AMS 019676	3268-4435
CKC3	180.5 - 181.5	4843 ± 40	BO	D-AMS 019678	3612-3750
PC4	18 - 19	367±24	T	D-AMS 013071	426-498
PC4	50.5 – 51.5	1153±24	T	D-AMS 013072	1044-1150
PC4	75.5 - 76.5	1825±24	C	D-AMS 013077	1706-1823
PC4	93 - 94	1876±26	T	D-AMS 013070	1734-1877

Table A.2: Core data used for salinity calibration curve. Abbreviations for lithologies are as follows- M: Mud, G: Gyttja, CR: Calcite Raft. Abbreviations for site are C for core taken in a cave, and L for core taken in a surface lake. Estimated salinity was calculated using the equation in Figure 3.

Sample Name	Core Location	Site	Type	Water Depth (m)	Cl original counts	Salinity (ppt)	Estimated Salinity (ppt)	Difference (ppt)	Rinsed Cl counts
JH2	Jailhouse	C	G	26.6	14924	28.6	28.09	0.51	293
YC1	Isod	C	G	13.2	8650	16.5	16.16	0.34	240
YC3	Yax Chen	C	M	7.8	3792	4.9	6.93	-2.03	51
T1	Tortuga	C	M		855	1.5	1.35	0.15	34
R1	Regina	C	CR	17.2	1479	1.8	2.54	-0.74	214
R2	Regina	C	M	20.2	11141	30.5	20.9	9.6	185
MB1	Mayan Blue	C	M	16.8	2712	6	4.88	1.12	145
MB2	Mayan Blue	C	M	13.5	1012	2.3	1.65	0.65	151
YC2	Lil Chen	C	M	15.2	6587	13.7	12.24	1.46	236
XH2	Xunnan Ha	C	M	14.7	9056	27.8	16.94	10.86	249
CKC3	Chumkopo	L	M	0.5	687	1.1	1.04	0.06	-
PC4	Pac Chen	L	G	0.4	259	0.5	0.22	0.28	-
YC_C33	Yax Chen	C	G	9.1	43529	6	8	-2	-
YC_C3	Yax Chen	C	G	9.1	6345	9	11.79	-2.79	-
YC_C37	Yax Chen	C	G	10.3	7372	10	13.74	-3.74	-

YC_C 2	Yax Chen	C	G	14	14913	18	28.07	-10.07	-
IB	Ich Balam	C	CR	2	810.1	1.1	1.27	-0.17	-

CHAPTER 3 FIGURES

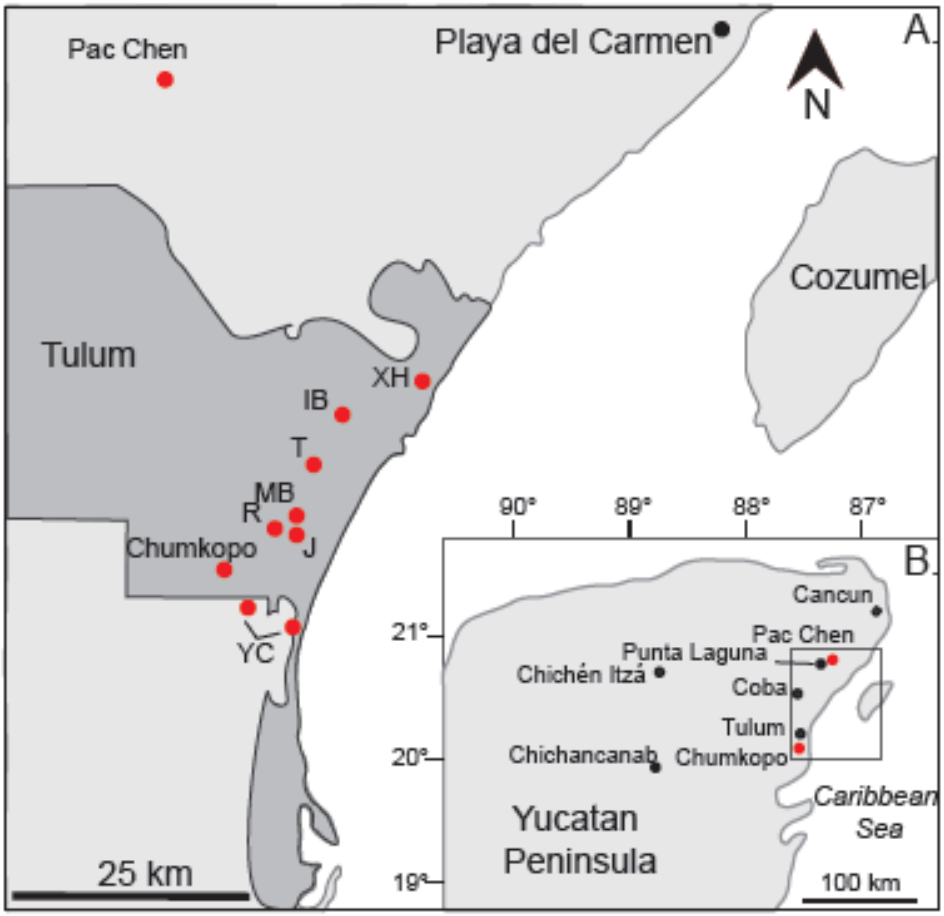

Figure 1. Map of the Yucatan Peninsula with core locations. A. Locations of cores for this study in red, cities in black. B (inset) map of Yucatan Peninsula.

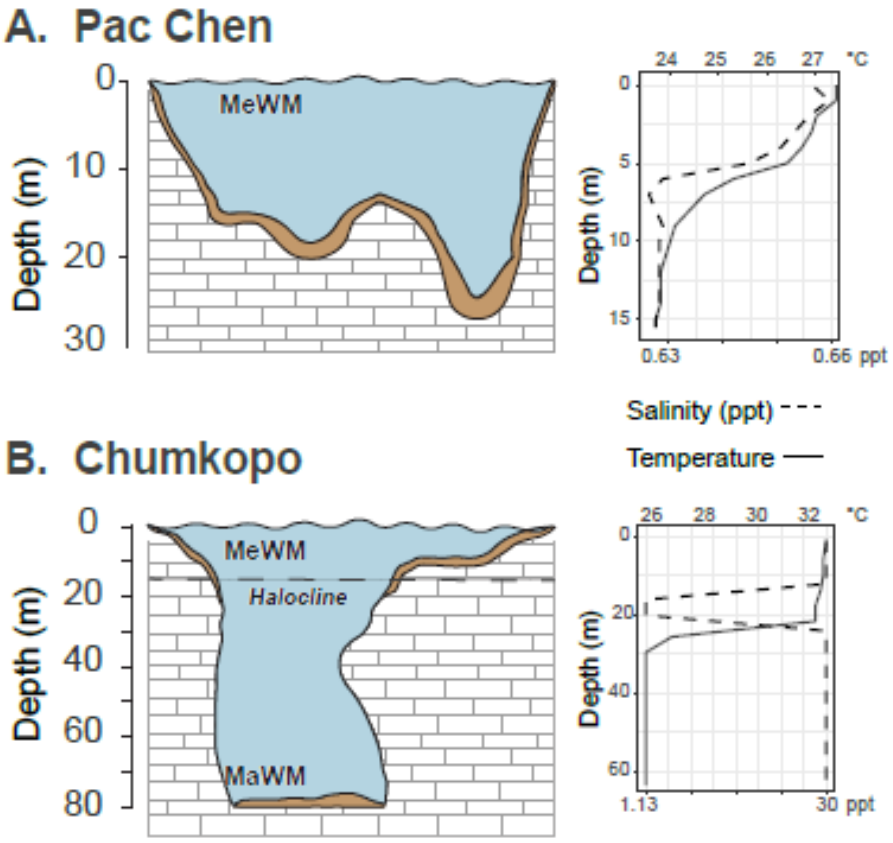

Figure 2. Depth profiles of Pac Chen (A) and Chumkopo (B) including water column salinity and temperature (from Krywy-Janzen et al., 2019; Fig 3 and Brown et al., 2014; Fig 3).

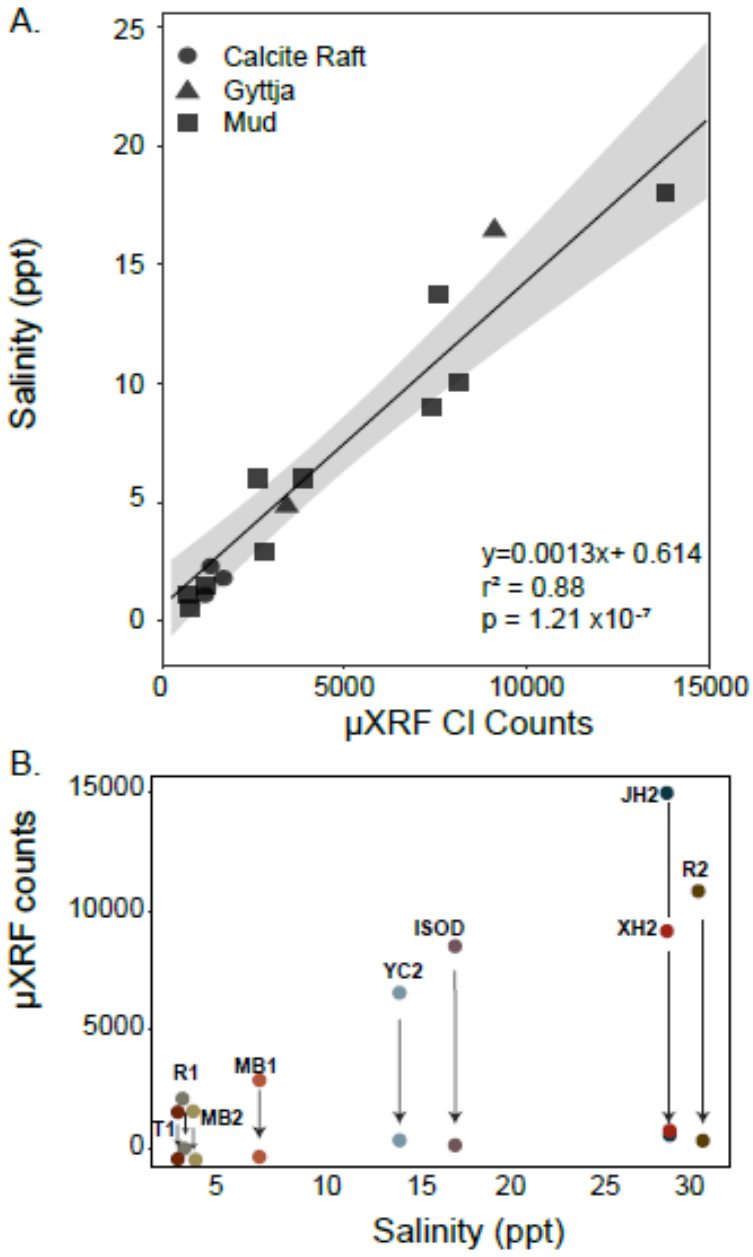

Figure 3. A) Relationship between sediment core-top Cl (counts) and measured environmental salinity (ppt) and the line of best fit. The grey bar represents standard error. B) Cl counts before and after washing with deionized water.

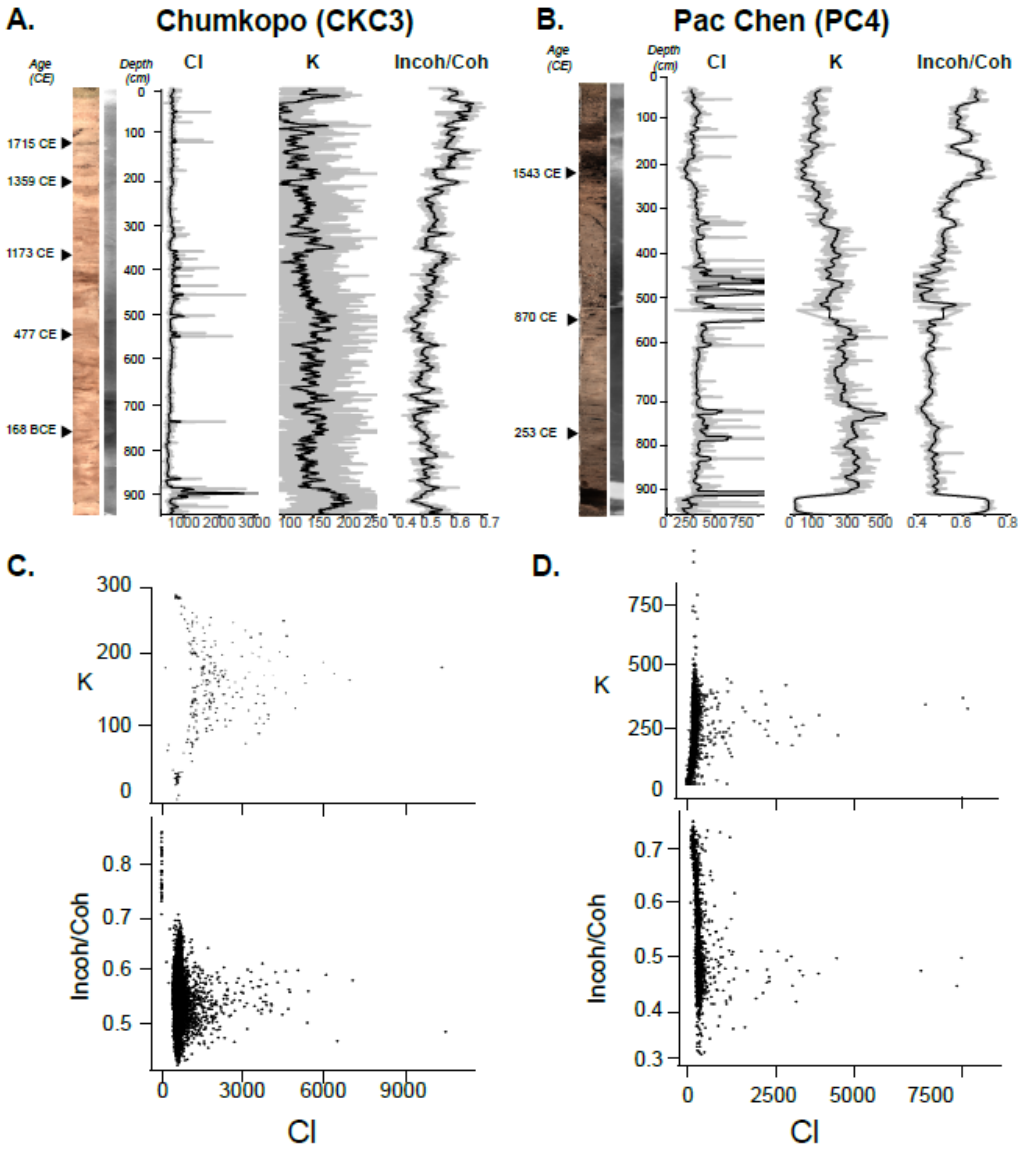

Figure 4. Core images with dates, intervals and cross plots of Cl, Incoherent/Coherent backscatter ratio and K. A) Chumkopo core image with radiograph and ^{14}C dates. Cl, K and Incoherent/Coherent backscatter values plotted with 10-year running mean. B) Pac Chen core image with radiograph and ^{14}C dates. Cl, K and Incoherent/Coherent backscatter values plotted with 10-year running mean. C) Cross plots of K and Incoherent/Coherent backscatter compared to Cl from Chumkopo. D) Cross plots of K and Incoherent/Coherent backscatter compared to Cl from Pac Chen.

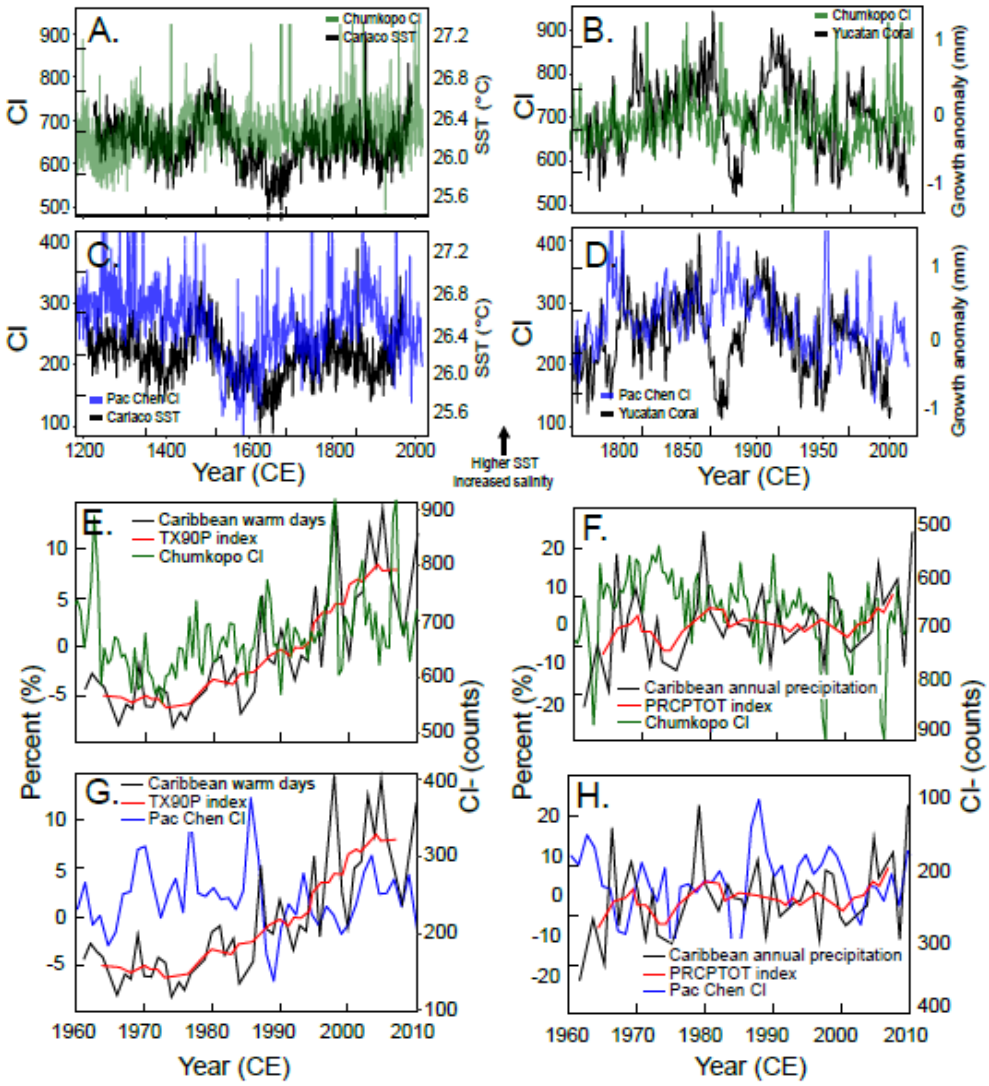

Figure 5. Comparison of various climate records with PC4 and CKC3. A) Chumkopo Cl record with Cariaco Basin SST record from 1200 to 2000 CE. B) Chumkopo Cl record with Yucatan coral growth anomalies from 1800 to 2000 CE. C) Pac Chen Cl record with Cariaco Basin SST record from 1200 to 2000 CE. D). Pac Chen Cl record with Yucatan coral growth anomalies from 1800 to 2000 CE. E) Recent Caribbean warm days index with Chumkopo Cl record from 1960 to 2010. F) Recent Caribbean annual precipitation index with Chumkopo Cl record from 1960 to 2010. G) Recent Caribbean warm days index with Pac Chen Cl record from 1960 to 2010. H) Recent Caribbean annual precipitation index with Pac Chen Cl record from 1960 to 2010.

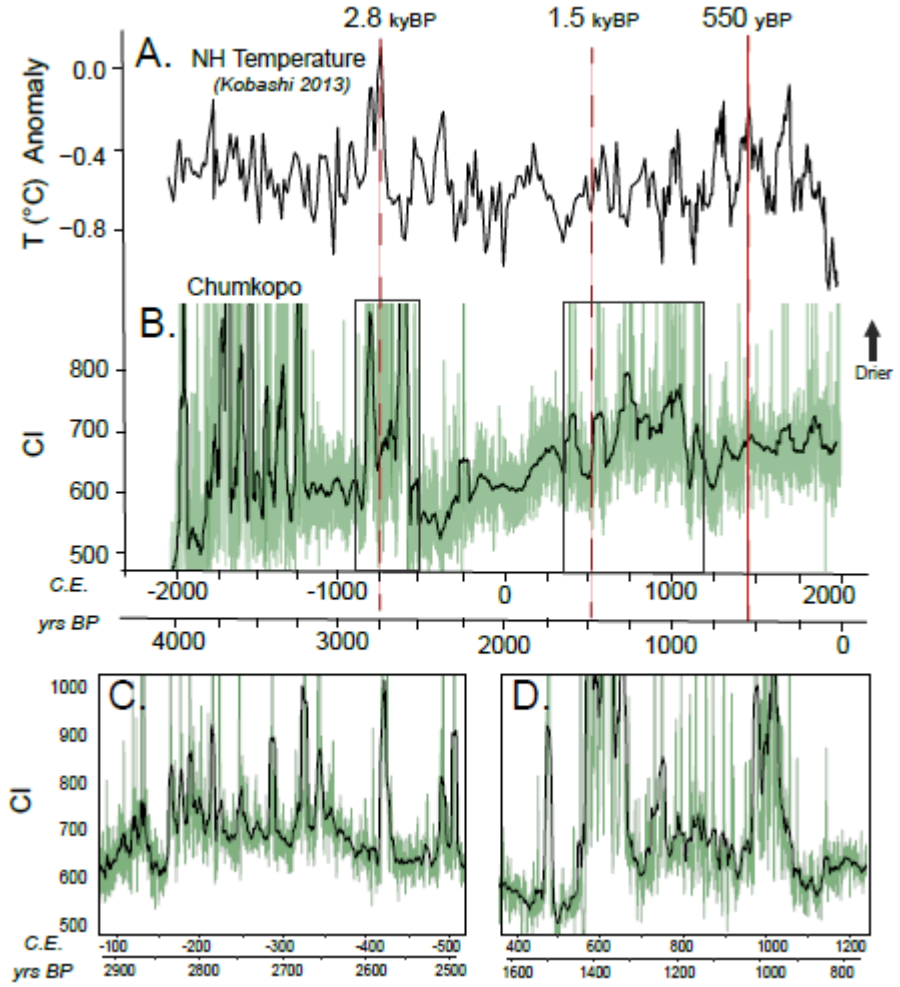

Figure 6. Comparison of Northern Hemisphere reconstructed temperature with Greenland reconstructed temperature and Chumkopo Cl record highlights similarities between major events in Yucatan and the broader Northern Hemisphere. A) Northern Hemisphere temperature anomaly reconstruction by Kobashi 2013. B) Chumkopo Cl record spanning the last 4000 years. C) Chumkopo Cl record from 1600 to 800 years BP. D) Chumkopo Cl record from 2900 to 2500 years BP highlighting the 2.8 ky BP dry event.

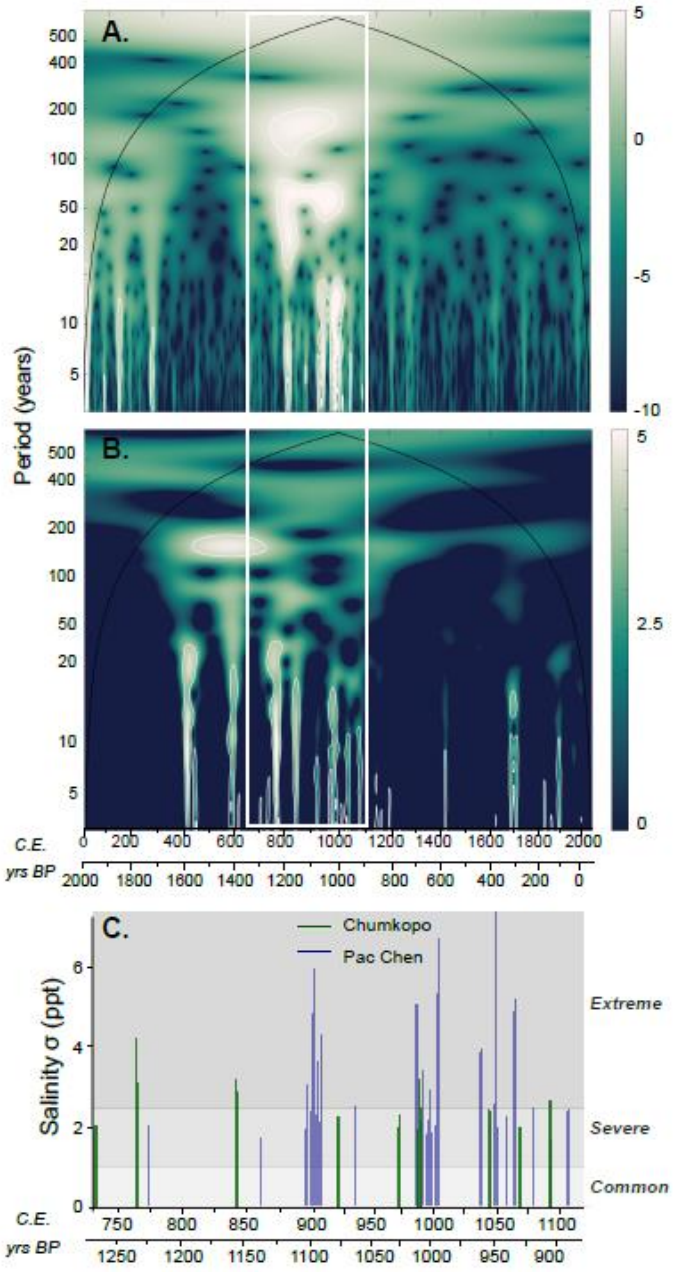

Figure 7. Individual wavelet plots for PC4 and CKC3 with water stress indicator**.** A) PC4 wavelet plot. B) CKC3 wavelet plot. C) Water stress indicator based on standard deviation of salinity values during the highlighted period in A and B (600-900 CE).

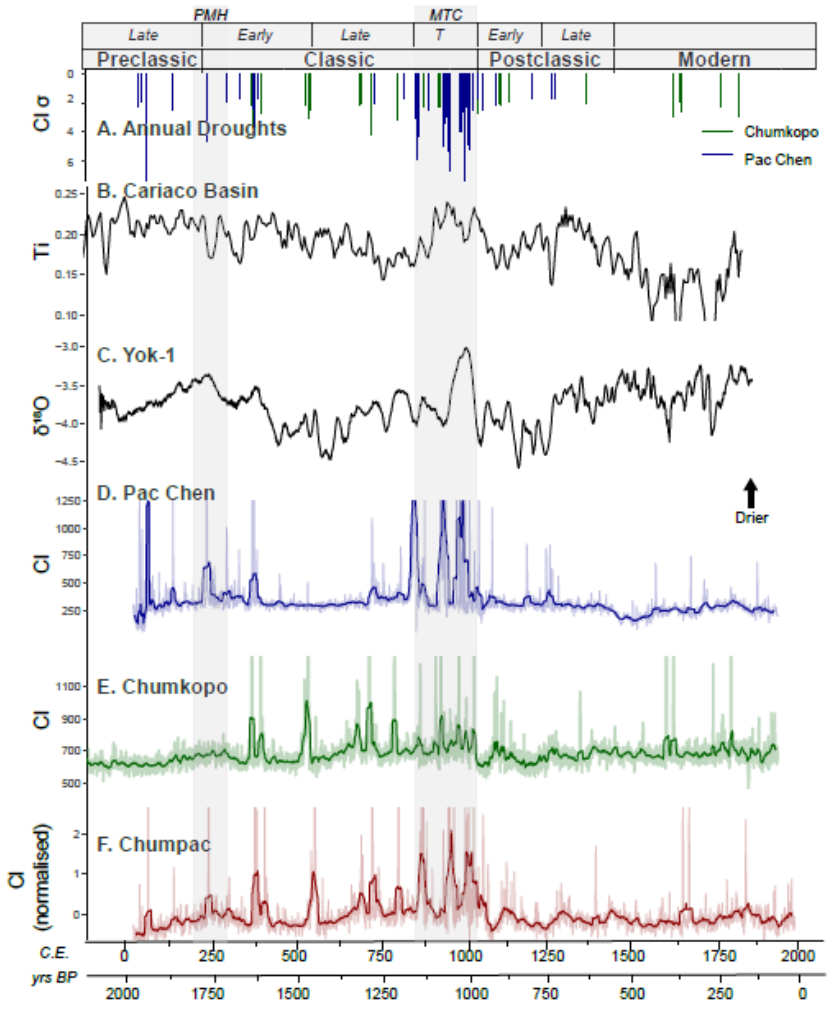

Figure 8. Multiproxy paleoclimate record comparison of Chumkopo and Pac Chen Cl with Yok Balum speleothem, and Cariaco Basin. A) Yearly drought record based on Cl standard deviation. B) Cariaco Basin Ti record. C) Yok Balum speleothem $\delta^{18}O$ record. D) Pac Chen Cl record. E) Chumkopo Cl record. F) Combined 'Chumpac' Cl record.

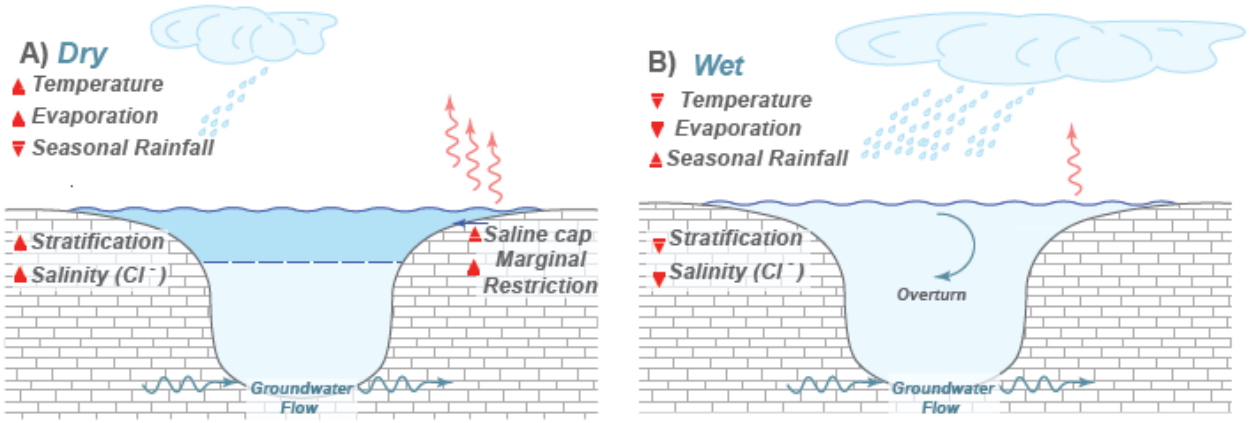

Figure 9. Proposed schematic of lake mixing and evaporation dynamics with comparison of Pac Chen Cl signals with depth. A) Parameters involved in lake evaporation and concentration during an anomalous dry period. B) Parameters involved in lake evaporation during wet periods.

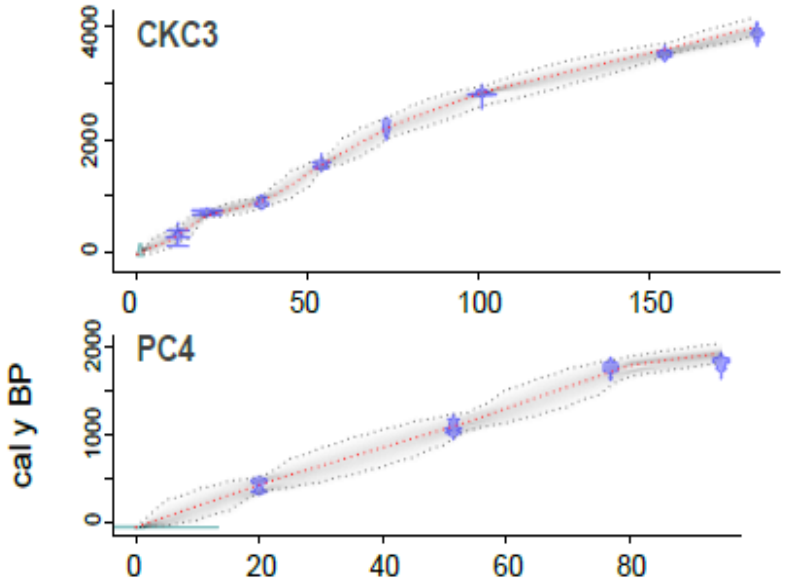

Figure A.1: BACON age models for Pac Chen and Chumkopo.

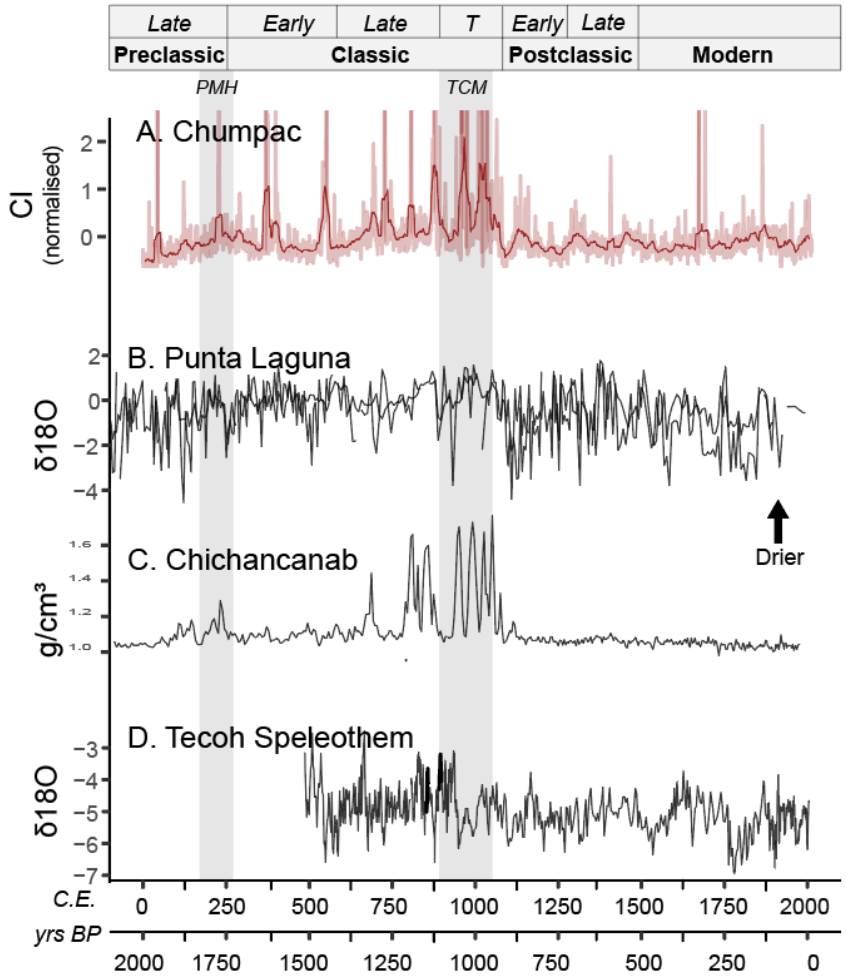

Figure A.2. Regional Yucatan Peninsula climate proxies compared to normalised Chumpac record. A) Chumpac record (Pac Chen, Chumkopo, Quintana Roo. B) Punta Laguna $\delta^{18}O$ of ostracod species *Cytheridella ilosvayi* and *Pyrgophorus coronatus* (Punta Laguna, Quintana Roo; Curtis et al., 1996). C) Lake Chichancanab sediment density record (Dzuiché, Yucatan; Hodell et al., 2008). D) Tecoh speleothem (Tzabnah Cave, Yucatan; Medina-Elizalde et al., 2010).

Mixing-induced salinity change in deep coastal Yucatan aquifer caused by hurricanes over the past 4 KY

McNeill-Jewer, C.A.[a], Reinhardt, E.G. [a], Coutino, A. [b], Stastna, M. [a], Devos, F., Meacham, S. and LeMaillot, C.[c]

[a] School of Earth, Environment and Society, McMaster University, 1280 Main St W, Hamilton Ontario

[b] Department of Applied Mathematics, University of Waterloo, 200 University Ave, Waterloo Ontario

[c] Mexico Cave Exploration Project (MCEP), Centro Investigador del Sistema Acuifero de Quintana Roo A.C. (CINDAQ), Global Underwater Explorers (GUE), Mexico

KEYWORDS: Hurricane, paleohurricane, chlorine, μXRF-CS, paleoclimatology, Yucatan Peninsula, Caribbean climate, groundwater mixing, ITCZ

ABSTRACT

Recently, instrumental monitoring has revealed that the passing of hurricanes near the eastern Yucatan Peninsula (Quintana Roo, Mexico) induces salinity changes in the coastal aquifer that can last weeks, a consequence of mixing of marine and meteoric groundwater masses. This phenomenon, however, has not been fully investigated in the paleo-record, as currently there is only limited evidence that rainfall-induced mixing occurred in the aquifer in the past. The position/depth of the mixing zone within the coastal aquifer responds to long-term changes in wetness and aridity, which when better understood, can be used to elucidate the effect of climate change on the aquifer and future availability of potable groundwater. This study used sediment cores (~1-2 m long) from two cenotes (Angelita, Zapote) and one cave system (Yax Chen), which were located at four different water depths

(ISODC2; 13 m; ANGC3; 15 m, ZAPC1; 50 m; ANGC1; 75 m). These radiocarbon-dated cores show stratigraphic fluctuations in Cl, Fe, Ti, S and K (µXRF core scanning) since the-mid Holocene (~4000 yr BP) that correspond with established paleo-climate records for the Caribbean region. The core locations are presently positioned at the transition between the meteoric and marine water masses (halocline and the mixed water mass; ISOD C2 and ANGC3), and within the marine water mass (ZAPC1, ANG C1). The shallower-water cores (ISODC2, ANGC3) show increased salinity (Cl) from ~ 2750-1250 yr BP, but over the same time period, the deeper core (ZAPC1) shows decreasing salinity (Cl). That period corresponds to a time of increased hurricane activity in the Caribbean, previously documented at Blackwood Sinkhole, Bahamas. The two cores taken near/above the halocline in the meteoric water mass exhibit geochemical responses to rainfall-induced mixing events opposite those in two cores taken from below the halocline in the marine water mass. This implies that there were long-term impacts of rainfall-induced mixing in the Yucatan aquifer, but also provides the first paleo-mixing record based on Cl and evidence of water-mass mixing as a result of increased hurricane frequency caused by climate change. The long-term impacts of hurricanes and heavy rainfall on the Yucatan Peninsula aquifer imply that greater rainfall (predicted for the near future) causes more mixing between the two water masses and reduces aquifer water quality because of salinization.

1. INTRODUCTION

The Yucatan Peninsula exhibits complex geoarcheology, paleoecology and paleoclimatology because it is affected by multiple climate phenomena and has an extensive history of human settlement, extending back > 3000 years. Evidence for the impacts of past hurricanes and droughts on ancient Maya Civilization, and instrumental evidence from recent hurricanes and dry periods highlight the importance of studying the effect of wetness and dryness on the Yucatan Peninsula aquifer over time (Medina-Elizalde et al., 2014; Kovacs et al., 2017; McNeill-Jewer et al., submitted). Whereas hurricanes deliver necessary moisture to the Yucatan Peninsula, they also destroy property and ecosystems that are valuable to the local tourist economy (Boose et al., 2003; Medina-Elizalde et al., 2016). Fifty-eight hurricanes have hit the Caribbean Coast of Mexico in recorded history (Jaugregi, 2003), and projections indicate hurricane frequency will increase along with future climate warming. This highlights the importance of understanding how groundwater resources will respond to ongoing climate change so that informed management strategies and preventive measures can be developed for the Mexican Caribbean (Saunders & Lea, 2008; Manuel-Navarrete et al., 2011; Sobel et al., 2016). Models predict a near doubling of the frequency of category 4 hurricanes and higher by the end of the 21st century, though there will be an overall decrease in total hurricane numbers (Bender et al, 2010; Grinstead et al, 2013; Holland & Bruyere, 2014). Coastal areas are particularly vulnerable to infrastructure destruction because they have been highly developed for tourism, and are thus at great risk of devastation

by natural disasters such as hurricanes (Saunders & Lea, 2008; Grinstead et al, 2013). Research suggests that meridional shifts in the ITCZ on geologic timescales can modulate hurricane activity, but continuous high-resolution paleoclimate records from multiple sites within the zone of ITCZ migration are needed to assess this (van Hengstum et al., 2016). Salinity of the meteoric water mass (MeWM) in the local aquifer varies over seasonal and longer-term wet/dry cycles and is dependent on the position of the halocline, which in turn is influenced by factors such as sea level (SL) position, tidal oscillations, drought, and storm frequency (Coutino et al., 2016; Kovacs et al., 2017; Brankovits et al., 2019; Ritter et al., 2019). Mixing occurs between the Meteroric Water Mass (MeWM) and Marine Water Mass (MaWM) to form a Mixed Water Mass (MxWM; mixing zone) that may be narrow or thick, depending on proximity to the coast. This mixing is a consequence of tides and rainfall that seem to be driven by intense meteorological events (e.g. hurricanes and tropical storms), causing instability between the water masses that can last for days to weeks (Kovacs et al., 2017; Kovacs et al. 2018, Coutino et al, 2017). Although rainfall-induced aquifer mixing has been observed with *in situ* measurements, only a few studies have examined the phenomenon over the long term (Holocene), using sediment cores (van Hengstum et al. 2010; Kovacs et al., 2017). This is because, until recently, there were few paleoclimate proxies or methods to investigate bottom-water mixing, though Brankovits et al. (2019) used instrumental monitoring to investigate bottom-water re-oxygenation and seasonal methane accumulation in a pit cenote on the Yucatan Peninsula.

Because mixing in the water column leads to salinity changes across the MeWM and MaWM, measurements of Cl preserved in sediment cores can provide a way to identify past changes in water mixing. Porewater Cl measured in sediment cores provides information on water salinity at the time of deposition (Lazar et al, 2014; Kiro et al, 2017; Levy et al, 2017; Kovacs et al., 2017; McNeill et al., submitted; Peros et al., 2017) and has been traditionally analyzed at fairly coarse resolution. With the advent of µXRF core scanning, sub-annual measurement has become feasible, even when sediments are not visibly laminated (Orme et al., 2015; McNeill-Jewer et al., submitted). Cl-based µXRF records have been used to document past wet and dry conditions (Peros et al., 2017; Kovacs et al., 2017a; McNeill-Jewer et al., submitted) and seawater intrusion (Chague-Goff et al., 2016).

2. SITE BACKGROUND

2.1. YUCATAN PENINSULA GEOLOGY AND AQUIFER

The Yucatan Peninsula (Figure 1) is a Cretaceous/Cenozoic-age karst limestone platform > 350,000 km^2 in area and is bordered by the Gulf of Mexico and the Caribbean Sea. The coastal deposits are relatively flat, resulting in a low hydraulic gradient (10-15 cm/km) towards the coast (Beddows, 2004). The limestone has a high net porosity, ranging from 14-23% that is both vertically and horizontally anisotropic, with increased porosity near fracture zones and the “Ring of Cenotes” in northern Yucatan (Smart et al., 2006; Beddows et al., 2007; Bauer-Gottwein et al., 2011). Multiple phases of dissolution associated with sea-level change have created extensive wet and dry cave conduits as well as sinkholes and karst

windows, locally known as cenotes (Back and Hanshaw, 1970, Beddows, 2004; Paytan et al., 2005; Smart et al., 2006). The coastal systems have multiple-scale porosity that consists of matrix, fracture, and cave conduit flow, with the majority of flow (~99%) within the conduits (Beddows et al., 2004; Smart et al., 2006). The karst geology of coastal Quintana Roo contributes to a lack of surficial lakes and sediment. Although there are many caves where speleothem records can be obtained, the uncertainties, time and cost associated with the analysis of speleothems make this method less feasible than sediment core collection. As more areas of the coastal Yucatan Peninsula are explored, shallow flooded caves and deep pit cenotes have become new prospects for the collection and interpretation of paleoclimate records. However, processes that preserve climate signals in the sediment are not yet fully understood, generally leaving them overlooked as paleoclimate archives. Recently there has been a move to using deep pit and cave-based proxies in the eastern Yucatan Peninsula, and preliminary studies indicate that they are reliable for recording wet and dry periods (van Hengstum et al., 2010; Collins et al., 2015; Kovacs et al., 2017; Stinnesbeck et al., 2018; Brankovits et al., 2019; McNeill-Jewer et al., 2019).

The Yucatan Peninsula aquifer is unconfined near the coast and is stratified according to salinity. Fresher, yet cooler MeWM sits on top of the warmer and more saline MaWM, which are separated by an interface, termed the halocline, or mixed water mass (MxWM). This can be observed in the salinity profiles in Figure 2. The salinity of the MeWM varies over wet and dry seasons and is influenced by

precipitation-induced mixing, tides and sea level, as well as mixing caused by movement of the halocline. The dry season in the Yucatan Peninsula is characterized by less mixing between the MeWM and MaWM than during the wet season (Coutino et al., 2017; Kovacs et al., 2017a; Brankovits et al., 2018). Measurements of salinity and temperature in the Yax Chen cave system revealed episodes of mixing between the MeWM and the MaWM, driven by meteorological events such as hurricanes and other large storms (Coutino et al, 2017). Rainfall-induced mixing is also responsible for rapid methane transport from shallow groundwater into the MaWM (Brankovits et al, 2018).

The MeWM becomes more saline moving towards the coast by virtue of increased mixing between the MeWM and MaWM as the former flows towards the coast. Flow within the MeWM increases towards the coast where tidal currents cause increased mixing with the MaWM and salinization of the MeWM. The consequent MxWM thins moving landward (Kovacs et al., 2017). This landward gradient differs spatially, depending on the predominance and density of cave passages and the extent of “coastal plugging,” which retards the flow of the MeWM to the coastal ocean. Water wells tend to have lower salinity than conduits, indicating that the water in the matrix portion of the aquifer is fresher because it is not subject to mixing, as in the more open conduits (Beddows et al., 2004; Coutino et al., 2017). As initially proposed in van Hengstum et al. (2010), during the dry season or protracted dry periods, the water column becomes more stably stratified, causing the MeWM to become fresher and the MaWM to become stagnant and anoxic.

During wetter times, the MeWM becomes more mixed and saline, while the MaWM gets fresher and oxygenated (Brankovits et al., 2018; Kovacs et al., 2017b). During wet periods, there is more mixing throughout the water column, resulting in more 'diffuse' salinity profiles that can extend into the MaWM.

Geochemical records from calcite raft deposits in Hoyo Negro and Ich Balam (near Playa del Carmen) indicate that during the last ~8500 years, salinity in the upper MeWM was higher during wetter times and lower during drier times (Kovacs et al, 2017b). There is, however, no information on how these water masses behaved spatially, either vertically or laterally, relative to the coast. This mixing relationship has important implications for aquifer quality, but we have little information about such mixing over larger climate cycles, especially with sea-level change during the Holocene. Groundwater level has been found to largely track Holocene sea-level rise, however there is little information on how water masses responded when the predominantly shallow (currently 10-15 m water depth) cave passages first flooded at ~ 8-7 ka (Kovacs et al., 2017, Collins et al, 2015, Krywy-Janzen et al 2019).

2.2. YUCATAN PENINSULA CLIMATE

The climate of the Yucatan Peninsula is dominated by evaporation, with annual rainfall maxima across the region as high as 1500 mm/y and as low as 500 mm/y, and evaporation potentials of 350-2500 mm/y (Brenner et al., 2001; Gianinni et al., 2001; Kushner, 2001; Bauer-Gottwein et al, 2011). Because of the high rates of evapotranspiration, the region is dependent on annual tropical depressions, storms

and hurricanes to maintain a positive net water balance (Bauer-Gottwein et al., 2011; Medina-Elizalde and Rohling, 2012; Nooren et al., 2018). Hurricane season reaches maximum activity in September on both Atlantic and Pacific coasts of Mexico (Jáuregui, 2003). Although hurricane frequency is lower for the Yucatan Peninsula than other coastal regions of Mexico, it is hit by more intense hurricanes than other areas, with five category 5 storms on the Gulf/Caribbean coast for every one on Pacific side (Jáuregui, 2003). According to Frappier et al. (2014), from 1951 to 2006 northern Yucatan and Quintana Roo were struck by 18 hurricanes, with a mean recurrence interval of 3.3 years. Most hurricanes approach the Yucatan Peninsula from the east-southeast with the greatest density of storms offshore to the north or northeast (Boose et al., 2003).

The Caribbean Basin experiences wet and dry extremes throughout El Niño Southern Oscillation (ENSO) cycles. Interannual variability in Mesoamerican rainfall is tied to ENSO, NAO, and changes in tropical North Atlantic SST (Giannini et al., 2000; Magana et al., 2003; Wang et al., 2009; Xie and Carleton, 2004). In warm El Niño conditions, there is dryness before the event, and wetness after, which is a direct response to warmer SST in the northern equatorial Pacific (Giannini et al., 2001). The annual precipitation cycle over south Mexico and Central America has a bimodal distribution, with maxima in June and September-October, and a relative minimum in July and August, known as the midsummer drought or ‘canicula.’ Mean annual precipitation in the northwest Caribbean is synchronous with variations in NAO, and wet (dry) years in the Caribbean and

central America are associated with warm (cold) north Atlantic and cold (warm) south Atlantic (Nyberg et al., 2001). A cooler north Atlantic relative to south increases surface pressure over the North Atlantic and promotes southward migration of the Inter Tropical Convergence Zone (ITCZ), which is a zone of deep convection and the most intense region of rainfall on Earth, generated by convergence of trade winds that migrate between 9 °N and 2 °N (Schneider et al., 2014). The mean position of the ITCZ (6 °N of the equator) is determined by energy transport from the Atlantic Ocean northward across the equator, which causes the Northern Hemisphere to be warmer than the Southern Hemisphere (Schneider et al., 2014). On seasonal and longer timescales, the ITCZ migrates towards whichever hemisphere is warmer, though there are exceptions (i.e., ENSO-Niño events). The ITCZ has likely helped modulate intense hurricanes across the western North Atlantic margin on millennial to centennial scales, and future northward shifts of the ITCZ may influence hurricane frequency and intensity in the North Atlantic (van Hengstum et al., 2016; Schneider et al., 2014).

2.3. CENOTES

Two distinct types of cenotes have resulted from dissolution of the limestone bedrock of the Yucatan Peninsula. The first type (lotic) is created through local collapse of a cave conduit ceiling, producing a sinkhole that is directly connected to the regional aquifer via cave passages (Schmitter-Soto et al., 2002; Smart et al., 2006). These cenotes are generally well oxygenated and wider than they are deep. The second type of cenote is called a lentic or pit cenote, which is produced by

dissolution at a discrete point, creating a deep sinkhole that is not connected to the aquifer via cave passages, but rather through matrix and fracture flow (Beddows, 2004). Pit cenotes are often deeper than they are wide, sometimes extending >100 m below the water table, and have anoxic bottom waters by virtue of reduced circulation within the water column. They have less hydraulic connection to the aquifer and are known to have turbid water with high concentrations of chlorophyll, and a hypolimnion rich in sediment and organic matter (Schmitter-Soto et al., 2002).

2.3.1. CENOTE ANGELITA

Cenote Angelita is a pit cenote located 10 km south of the town of Tulum, and 11.7 km inland. It is 60 m deep, with a large breakdown pile that begins 45 mbsl (Figure 2A). The hydrolab profile shows a distinct transition (MxWM) between the MeWM and MaWM at 30 mbsl, with marked changes in pH, temperature, salinity and dissolved oxygen. The bottom of Angelita is anoxic and is blanketed with dark organic sediment and debris of sticks and decomposing leaf litter. Two sediment cores were taken from Cenote Angelita. ANGC1 was taken at a water depth of approximately 75 m, at the base of the breakdown pile, whereas ANGC3 was taken at ~30 m depth, at the top of the breakdown pile.

2.3.2. ZAPOTE CENOTE

Zapote Cenote is a pit cenote located approximately 20 km northwest of Playa Del Carmen and 21 km from the coast. Zapote is 54 m deep and has a substantial

breakdown pile that rises to approximately 29 m, and has been the site of research that investigated the biological speleothems that grow there (Figure 2B; Stinnesbeck et al., 2018; Ritter et al., 2019). The growth of the biological speleothems is an episodic process that depends on the position of the halocline, which can vary in response to droughts, recharge, annual tidal fluctuations and sea level change (Ritter et al., 2019). Zapote is located in the Holbox fracture zone, which is characterized by north-south trending zones of increased permeability (Bauer-Gottwein et al, 2011; Ritter et al., 2019). The debris mound and cenote floor are covered in a thick layer (>1 m) of OM consisting mostly of decomposing leaf and other plant materials (Ritter et al., 2019). Zapote is stratified, with the MeWM from 0-34 mbsl, the 10-m-thick transitional halocline from 34-44 mbsl, and MaWM below 44 (Stinnesbeck et al., 2017). The sediment core (ZAPC1) was taken at ~ 50 m water depth in the MaWM.

2.3.3. YAX CHEN - ISODII

The Yax Chen cave system has seven large collapse cenotes along its length and is mostly 8 to 11 m deep. The sediment core (ISODC2) was taken 100 m downstream of Cenote ISODII in Yax Chen, which is part of Ox Bel Ha Cave System (Figure 2C). This section of the cave is mostly 10-11 m deep and is 1.8 km from the Caribbean coast, but there are deeper portions that extend to 15-20 m. ISODC2 was collected at ~12.5 m water depth and just below a stepped halocline within the MxWM (Figure 2). This location is considerably shallower and closer to the coast than Angelita and Zapote, and the cave system spans both the

MeWM and MaWM. The MZ and MaWM begin at approximately 13 m depth in this area. The sediment at ISODII is mainly light brown organic floc material that flows into the cave system directly from the open cenote (Collins et al., 2015; McNeill-Jewer et al., 2019).

3. METHODS

3.1. CORING, µXRF AND AGE ANALYSIS

Two sediment push cores were taken in 2007 from Cenote Angelita at depths of ~75 m (ANG C1, 85 cm long) and 28 m, the latter (ANGC3, 163 cm long) on top of the breakdown pile. One core was taken from Cenote Zapote in 2017, at a depth of ~50 m (ZAPC1, 85 cm long). One sediment core (ISODC2) was taken from ISODII in 2013 at 13 m (~3 m above the top of the upper halocline). All cores were taken by trained cave divers who used SCUBA. All cores were analyzed at the McMaster University Core Scanning Laboratory (MUCS Lab) in 2017 using a Cox Analytical ITRAX X-Ray Fluorescence Core Scanner (XRF-CS) Cr X-Ray source. All cores except ANG3 were scanned at a resolution of 200 µm. ANGC3 was scanned at a resolution of 500 µm. All cores were scanned with a 15-second exposure time. ANGC1 was scanned at 50 kV, 28 mA. ANGC3 was scanned using the Sequential Sample Reservoir (SSR- see Gregory et al., 2017 for full details) at 40 kV, 10 mA. ZAPC1 was scanned at 19 kV and 9 mA. Calibrated radiocarbon age-depth models for each core were calculated using the Bayesian linear modelling package BACON in statistical software R (Blaauw and Christen, 2011).

3.2. GAMMA ANALYSIS

The gamma method is a simple and 'computationally inexpensive' feature-identification tool that uses multiple time series to identify events in geophysical data (Shaw et al., 2019). It is based on the idea that within geophysical data such as µXRF-CS, multiple physical variables (e.g., elemental counts) are perturbed nearly simultaneously. Each time series is rescaled to values between 0 and 1 and the minimum deviation, or 'gamma' time series is computed. Dataset perturbations are calculated by subtracting the mean and taking the absolute value. The dataset is then divided by its maximum to have the index vary from 0 to 1. Events can therefore be detected as time periods during which the 'gamma' has a significant deviation from zero.

Variants of the basic method allow the user to implement contextual knowledge to choose inputs that best suit the goals of the analysis. To perform the analysis for this study, the Cl records of all four cores were combined to create the gamma index in MATLAB from Mathworks. Because the absolute values of the dataset are used, variation in the Yucatan gamma record corresponds to water-column mixing, as perturbations in Cl within all four cores occurs simultaneously during mixing events.

3.3. PCA and Correlation

PCA and correlation analyses were performed on all four cores to investigate the relationships of elements within and across cores. PCA is a method used to identify

patterns of variability ranked by variance captured. In a PCA biplot, variables (in this case, µXRF-CS elements) that have similar expression profiles are clustered together, with close angles representing positive correlation, orthogonal angles representing no correlation and obtuse angles (~180°) representing negative correlation. PCA and correlation analysis were carried out using the statistical software R with packages “FactoMineR” and “corrplot.” A set of weathering elements (Ti, Fe, Si, K and S), along with Cl, was selected for each record. These were used to compute a correlation matrix and PCA biplot.

RESULTS

3.4. Sediment profiles, Age Models and µXRF

Overall, the sediment of ISODC2 is composed of medium-brown organic-rich sediment, with lower OM near the base of the core (Figure 3A). There is a lithological change from marl to OM at ~75 cm that is related to the flooding of cave passages as sea-level rose in the late Holocene (Collins et al., 2015). The sediment of ZAPC1 and ANGC1 consists of dark brown organic-rich mud with inclusions of whole seeds and a strong smell of oxidation (Figures 3B, C). The sediment of ANGC3 is primarily dark brown organic-rich mud with inclusions of whole seeds and sticks, with occasional intervals of sandy carbonate sediment (Figure 3D). At 145 cm in ANGC3, there is charcoal within the organic sediment (Table S1). Age model dates were interpolated linearly using BACON. There are small age reversals for ZAPC1 and ANGC3, but not for ISODII and ANGC1 (Figure A.1).

These too-old, outlier ages are likely a consequence of downslope failures of sediment from the sides of the breakdown pile. The maximum basal age among the records, ~8 ky BP, was from ANGC1. The minimum basal age among the records was from ISODII, ca. 3 ky BP.

The Cl counts for all records range from approximately 10,000 to 20,000. Using the salinity calibration equation completed by McNeill-Jewer et al (submitted; Chapter 3) the averaged reconstructed salinity corresponding to each core is 12 ppt for ANGC3 (taken at ~15 m, ~ 10 ppt), 19.2 ppt for ISODII (taken at ~13 m depth, ~20 ppt), 25.5 ppt for ZAPC1, (taken at ~55m, 25 ppt) and 19.3 for ANGC1 (taken at ~60 m depth, 35 ppt). In the ISODC2 record, Cl is low near the base and increases around 70 cm, coincident with the transition to more organic sediment (Figure 3A). The ISODC2 Cl values decrease slightly near the top of the core. The ZAPC1 record has relatively constant Cl values from 100 to 50 cm, followed by a small peak, and decreases again from about 20 to 0 cm (Figure 3B). Cl counts from ANGC1 remain relatively constant throughout the core, with only small deviations (Figure 3C). The ANGC3 record shows relatively constant Cl values from about 160 to 80, which then decrease thereafter (Figure 3D).

Concentrations of Fe are high for all cores, but highest for ANGC1, whereas concentrations of Ti, K and S are low and similar for all four cores (Figure 3). There are generally positive relationships between Cl and Si for all cores, except ZAPC1 (r= 0.07 for ISODC2; r= 0.32 for ANGC3; r= 0.18 for ANGC1; r= -0.88 for ZAPC1). ISODII has the highest Si of all four cores (Figure 3E) as a result of a higher diatom

abundance (McNeill-Jewer et al., 2019). All cores have a positive relationship between Cl and Fe except for ANGC1 (r=0.41 for ISODC2; r=0.31 for ANGC3; r= -0.18 for ANGC1; r=0.46 for ZAPC1). ZAPC1 has the lowest Fe count, while ANGC1 has departures with the highest amounts of Fe (Figure 3F). There is a weakly positive relationship between Cl and Ti as well as between Cl and S for all cores, and a strong positive relationship between Cl and K for all cores, which all have K values ranging from 0 to 3000 counts.

3.5. PALEO-MIXING INDICATORS (CL, FE, S, K)

Cl has been shown to be an effective proxy for salinity and wetness/drought-driven changes in the mixing of the MeWM and MaWM (Kovacs et al., 2017). It has been used in the Yucatan Peninsula to document changes in shallow-lake salinity (McNeill-Jewer et al., submitted), though it has not been used extensively to investigate groundwater mixing. Fe, Ti, and K are used as terrigenous weathering proxies and McNeill-Jewer et al. (2019) examined relationships between them and rainfall using sediment traps in the Yax Chen Cave System. K is a product of leaf litter decomposition. Fe can be a terrigenous weathering proxy or an indicator of redox changes in the water column. Ti is often used as a proxy for terrigenous erosional input because it is not subject to weathering and is not redox sensitive (Figure A.2). Titanium oxide is one of the most stable components of the soil against weathering which makes it a good indicator of weathering intensity.

In the cores close to the halocline (ANGC3, ISODC2), Cl is positively correlated with the weathering elements and therefore is positively correlated with rainfall (ANGC3: Cl-S r= 0.43, Cl-K r=0.72, Cl-Si r= 0.32, Cl-Fe r= 0.31, Cl-Ti r= 0.27 and ISODC2 Cl-S r = 0.5, Cl-K r = 0.47, Cl-S r = 0.5; Figure A.2). The correlation plots in Figure A.2 show that all chosen elements are positively correlated with Cl (salinity) in ANGC3, indicating increase in salinity (mixing) is accompanied by increases in erosional proxies. In contrast, in ANGC1, Cl (salinity) is negatively correlated to all other elements (ANGC Cl-S r= -0.38; Cl-K r=-0.53; Cl-Si r= -0.18; Cl-Fe r = -0.16; Cl-Ti r= -0.24; Figure A.2). The relationship between Cl and the other elements is less straightforward in ZAPC1, as Cl is positively related to Fe, but shows no correlation to Ti (ZAPC1 Cl-S r= -0.43; Cl-K r=-0.63; Cl-Si r= -0.68; Cl-Fe r = 0.45; Cl-Ti r= 0.05; Figure A.2). This indicates that when salinity (Cl) is high in the MaWM, Fe is low, and when salinity is low in the MaWM (through rainfall), Fe is high.

The four cores in this study reflect certain relationships between precipitation and elemental abundance found from biannual in situ sediment collection in McNeill-Jewer et al. (2019). The ISODII record has the closest relationship to the elements from Yax Chen because ISODII is within that cave system, though ISODC2 represents a long-term climate record rather than a biannual in situ measurement. McNeill-Jewer et al. (2019) showed that K and Fe are highly correlated (r= 0.46) within the Yax Chen cave system. This is true for the shallower cores in this study (ISOD K-Fe r= 0.47; ANGC3 K-Fe r= 078), but not for the deeper ones (ZAPC1 K-

Fe r= -0.38; ANGC1 K-Fe r= 0.05). Fe and Ti are positively correlated within the four cores in this study (ISOD r= 0.73; ANGC3 r= 0.94; ZAPC1 r= 0.59; ANGC1 r= 0.16; Figure A.2), as well as throughout the Yax Chen cave system (r=0.75; McNeill-Jewer et al., 2019). The correlation between biogenic elements is positive in all four cores, except ANGC1 where K and Si are not closely tied (Figure A.2). In the Yax Chen cave system, biogenic weathering elements K and S are highly correlated (r=0.81), as are K and Si (r= 0.63; McNeill-Jewer et al., 2019). Precipitation is negatively correlated with Si (r= -0.27), S (r= -0.62) and K (r= -0.28) because of the ponding of water on top of mangrove peat, and the seasonal lag associated with the growth of Si-rich phytoplankton in cenotes (McNeill-Jewer et al., 2019).

Ti was removed from the set of paleo-mixing elements, as it had little relationship to Cl across all sites (Figure A.2). The remaining elements (Cl, Fe, S, K) were plotted (Figure 4) and co-vary throughout the ZAPC1, ANGC1 and ANGC3 ISODC2 records. Certain periods of time show more variability than others (e.g. less fluctuation after 2 ky BP in most cores). After 1000 y BP, the Cl, Fe, K and S records in ZAPC1 become less variable and all values decrease slightly (Figure 4).

4. DISCUSSION

4.1. CL AS AN INDICATOR OF WATER MASS STRATIFICATION AND MIXING

The relationship of salinity (Cl) changes above and below the halocline is highlighted in Figure 5, and as Figure 5A shows, there is covariance between the shallower cores, ISODC2 and ANGC3, whereas Figure 5B shows an opposing trend between ISODC2 and ZAPC1, which is a deeper core (Figure 6). Cl values in ISODC2 and ANGC3 covary over the last ~ 4 ka even though Angelita is less connected to the aquifer, being a pit cenote, and ISODII is part of a large cave system with a direct connection to the aquifer. The two records show increased salinity between 2750 and 1250 y BP, which corresponds to wetter conditions with more frequent hurricanes (van Hengstum et al. 2016). In contrast, the deeper core from Zapote (ZAPC1) shows decreasing salinity during the same time interval. This temporal change in aquifer salinity also closely corresponds with other documented climate proxies for the circum-Caribbean that show relatively wet and dry periods (Chumkopo Cl and Cariaco Basin Ti; Figure 7), which will be discussed further in 4.3.

Comparison of ISODC2 and ZAPC1 shows substantial differences from approximately 2750 to 1250 y BP, a time when the ITCZ was farther north, resulting in increased wetness in the region (Figure 5B). The shallower ISODC2 core indicates greater salinity at that time, whereas the ZAPC1 indicates fresher

conditions, suggesting this time of increased wetness impacted the salinity in both these records, but in opposite ways. Below the halocline, the ANGC1 and ZAPC1 records tend to covary because both are deeper cores, although ANGC1 lies further below the halocline (Figure 5C). This increase and decrease of salinity with depth during wet periods indicates change in the position of the water masses. During wet periods there is more flow in the MeWM from increased rainfall associated with hurricanes and tropical storms, which causes increased entrainment of the underlying MaWM and creates a more gradual salinity transition (MxWM; Figure 6). Cores from shallower sites (ANGC3, ISODC2) closer to the halocline recorded increased salinity with greater rainfall, relative to dry periods, because of increased mixing of the overlying water masses. Deeper core sites farther from the halocline experienced relative freshening, as the MeWM or MxWM extended deeper into the water column because of the increased freshwater input, i.e. the MeWM was thicker (Figure 6). This is corroborated by instrumental data that show increased salinity in the MeWM associated with entrainment of the MaWM during heavy rainfalls (Coutino et al., 2017, Kovacs et al., 2017, 2018) and also over longer Holocene records (Kovacs et al., 2017; van Hengstum et al., 2010), albeit only for the upper MeWM.

Supporting information regarding this mixing relationship is provided by terrigenous weathering products. Potassium had the best overall correlations with Cl (ISODC2 =0.47, ANGC3=0.72, ZAPC1=-0.63, ANGC1= -0.53; Figure S2; Figure 6) and was found to have a good relationship with rainfall, although it showed a lagged

response in sediment trap studies from Yax Chen (McNeill-Jewer et al., 2019). Likewise, K was also used as a weathering proxy in lake cores from Pac Chen (Krywy-Janzen et al., 2019). In cores from below the halocline (ZAPC1, ANGC1), Cl was negatively correlated with the weathering proxies, indicating that in times of less mixing between the MeWM and MaWM (dry periods), there is less input of weathering elements, and this is accompanied by a higher concentration of Cl. In contrast, during periods of increased rainfall, higher input of weathering elements is accompanied by reductions in Cl (MxWM or MeWM extends deeper). Cores collected at, or slightly below the halocline show the reverse trend, with higher salinity (Cl) corresponding to higher weathering proxies during wet periods and lower values of both during dry periods.

4.2. AQUIFER RESPONSE TO CLIMATE, MID-HOLOCENE TO PRESENT

Cores above or close to the halocline reflect water column freshening when climate is more arid, and contain lower concentrations of erosional inputs because of reduced rainfall and runoff. Conversely, during wetter intervals, cores above the halocline become more saline from rainfall-induced mixing that entrains the higher-salinity MaWM into the MeWM, while also inputting more erosional elements. These wet periods induce relative ‘thickening’ of the MxWM within the MeWM because of saline entrainment, but the MeWM also becomes thicker with increased rainfall input. This relationship between Cl (salinity) and erosional proxies (Si, K, S, Fe, Ti) is shown in Figure 6 A and B, with the PCA plots of ANG C3 and ISODC2,

noting the positive correlations (close angles) of the elements. Salinity in the ANGC3 record is likely more positively correlated to the erosional proxies than in ISODC2, because it is located in the open water, whereas ISODC2 is located within a cave system, where slightly different processes impact sedimentation (McNeill-Jewer et al., 2019).

Cores below the halocline exhibit fresher conditions when the climate is wetter because of increased mixing of the MeWM down into the MaWM with entrainment, which induces a period of reoxygenation and freshening (Coutino et al., 2016; Brankovits et al., 2018). The freshening of deeper waters is accompanied by the input of erosional elements, which accounts for the negative relationship between Cl (salinity) and erosional proxies (Figure 6C and D [Zapote] and C1 [Angelita]). On the other hand, during periods of quiescence, the bottom waters become stagnant as the MeWM expands and stratifies, causing the MZ MxWM to move 'upward,' which causes Cl to increase in bottom waters because of the lack of fresher inputs. This stratification is accompanied by a relative lack of erosional elements, further demonstrating the negative relationship between Cl and the erosional proxies in Figure 6 C and D. Movement of the halocline over the Holocene in response to wet and dry periods is also addressed in Stinnesbeck et al. (2017) and Ritter et al. (2019), as growth of the biological speleothems in Zapote Cenote were dependent on the position of the halocline during the late Holocene.

ISODC2 is the most sensitive indicator of changes in rainfall and mixing between the MeWM and MaWM, and corresponds well with ANGC3, which is of lower

resolution. There is very good correspondence between ISODC2 and the Chumkopo Cl record, only several km away (Figure 1; McNeill-Jewer et al., submitted). From ~ 3900 to 3200 y BP, the Chumkopo record shows rapidly fluctuating wet and dry conditions, which are also apparent in the ISOD II core, followed by wetter climate (decreased Cl=fresher) from 2600 to 2200 y BP, which caused a corresponding increase in salinity in ISODC2. This peak in Cl is followed by a general decrease in salinity to the present, which is expressed as a corresponding increase in salinity at Chumkopo. A similar correspondence is also found in the marine Cariaco Basin Ti record, which lies off the coast of Venezuela and was shown to reflect ITCZ migration over the Holocene (McNeill-Jewer et al., submitted; Haug et al., 2001). Holocene-scale hydroclimate records generally indicate there was increased precipitation during the Holocene Climatic Optimum 8000-6000 years ago, followed by general drying for the last 5 ky (Schneider et al, 2014; van Hengstum et al., 2018). The ISODII Cl record, Chumkopo drought record and Cariaco Basin Ti record all show slight drying trends over the past 4 ky, but also periods of Rapid Climate Change (RCC) (Figure 7). Similarities between these records indicate that aridity and mixing in the eastern YP are connected and respond to movement of the ITCZ. Figure 7C indicates that from ~2500 to 1200 y BP, when there was greater wetness across the Yucatan Peninsula because of the more northerly position of the ITCZ, variability in Cl counts in the Chumkopo record was greatly reduced, particularly from ~2200 to 1700 y BP, which also corresponds to increased activity in the gamma mixing record (Figure 8). This was likely caused

by increased wetness in the region from the more northerly position of the ITCZ, which would have amplified variability in mixing, but reduced variability in the freshening of the shallow Chumkopo waters, as freshening cannot be detected in already ‘fresh’ water, as discussed in McNeill-Jewer et al., submitted).

Because the gamma method is a combination of the four Cl records and is based on absolute values (change), it is a reliable and robust proxy for observing relative variation in water mass mixing. It does not distinguish between positive and negative changes in salinity, but only indicates there was a relative change in all records at a particular time. Broad variations in the gamma index correspond to changes in the Cl (salinity) of the MeWM and MaWM and reveal times of increased variability (wetness) and decreased variability (dryness) over the past 4000 years. Figure 7 shows that the ISODC2 record matches well with other regional records of drought and rainfall (Chumkopo, Yucatan Peninsula, Figure 7A, and Cariaco Basin, Venezuela, Figure 7B), however, we propose here that the gamma record reveals rapid changes that occur with periods of increased or decreased hurricanes/tropical storms. Two of the most noticeable and long-lasting times of reduced gamma index coincide with the Preclassic and Classic Maya periods (Figure 8). The early Preclassic period was characterized by relatively dry conditions that shifted to wetter conditions in the Middle Preclassic, about the time of the widespread 2.8 ky event (Nooren et al., 2018). In our records from that time, the ISODC2 (shallower) and ZAPC1 (deeper) cores decouple, indicating there

were wetter conditions in the coastal Yucatan Peninsula 2800 years ago. This is shown in the gamma record, as well (Figure 8), as a peak from 2.9 to 2.8 ky BP.

The Preclassic Maya Hiatus (PMH) and abandonment of major population centers was synchronous with two distinct droughts centered around approximately 200 and 250 CE (Medina-Elizalde et al., 2016) that are also observed in our shallow-water core records (ANGC3, ISODC2, Figure 5A), which show a defined peak at that time (ca. 220 to 260 CE), as do the drought records from Chumkopo and the Cariaco Basin (Figure 7). These droughts are reflected as relative maxima in the gamma index during the highlighted PMH time period (Figure 8). The PMH was the period of reduced building that marks the transition from the Preclassic to the Classic Periods. The time period between the PMH and the TCM is defined by a low gamma index that indicates little mixing change during the majority of the Maya Classic Period (Figure 8), while the individual records indicate long-term drying (Figure 5, 7). The Terminal Classic Maya (TCM) period coincides with a rapid increase in variability of the gamma index, which suggests rapid changes in wetness occurred approximately 1.1 ky BP. The Chumkopo Cl record (McNeill-Jewer et al. submitted) shows that the TCM coincides with a series of annual to sub-annual dry events, with short intervening periods of reduced salinity, suggesting that increased variability in hydroclimate was temporally associated with societal disintegration. The changes in variation within the gamma index as well as the individual records support this hypothesis of rapid change.

The response of the groundwater mass to arid and wet periods differs from what occurs in shallow water bodies (e.g. Chumkopo), which become increasingly saline during times of extended drought and remain relatively fresh during times of increased wetness (Figure 7). Despite simultaneous changes in these surface water and groundwater systems, they display opposite responses to wet and dry periods. Greater rainfall results in fresher surface water and more saline groundwater, whereas drought results in fresher groundwater, but more saline surface waters. This relation between rainfall amount and the salinity of surface and groundwaters was also observed in instrumental records (Kovacs et al. (2017a); Coutino et al (2017).

4.4. HURRICANE IMPACTS ON COASTAL KARST AQUIFERS

Groundwater resources on islands and peninsulas are particularly vulnerable to impacts of hurricanes, sea level rise and other effects initiated by climate change. We demonstrated that past hurricanes and aridity impacted MeWM salinity in the coastal Yucatan Peninsula aquifer over the past 4 ky and predict that this will continue into the future. Increased understanding of past and present mixing in the coastal groundwater is important to inform sustainable development practices that can mitigate the effects of climate change on groundwater salinity. Future research should focus on further elucidating the mixing dynamics associated with rainfall. Simultaneous covariance of paleosalinity records from pit cenotes (ANGC1, ANGC3, ZAPC1) and a coastal cave system (ISODC2) suggest the mixing response is aquifer-wide, at least at the coast. Further investigation into the spatial

complexities related to cave passage density, coastal plugging (caliche), and other physical variables will help inform how the MeWM and MxWM will behave in light of future climate and human pressures.

Multiple paleoclimate proxies indicate increased precipitation and hurricanes from 2750 to 1250 years BP, suggesting the ITCZ was in a more northerly position. This is also illustrated in Figure 7 by covariance between the Cariaco Basin Ti record (Haug et al., 2001) and the shallow-water ISODC2 core Cl record (van Hengstum et al., 2016). Should the ITCZ move south and trigger increased aridity across the Yucatan Peninsula, it is likely the MeWM will become thinner and fresher as it stagnates, and there will be less erosional elements input into the cenote and cave systems. In contrast, increased hurricanes and wetness across the Yucatan Peninsula, such as occurred in the interval 2750 to 1250 y BP, will cause the MeWM near the coast to become more saline on average, as the MxWM extends farther inland. This suggests that groundwater wells located close to the coast may exhibit higher salinity in the future because of increased hurricane frequency and/ or intensity, which will induce mixing of subsurface water masses. Predictions of decreased frequency, but increased magnitude of hurricanes, suggest that although the coastal groundwater mass may stratify more in the long run because of the general drying trend observed over the past 1000 years, more intense hurricanes will cause more intense short-term changes in the mixing of the water masses. This is particularly important to take into account when planning coastal development, as it will affect groundwater geochemistry.

5. CONCLUSIONS

Our high-resolution paleo-mixing proxy (Cl), measured by μXRF-CS in cores collected at different water depths and distances from the halocline, indicated long-term mixing between the MeWM and MaWM, associated with high rainfall. We showed that the MeWM/MxWM responds to rainfall-induced flow and mixing with the MaWM, and that rainfall also changes the vertical position of the halocline. The records in this study indicate that long-term changes in groundwater dynamics are controlled by local, regional and hemispheric hydroclimate, i.e. wetter vs drier. These findings corroborate independent studies of instrumental monitoring of salinity in coastal Yucatan Peninsula cave systems (Kovacs et al., 2017; Coutino et al., 2017; Brankovits et al., 2019), calcite raft and microfossil-based paleosalinity records (Kovacs et al., 2017; van Hengstum et al., 2010).

ACKNOWLEDGEMENTS:

The authors gratefully acknowledge the support of The Mexican Cave Exploration Project (MCEP), CINDAQ, and the staff at Zero Gravity for dive support and logistics. This research was possible through the MCEP Science Week volunteers from around the world.

FUNDING: Natural Sciences and Engineering Research Council (NSERC) Discovery Grants (EGR - 2015-057250) and the Canada Foundation for Innovation John R. Evans Leaders Fund (CFI-JELF grant 105-04523).

REFERENCES

1. Aragón-Moreno, A. A., Islebe, G. A., & Torrescano-Valle, N. (2012). A~ 3800-yr, highresolution record of vegetation and climate change on the north coast of the Yucatan Peninsula. Review of palaeobotany and palynology, 178, 35-42.

2. Aragón-Moreno, A. A., Islebe, G. A., Roy, P. D., Torrescano-Valle, N., & Mueller, A. D. (2018). Climate forcings on vegetation of the southeastern Yucatán Peninsula (Mexico) during the middle to late Holocene. Palaeogeography, Palaeoclimatology, Palaeoecology, 495, 214-226.

3. Beddows, P. A., Smart, P. L., Whitaker, F. F., & Smith, S. L. (2002). Density stratified groundwater circulation on the Caribbean Coast of Yucatan peninsula, Mexico. In Karst Waters Institute Special Publication 7: Hydrogeology and Biology of Post-Paleozoic Carbonate Aquifers.

4. Bender, M. A., Knutson, T. R., Tuleya, R. E., Sirutis, J. J., Vecchi, G. A., Garner, S. T., & Held, I. M. (2010). Modeled impact of anthropogenic warming on the frequency of intense Atlantic hurricanes. Science, 327(5964), 454-458.

5. Climate Change Effects on Groundwater Resources: A Global Synthesis of Findings and Reccomendations (Bowleg, J., Allen, D.M., 2011)

6. Bhattacharya, T., Chiang, J. C., & Cheng, W. (2017). Ocean-atmosphere dynamics linked to 800–1050 CE drying in mesoamerica. Quaternary Science Reviews, 169, 263-277.

7. Brankovits, D., Pohlman., J.W., Ganju, N.K., Iliffe., T.M., Lowell, N., Roth, E., Sylva, Emmert, Lapham (2018). Hydrologic controls of methane dynamics in karst subterranean estuaries

8. Boose, E. R., Foster, D. R., Plotkin, A. B., & Hall, B. (2003). Geographical and historical variation in hurricanes across the Yucatan Peninsula. The lowland Maya area. Haworth. New York, NY, EEUU, 495-516.

9. Bouwer SD (1992) Periodicities of solar irradiance and solar activity indices. II. Sol Phys 142(2):365–389

10. Calvert, S. E., & Pedersen, T. F. (1993). Geochemistry of recent oxic and anoxic marine sediments: implications for the geological record. Marine geology, 113(1-2), 67-88.

11. Coutino, A., Stastna, M., Kovacs, S., & Reinhardt, E. (2017). Hurricanes Ingrid and Manuel (2013) and their impact on the salinity of the Meteoric Water Mass, Quintana Roo, Mexico. Journal of Hydrology.

12. Croudace, I.W., Rothwell, R.G., (2015). Micro-XRF studies of sediment cores in Developments in Paleoenvironmental Research. Springer

13. Frappier, A. B., Pyburn, J., Pinkey-Drobnis, A. D., Wang, X., Corbett, D. R., & Dahlin, B. H. (2014). Two millennia of tropical cyclone-induced mud layers in a northern Yucatán stalagmite: Multiple overlapping climatic hazards during the Maya Terminal Classic "megadroughts". Geophysical Research Letters, 41(14), 5148-5157.

14. Garman, K. M., & Garey, J. R. (2005). The transition of a freshwater karst aquifer to an anoxic marine system. Estuaries, 28(5), 686-693.

15. Giannini, A., Kushnir, Y., & Cane, M. A. (2001). Seasonality in the impact of ENSO and the North Atlantic high on Caribbean rainfall. Physics and Chemistry of the Earth, Part B: Hydrology, Oceans and Atmosphere, 26(2), 143-147.

16. Grinsted, A., Moore, J. C., & Jevrejeva, S. (2013). Projected Atlantic hurricane surge threat from rising temperatures. Proceedings of the National Academy of Sciences, 110(14), 5369-5373.

17. Harbison, P. A. T. (1986). Mangrove muds—a sink and a source for trace metals. Marine Pollution Bulletin, 17(6), 246-250.

18. Holland, G., & Bruyère, C. L. (2014). Recent intense hurricane response to global climate change. Climate Dynamics, 42(3-4), 617-627.

19. Humphreys, W. F. (1999). Physico-chemical profile and energy fixation in Bundera Sinkhole, an anchialine remiped habitat in north-western Australia. Journal of the Royal Society of Western Australia, 82, 89.

20. Hurrel JW (1995) Decadal trends in the North Atlantic oscillation: regional temperature and precipitation. Science 269:676–679

21. Jáuregui, E. (2003). Climatology of landfalling hurricanes and tropical storms in Mexico. Atmósfera, 16(4), 193-204.

22. Jouve, G., Francus, P., Lamoureux, S., Provencher-Nolet, L., Hahn, A., Haberzettl, T., & Team, T. P. S. (2013). Microsedimentological characterization using image analysis and μ-XRF as indicators of sedimentary processes and climate changes during Lateglacial at Laguna Potrok Aike, Santa Cruz, Argentina. Quaternary Science Reviews, 71, 191-204.

23. Ketabchi, H., Mahmoodzadeh, D., Ataie-Ashtiani, B., & Simmons, C. T. (2016). Sea-level rise impacts on seawater intrusion in coastal aquifers: Review and integration. Journal of Hydrology, 535, 235-255.

24. Kohout, F. A. (1960). Cyclic flow of salt water in the Biscayne aquifer of southeastern Florida. Journal of Geophysical Research, 65(7), 2133-2141.

25. Kovacs, S. E., Reinhardt, E. G., Stastna, M., Coutino, A., Werner, C., Collins, S. V., ... & Le Maillot, C. (2017). Hurricane Ingrid and Tropical Storm Hanna's effects on the salinity of the coastal aquifer, Quintana Roo, Mexico. Journal of Hydrology.

26. Kovacs, S. E., Reinhardt, E. G., Chatters, J. C., Rissolo, D., Schwarcz, H. P., Collins, S. V., ... & Erreguerena, P. L. (2017). Calcite raft geochemistry as a hydrological proxy for Holocene aquifer conditions in Hoyo Negro and Ich Balam (Sac Actun Cave System), Quintana Roo, Mexico. Quaternary Science Reviews, 175, 97-111.

27. Kumar P, Foufoula-Georgiou E (1997) Wavelet analysis for geophysical applications. Rev Geophys:385–412

28. Kuo C, Lindberg C, Thomson DJ (1990) Coherence established between atmospheric carbon dioxide and global temperature. Nature 343:709–713

29. Lachniet, M. S., Bernal, J. P., Asmerom, Y., Polyak, V., & Piperno, D. (2012). A 2400 yr Mesoamerican rainfall reconstruction links climate and cultural change. Geology, 40(3), 259-262.

30. Lechleitner, F. A., Breitenbach, S. F., Rehfeld, K., Ridley, H. E., Asmerom, Y., Prufer, K. M., ... & Polyak, V. (2017). Tropical rainfall over the last two millennia: evidence for a lowlatitude hydrologic seesaw. Scientific reports, 7(1), 1-9.

31. Li, J., Xie, S. P., Cook, E. R., Morales, M. S., Christie, D. A., Johnson, N. C., & Fang, K. (2013). El Niño modulations over the past seven centuries. Nature Climate Change, 3(9), 822-826.

32. Little, S. H., Vance, D., Lyons, T. W., & McManus, J. (2015). Controls on trace metal authigenic enrichment in reducing sediments: insights from modern oxygen-deficient settings. American Journal of Science, 315(2), 77-119.

33. Malaizé, B., Bertran, P., Carbonel, P., Bonnissent, D., Charlier, K., Galop, D., ... & Pujol, C. (2011). Hurricanes and climate in the Caribbean during the past 3700 years BP. The Holocene, 21(6), 911-924.

34. Medina-Elizalde, M., Polanco-Martínez, J. M., Lases-Hernández, F., Bradley, R., & Burns, S. (2016). Testing the "tropical storm" hypothesis of Yucatan Peninsula climate variability during the Maya Terminal Classic Period. Quaternary Research, 86(2), 111-119

35. Medina-Elizalde, M., Burns, S. J., Polanco-Martínez, J. M., Beach, T., Lases-Hernández, F., Shen, C. C., & Wang, H. C. (2016). High-resolution speleothem record of precipitation from the Yucatan Peninsula spanning the Maya Preclassic Period. Global and Planetary Change, 138, 93-102.

36. Michael, H. A., Mulligan, A. E., & Harvey, C. F. (2005). Seasonal oscillations in water exchange between aquifers and the coastal ocean. Nature, 436(7054), 1145.

37. Morford, J. L., & Emerson, S. (1999). The geochemistry of redox sensitive trace metals in sediments. Geochimica et Cosmochimica Acta, 63(11-12), 1735-1750.

38. Mylroie, J. E., & Mylroie, J. R. (2011). Void development on carbonate coasts: creation of anchialine habitats. Hydrobiologia, 677(1), 15-32.

39. Nyberg, J., Kuijpers, A., Malmgren, B. A., & Kunzendorf, H. (2001). Late Holocene changes in precipitation and hydrography recorded in marine sediments from the northeastern Caribbean Sea. Quaternary Research, 56(1), 87-102.

40. Pérez, L., Lorenschat, J., Brenner, M., Scharf, B., & Schwalb, A. (2010). Extant freshwater ostracodes (Crustacea: Ostracoda) from Lago peten itza, Guatemala. Revista de Biología Tropical, 58(3), 871-895.

41. Peros, M., Gregory, B., Matos, F., Reinhardt, E., & Desloges, J. (2015). Late-Holocene record of lagoon evolution, climate change, and hurricane activity from southeastern Cuba. The Holocene, 25(9), 1483-1497.

42. Reeve, A., & Perry, E. C. (2000). Hydrogeology and tidal analysis along the western north coast of the Yucatan Peninsula, Mexico. In Hari Krishna, J. et al.(Eds.), Tropical Hydrology and Caribbean Water Resources: Proceedings of the International Symposium on Tropical Hydrology and Fourth Caribbean Islands Water Resources Congress. American Water Resources Association, Bethesda, MD (pp. 327-337).

43. Ritter, S. M., Isenbeck-Schröter, M., Scholz, C., Keppler, F., Gescher, J., Klose, L., ... & Stinnesbeck, W. (2019). Subaqueous speleothems (Hells Bells) formed by the interplay of pelagic redoxcline biogeochemistry and specific hydraulic conditions in the El Zapote sinkhole, Yucatan Peninsula, Mexico. Biogeosciences, 16(11), 2285-2305.

44. Santos, I. R., Burnett, W. C., Dittmar, T., Suryaputra, I. G., & Chanton, J. (2009). Tidal pumping drives nutrient and dissolved organic matter dynamics in a Gulf of Mexico subterranean estuary. Geochimica et Cosmochimica Acta, 73(5), 1325-1339.

45. Saunders, M. A., & Lea, A. S. (2008). Large contribution of sea surface warming to recent increase in Atlantic hurricane activity. Nature, 451(7178), 557-560.

46. Schmitter-Soto, J. J., Comín, F. A., Escobar-Briones, E., Herrera-Silveira, J., Alcocer, J., Suárez-Morales, E., ... & Steinich, B. (2002). Hydrogeochemical and biological characteristics of cenotes in the Yucatan Peninsula (SE Mexico). Hydrobiologia, 467(1-3), 215-228.

47. Shaw, J., Stastna, M., Coutino, A., Walter, R. K., & Reinhardt, E. (2019). Feature identification in time series data sets. Heliyon, 5(5), e01708.

48. Stinnesbeck, W., Frey, E., Zell, P., Avilés, J., Hering, F., Frank, N., ... & Ritter, S. (2018). Hells Bells–unique speleothems from the Yucatán Peninsula, Mexico, generated under highly specific subaquatic conditions. Palaeogeography, palaeoclimatology, palaeoecology, 489, 209-229.

49. Stinnesbeck, S. R., Frey, E., Olguín, J. A., Stinnesbeck, W., Zell, P., Mallison, H., ... & Sanvicente, M. B. (2017). Xibalbaonyx oviceps, a new megalonychid ground sloth (Folivora, Xenarthra) from the Late Pleistocene of the Yucatán Peninsula, Mexico, and its paleobiogeographic significance. PalZ, 91(2), 245-271.

50. Steyaert, M., Moodley, L., Nadong, T., Moens, T., Soetaert, K., & Vincx, M. (2007). Responses of intertidal nematodes to short-term anoxic events. Journal of Experimental Marine Biology and Ecology, 345(2), 175-184.

51. Stoessell, R. K., Moore, Y. H., & Coke, J. G. (1993). The occurrence and effect of sulfate reduction and sulfide oxidation on coastal limestone dissolution in Yucatan cenotes. Groundwater, 31(4), 566-575.

52. Torres-Talamante, O., Alcocer, J., Beddows, P. A., Escobar-Briones, E. G., & Lugo, A. (2011). The key role of the chemolimnion in meromictic cenotes of the Yucatan Peninsula, Mexico. Hydrobiologia, 677(1), 107-127

53. Torrence, C., & Compo, G. P. (1998). A practical guide to wavelet analysis. Bulletin of the American Meteorological society, 79(1), 61-78

54. Van Hengstum, P. J., Donnelly, J. P., Fall, P. L., Toomey, M. R., Albury, N. A., & Kakuk, B. (2016). The intertropical convergence zone modulates intense hurricane strikes on the western North Atlantic margin. Scientific reports, 6(1), 1-10.

55. van Hengstum, P. J., Maale, G., Donnelly, J. P., Albury, N. A., Onac, B. P., Sullivan, R. M., ... & MacDonald, D. (2018). Drought in the northern Bahamas from 3300 to 2500 years ago. Quaternary Science Reviews, 186, 169-185.

56. Wallace, E. J., Donnelly, J. P., van Hengstum, P. J., Wiman, C., Sullivan, R. M., Winkler, T. S., ... & Albury, N. (2019). Intense hurricane activity over the past 1500 years at South Andros Island, The Bahamas. Paleoceanography and Paleoclimatology, 34(11), 17611783.

57. Westerhold T, Röhl U (2009) High resolution cyclostratigraphy of the early Eocene—new insights into the origin of the Cenozoic cooling trend. Clim Past 5:309–327. (www.climpast.net/5/309/2009/)

58. Worthington, S, (2004). Hydraulic and geological factors influencing conduit flow depth Mixing-induced salinity change in deep coastal Yucatan aquifer controlled by wet and dry periods over the past 4 KY

CHAPTER 4 APPENDIX

1. Age Control and Models

Age models for ANGC1, ANGC3 and ZAPC1 were run at the Lalonde AMS Laboratory at University of Ottawa and ISODC2 was run at DirectAMS. The age reversals were not surprising, as ANGC1 and ZAPC1 are both from very deep spots that are adjacent to large breakdown piles, making it possible for old debris to fall and confound the age model.

2. PCA and Correlation Analysis

The PCA and correlation analysis clearly show that the records from above the halocline (ANGC3, ISODC2) have positive correlations between Cl and weathering products, whereas the records from below the halocline (ANGC1, ZAPC1) have negative correlations between Cl and weathering products.

CHAPTER 4 TABLES

Table S1: Radiocarbon information for ZAPC1 C1, AngC1, AngC3 and ISODC2

Core	Lab code	Material	Depth (cm)	14C Age	Age (y BP)	Age (CE)
ANGC1	UOC-6388	Seed	12 cm	195 ± 22	139	1811
	UOC-6389		31 cm	6497 ± 23	1516	434
	UOC-6390		57 cm	3251 ± 28	3300	-1305
	UOC-6391		73 cm	6487 ± 39	6826	-4876
ANGC3	UOC-6392		21 cm	566 ± 25	463	1487
	UOC-6393		61 cm	1268 ± 25	1114	836
	UOC-6394		81 cm	1896 ± 29	1699	251
	UOC-6395		104 cm	2225 ± 26	2130	-180
	UOC-6396	Charcoal	145 cm	3049 ± 27	3131	-1181
ZAPC1	UOC-6397	Seed	25 cm	5300 ± 37	2720	-770
	UOC-6398		56 cm	4160 ± 31	4312	-2362
	UOC-6399		83 cm	5147 ± 33	5893	-3943
	UOC-6400	Leaf	93 cm	5250 ± 36	6116	-4166
ISODC2			10.5 cm	845	613	1337
			23.5 cm	1042	815	1135
			36.5 cm	827	1178	772
			46.5 cm	1039	1485	465

CHAPTER 4 FIGURES

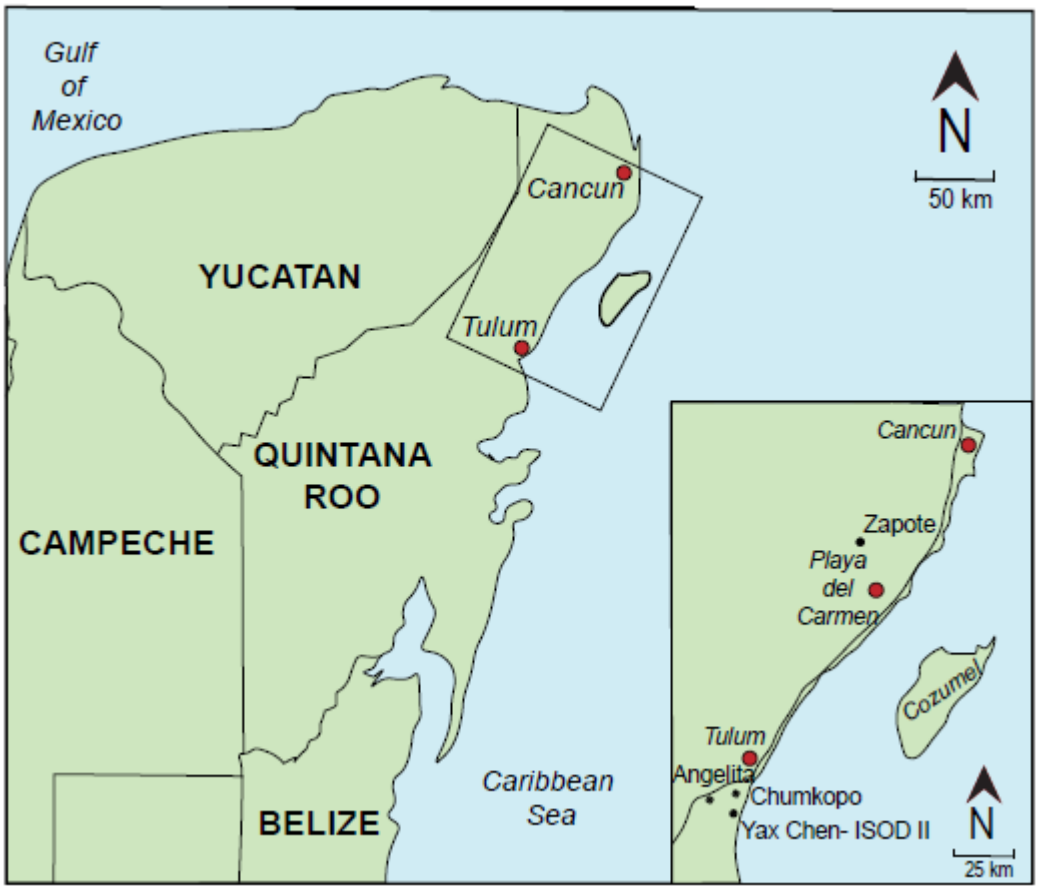

Figure 1. Yucatan Peninsula map with inset locations of cores**.**

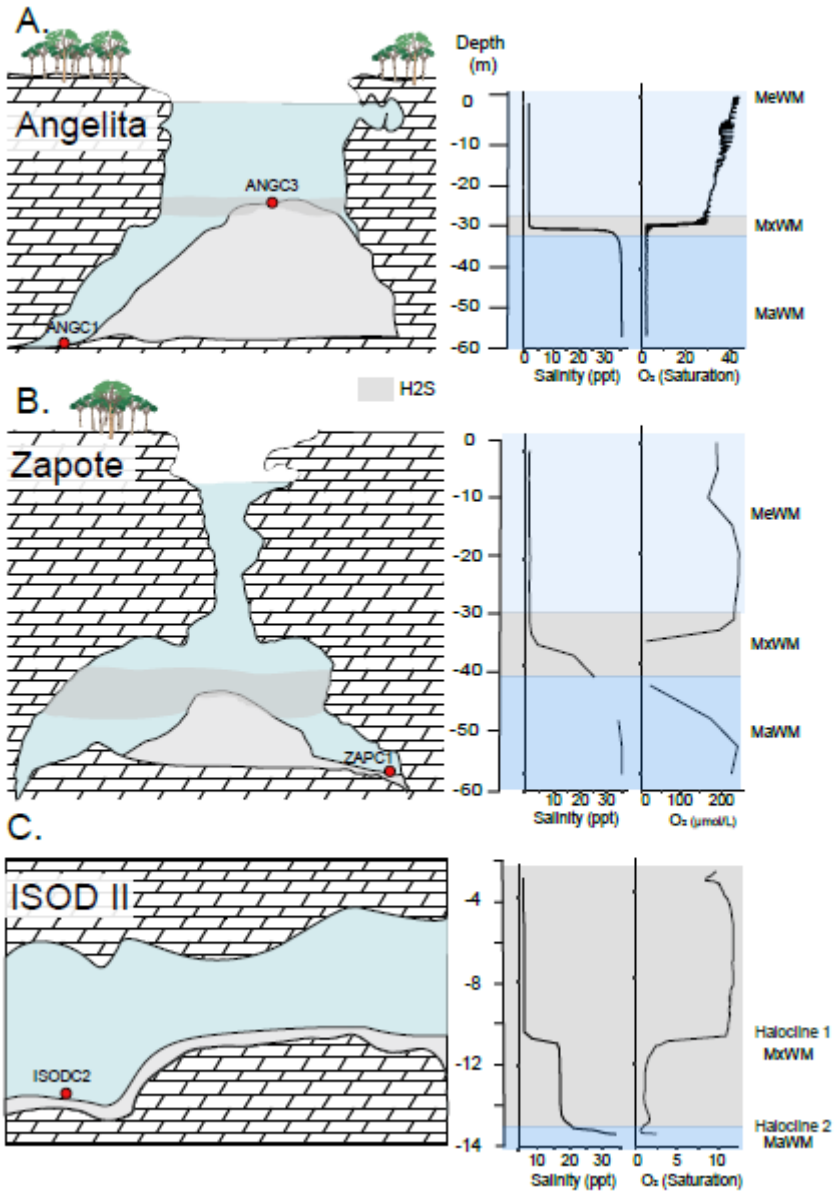

Figure 2. Site profiles. A) Angelita site profile with core locations of ANGC1 and ANGC3 and depth profiles of salinity (ppt) and oxygen saturation (%). B) Zapote profile with core location of ZAPC1 and depth profiles of salinity (ppt) and Oxygen (µmol/L). C) ISODII site profile with core location of ISODC2 and depth profiles of salinity (ppt) and oxygen saturation (%).

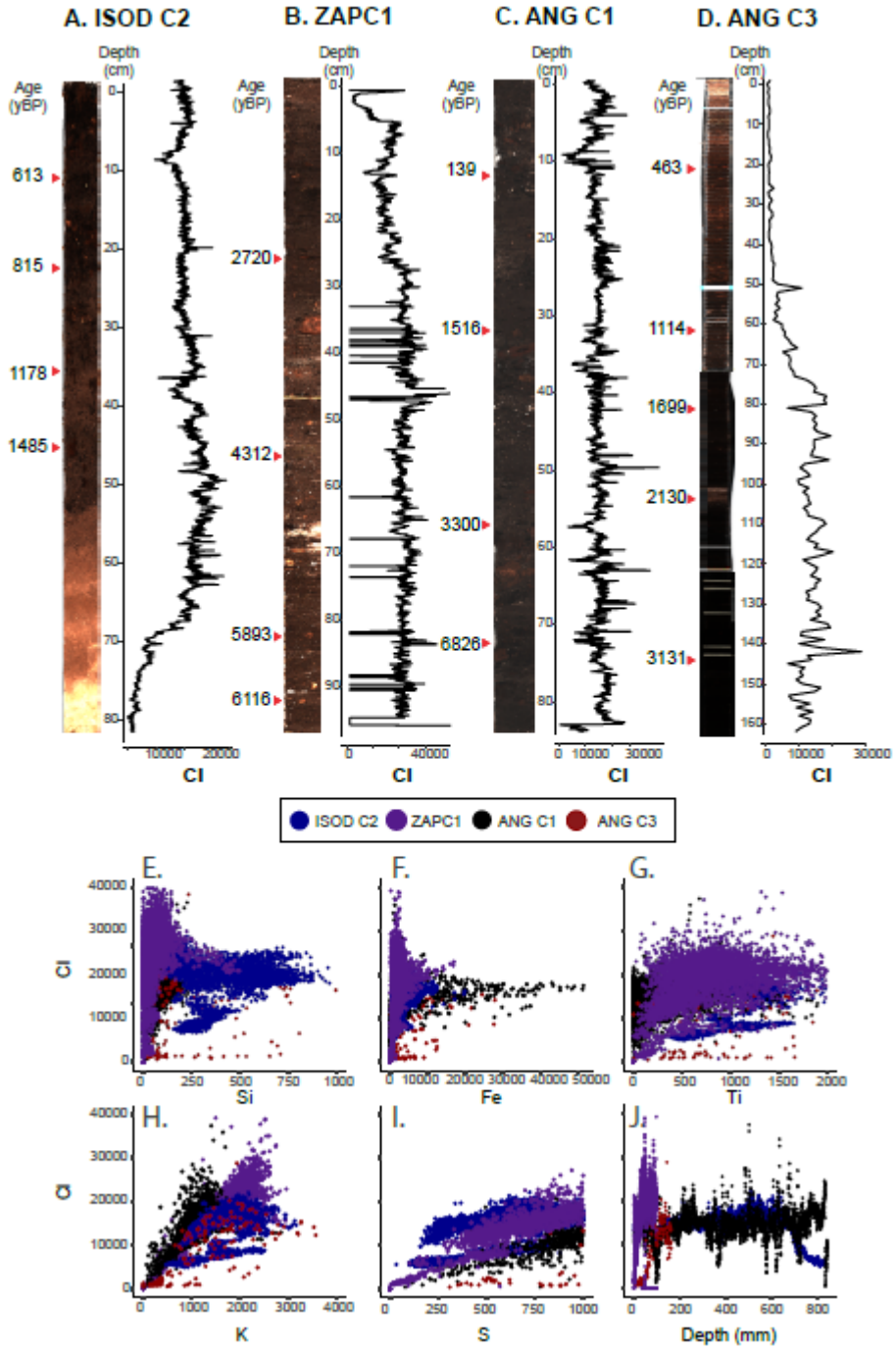

Figure 3. Core images with Cl plot for each record (above). Cross plots of Cl vs Si, Fe, Ti, K and S for all 4 cores (below).

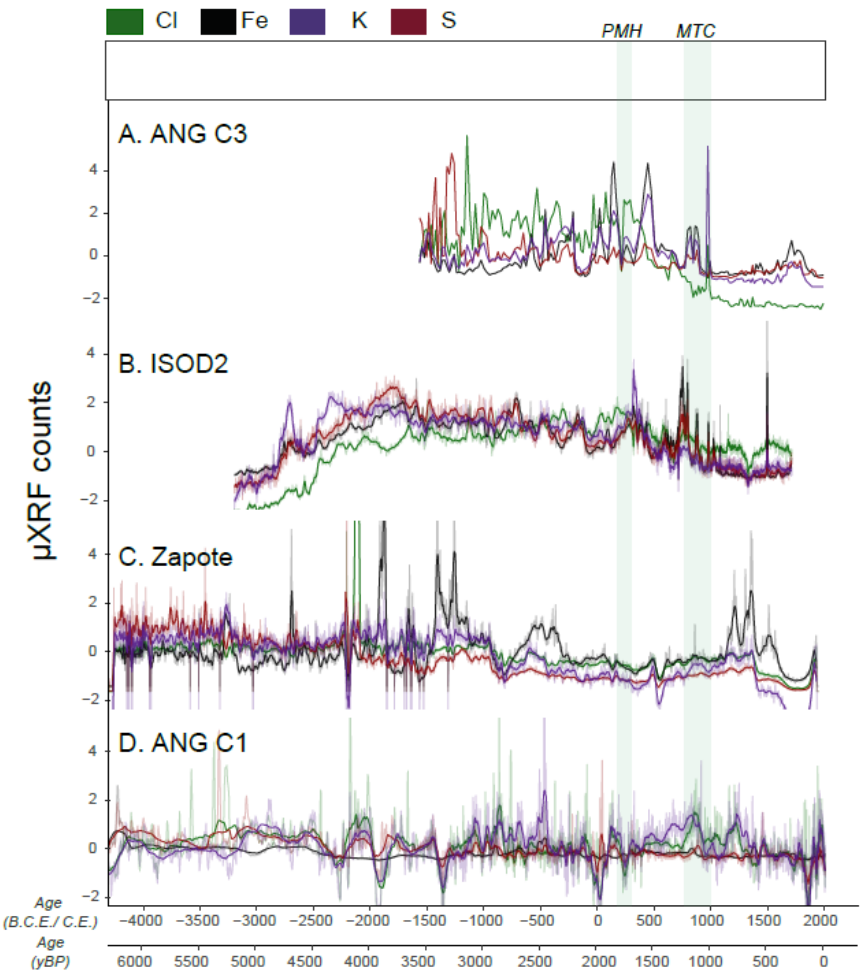

Figure 4. Normalized µXRF-CS counts of Cl (green), Fe (black), K (purple) and S (red) for A) ANGC3 B) ISODC2 C) ZAPC1 D) ANGC1.

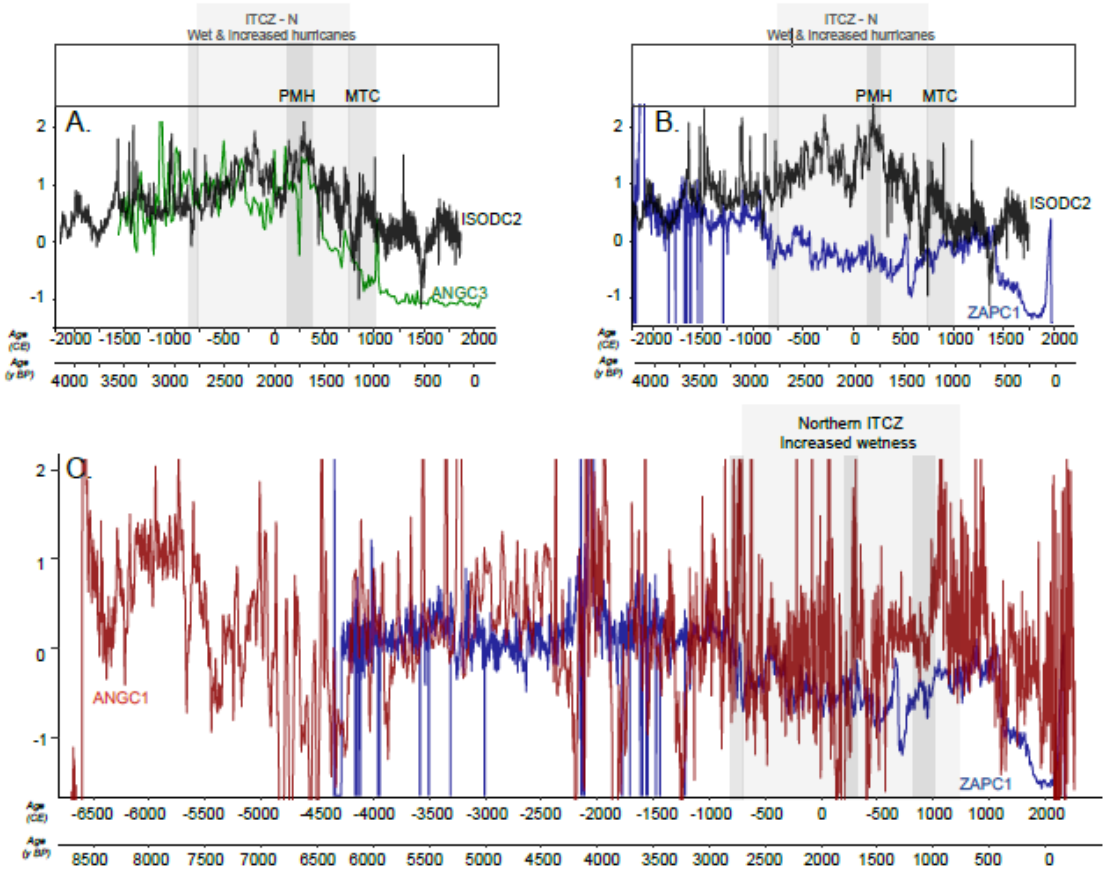

Figure 5. Records with wet and dry periods highlighted. A) ISODC2 and ANGC3. B) ISODC2 and ZAPC1. C) ANGC1 and ZAPC1.

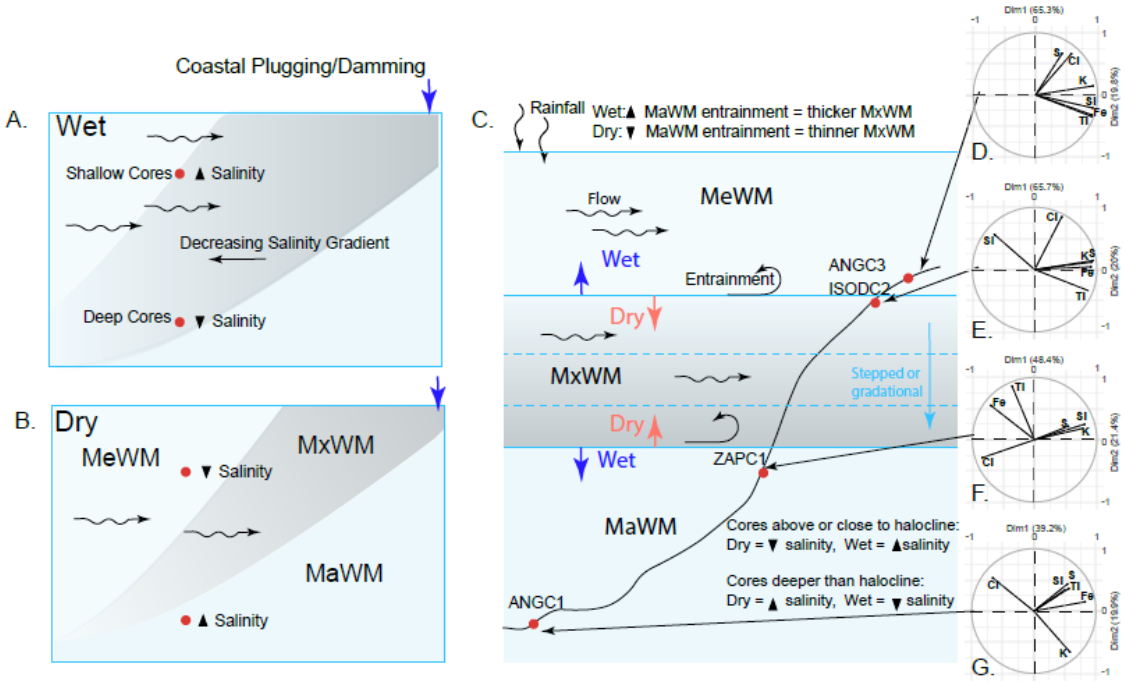

Figure 6. Conceptual model of hydrological changes associated with wet and dry periods with PCA plots corresponding to Cl and weathering proxies for each core arranged by depth. A) ANGC3. B) ISODC2 C) ZAPC1 D) ANGC1.

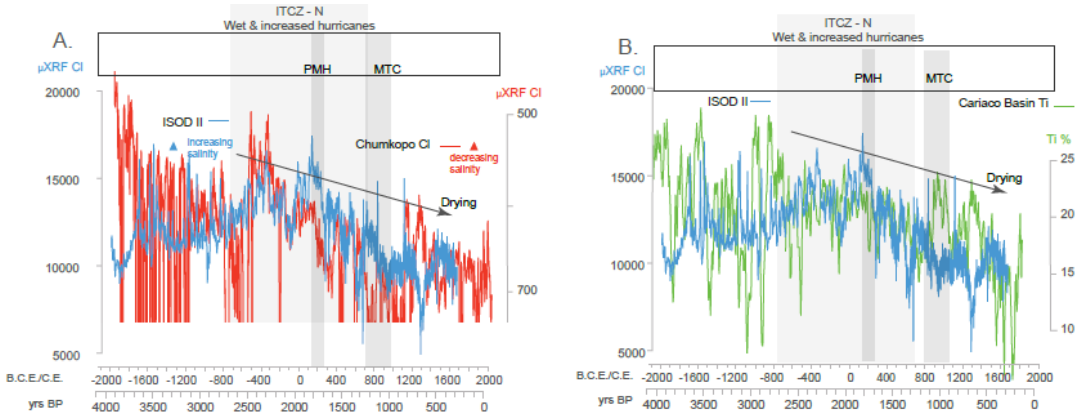

Figure 7. A. Chumkopo and ISODC2 Cl counts showing a drying trend over the past 2 ky. B. ISODC2 and Cariaco Basin Ti.

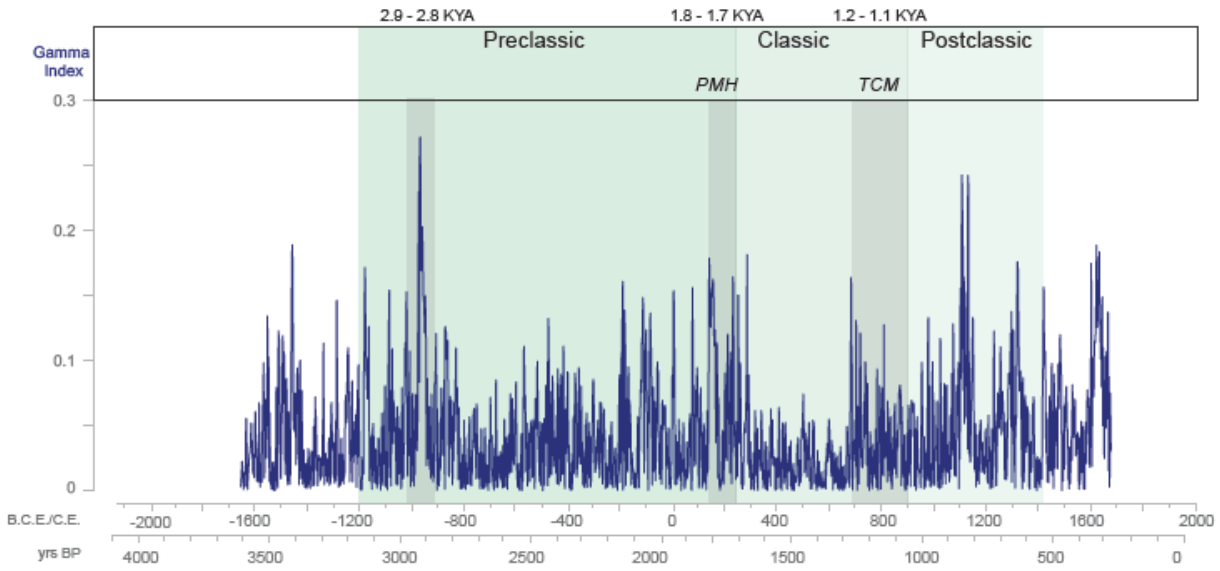

Figure 8. Gamma Index for the last 3.5 ky showing periods of rapid change amongst all four records (ANGC1, C3, ZAPC1, ISODC2). The gamma index shows periods when Cl values are either rapidly increasing or rapidly decreasing in all of the records.

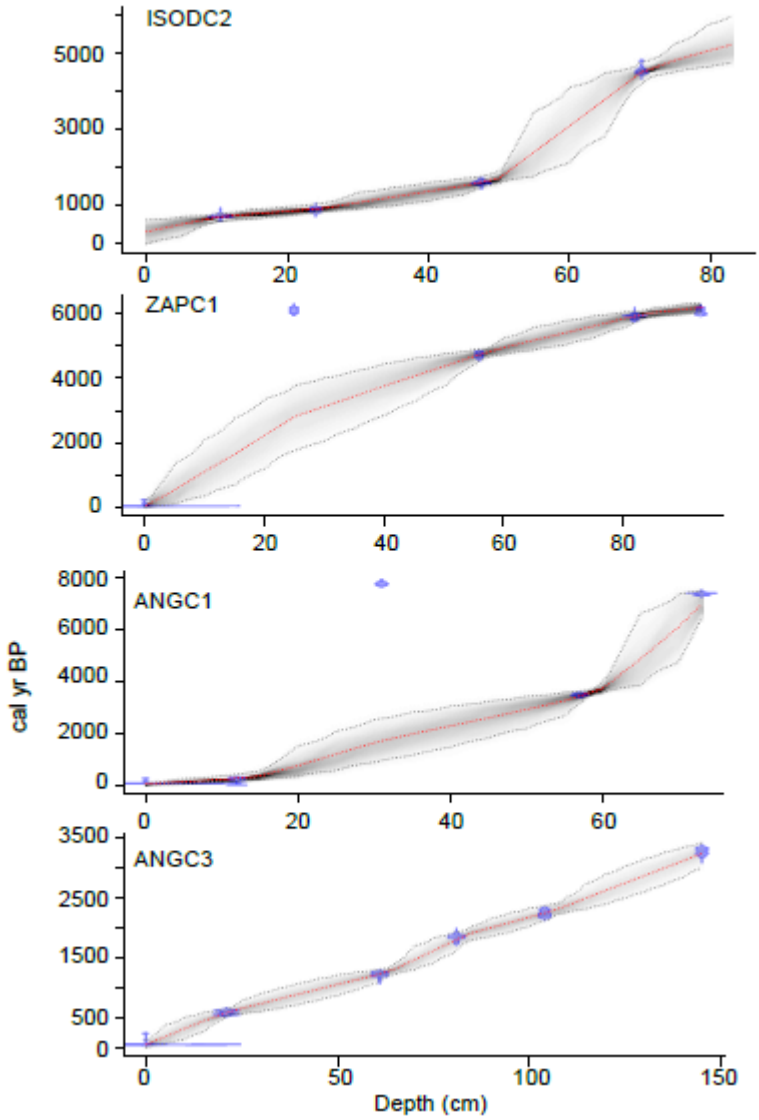

Figure A.1. BACON age models for ISOD, ZAPC1, ANGC1 and ANGC3.

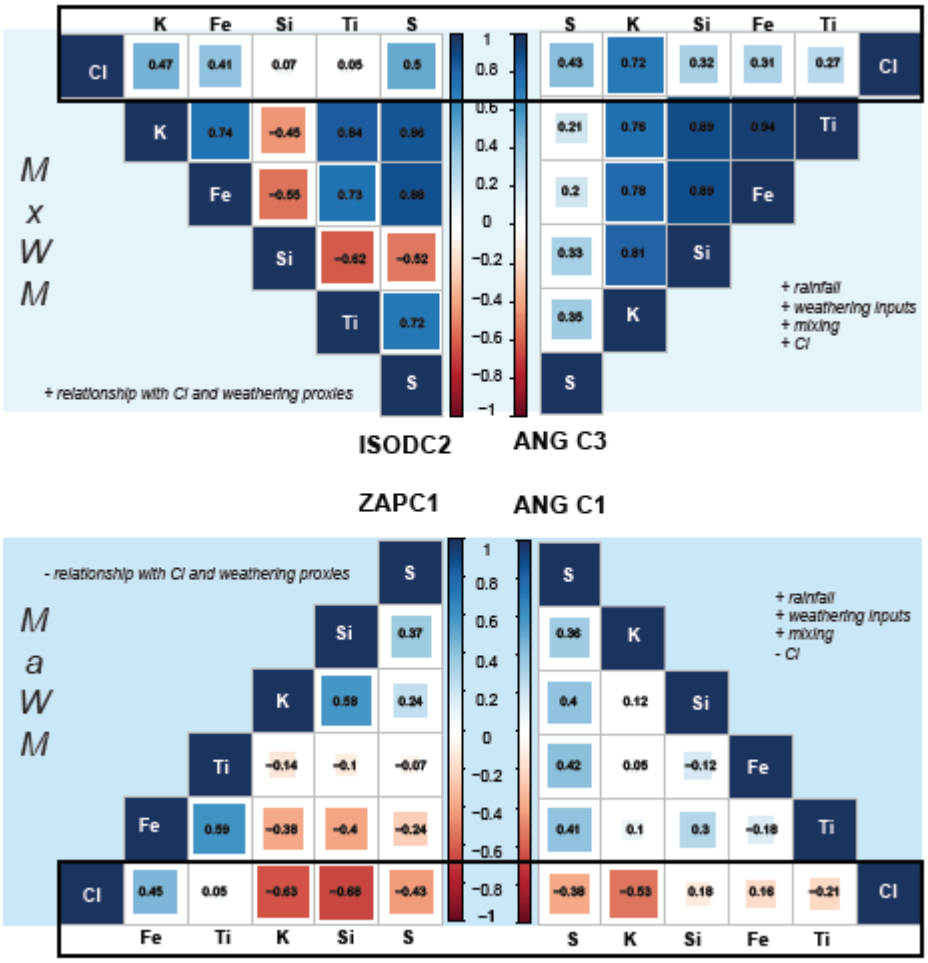

Figure S2. PCA and correlation charts for all 4 cores with correlation coefficients denoting their relative place in the water column and relationship with the halocline/ MZ.

CHAPTER 5: CONCLUSIONS

The sediment geochemistry of the caves, deep cenotes and shallow waters of the Yucatan Peninsula responds to wetness and dryness across the region because of changes in evaporation and water-mass mixing. This thesis describes the present interaction of land cover and precipitation on sediment geochemistry in a coastal cave system, the past response of shallow surface waters to drought, and the past interaction between the meteoric and marine water masses in response to precipitation and drought events. The combination of methods from Chapters 3 and 4 are useful to investigate changes in past aridity and wetness because Chumpac can be used to look at aridity and the Yucatan gamma mixing proxy can be used to look at wetness, thereby providing a reliable and comparable set of climate proxies that can be used to infer past hydroclimate conditions. The high resolution and comparability of these records makes them unprecedented in terms of climate reconstruction and the new proxies proposed here will be used by other researchers.

In Chapter 2, the effect of hurricanes on sediment accumulation in the Yax Chen cave subsystem was investigated. The magnitude of seasonal rainfall as well as the stature and extent of vegetation cover surrounding the cenote are important controls on sediment chemistry and accumulation. Hurricanes and large rainfalls result in a seasonally lagged increase in particulate organic matter from phytoplankton blooms, which grow in response to a rise in the water table and nutrient inputs. Cenotes surrounded by substantial mangrove have a more

restricted surface because of peat occlusion, which limits downward water percolation, promotes local ponding, and encourages phytoplankton blooms months later, when the water table drains. This was illustrated by the passing of Hurricane Ingrid in 2015, which had a small impact on sediment accumulation in the following months, but a substantial impact in the subsequent season. Chapter 2 discusses differences in sediment accumulation that arise because of differences in vegetation cover and cenote size, which is important to consider when searching for new sites to develop paleoclimate proxies, and to identify places where pollutants might enter the cave system. We also show in this chapter that the cave-cenote system is more complex than previously thought, which suggests more research is required to develop sound management strategies to protect the system in the future. Such studies might explore the consequences of these systems being destroyed, e.g. how sedimentation and downstream water quality will be affected if mangroves around a cenote are removed.

In Chapter 3, we used uppermost deposits from 16 sediment cores from a range of cave systems around Tulum, Quintana Roo to develop a salinity calibration that was applied to two sediment cores from shallow lakes. Dramatic increases in the standard deviation of past salinity within a short period of time, which coincided with the Maya Terminal Classic, suggested that rapid and unpredictable increases in salinity (and the climate shifts that caused them) may have been the drivers of cultural disintegration across the Yucatan Peninsula. The records also show correspondence with Bond events, movement of the ITCZ, and changes in regional

SSS and SST. The combined “Chumpac” record created in Chapter 3 has greater temporal resolution than other paleoclimate records from the Yucatan Peninsula, and is based on simpler assumptions than used when working with speleothems or lake sediment records.

In Chapter 4, the salinity of four cores from different depths and distances from the halocline were used to investigate responses to rainfall. It was discovered that cores within the MeWM respond differently from cores in the MaWM because of differences in rainfall-induced mixing. This was corroborated by other studies that used instrumental monitoring and showed mixing of the MeWM into the MaWM during big rainfalls that caused deep freshening, as well as drought-induced stagnation that causes freshening in the cave MeWM. Chapter 4 demonstrated that groundwater on the Yucatan Peninsula responds to larger-scale climate changes and has responded to movement of the ITCZ throughout the late Holocene. This is especially important to consider when developing management plans for coastal regions in Quintana Roo, and other coastal areas with similar hydrology. With increasing hurricanes and more development, these coastal aquatic ecosystems are subject to greater vulnerability, and it is thus important to explore how changes in hurricane frequency and magnitude impact groundwater salinity. This is important to understand for both agricultural and domestic purposes, and to identify adverse effects to local ecosystems that might be caused by changes in water-column salinity over time.